

UC Berkeley

UC Berkeley Electronic Theses and Dissertations

Title

Surface Modifications for Cell Culture Systems

Permalink

<https://escholarship.org/uc/item/0ht2z9q9>

Author

Reese, Willie M.

Publication Date

2017

Peer reviewed|Thesis/dissertation

Surface Modifications for Cell Culture Systems

by

Willie M. Reese

A dissertation submitted in partial satisfaction of the

requirements for the degree of

Doctor of Philosophy

in

Engineering - Materials Science and Engineering

in the

Graduate Division

of the

University of California, Berkeley

Committee in charge:

Professor Kevin E. Healy, Chair

Professor Phillip B. Messersmith

Professor Sanjay Kumar

Fall 2017

Surface Modifications for Cell Culture Systems

Copyright 2017
by
Willie M. Reese

Abstract

Surface Modifications for Cell Culture Systems

by

Willie M. Reese

Doctor of Philosophy in Engineering - Materials Science and Engineering

University of California, Berkeley

Professor Kevin E. Healy, Chair

This dissertation focuses on methods to understand and improve surface modifications for 2D and 3D cell culture platforms. In this work, novel methods are investigated for their ability to alter cell adhesion and block small molecule absorption, events that have the ability to alter cell behavior and phenotype.

Chapter 1 is an introduction to surface modification techniques, the mechanisms within the cell that are currently understood to probe these alterations of surface chemistry, topography, and other attributes, and the application of these methods. This chapter serves to tie together the investigations done in this dissertation.

Chapter 2 presents an investigation on the effects of change of topography using multi-photon ablation lithography to fabricate arrays of nanoscale craters in quartz substrates with a variety of geometries and spacing (i.e. pitch). This direct-write patterning method developed by a collaborator induced directed NIH 3T3 cell migration. In this work, I focused on understanding the mechanism of action for this phenomena. Briefly, the direct write patterning produced sub-micron sized pits in quartz that could be arranged in any number of spacial patterns. I investigated both isometrically spaced pits ($2-8\mu\text{m}$) as well as gradient spaced patterns, where pits were spaced at $1\mu\text{m}$ spacings toward the center of the pattern up to $10\mu\text{m}$ toward the perimeter of the pattern. Immunofluorescent labeling of intracellular focal adhesion Vinculin was used to quantify focal adhesion size and revealed significant differences based on pattern spacing. In isometric patterns, 2 and 4 μm patterns showed significantly smaller focal adhesion size distributions leading to the conclusion that the nanocraters restricted focal adhesion size and also maturity leading to higher turnover of these adhesion. Higher turnover in regions where the pits were densely arranged led to an observation of cells migrating away. With motion tracking on gradient patterns, cells were seen to migrate areas where the nanopits were spaced closer together along directions of the highest rate of increase in surface area, confirming that the pits were restricting the area available for cells to form larger stable focal adhesions. Other researchers have shown that area is a critical attribute for focal adhesion formation that can be overcome by intercellular adhesion protein activation. To investigate this, NIH3t3

cells were transfected with a plasmid containing the DNA for the first 405 amino acids of the Talin-1 protein, which has shown to perform as the full Talin molecule in intracellular signaling. After transfection, cells showed no significant difference on any of focal adhesion size on any of the isometric patterns and also lost their directed migration function on gradient patterns. This data supports our hypothesis that the physical restriction of area for adhesion causes cells to statistically migrate from regions of high pit density (low pitch) to regions where more area is available, but with intracellular signaling of talin this can be overcome by the cell. This study helps to elucidate the mechanism through which cells probe their substrate topography and if employed on more biologically relevant surfaces can be used as a way to decrease cell adhesion.

Chapter 3 presents a novel method using a macrocyclic polyphenol coating to block drug absorption in Poly(dimethylsilane) (PDMS) based microfluidic Microphysiological Systems (MPS). MPS can be used to combine genetically relevant cell lines in micro-environments that recapitulate not only genetically relevant organ specific structure, but also organ system relationships to access on and off-target toxicities and efficacies. Most MPSs are easily manufactured via soft lithography techniques using poly-dimethylsiloxane (PDMS), which has shown to be biologically compatible and amenable to many standard cell culture techniques due to its high transparency, high oxygen permeability, and low auto-fluorescence. Although PDMS has several positive attributes, many have shown that due to its hydrophobicity, small lipophilic molecules can be absorbed into PDMS creating unpredictable drug concentrations in MPSs.

To address this limitation, we designed and developed a novel macrocyclic polyphenol, which is able to reduce the absorbance of the model drug compounds rhodamine B, C₁-BODIPY-C₁₂, Brilliant Green, and Metanil Yellow into PDMS by 87, 96, 93, and 95 percent, respectively. This outperforms established polyphenol coatings such as polydopamine or pyrogallol. Initial experiments have shown low cytotoxicity allowing for the culture of iPSC-derived cardiomyocytes for at least one month. Preliminary experiments also show good coating stability not only on PDMS but also on other biologically relevant polymeric materials such as tissue culture polystyrene, polycarbonate, and Teflon. This coating is also advantageous over other solutions of drug absorption such as Sol-Gel methods or other glass like coatings, due to its ease of use, low cost, and high oxygen permeability.

Chapter 4 gives an overall conclusion and details future directions for investigations in Chapter 2 and 3.

To my parents, Richard James, Sr and Chan Im Reese.

Contents

Contents	ii
List of Figures	v
List of Tables	vii
List of Abbreviations	viii
1 Cell-Surface Interactions and Motivations for Surface Modifications	1
1.1 Overview: How Cells Interact with Interfaces	1
1.1.1 Integrins	1
1.1.2 Integrin Ligands in the Extracellular Matrix	2
1.1.3 Focal Adhesions	5
1.1.4 The Cytoskeleton	7
Actin filaments	8
Microtubules	9
Intermediate Filaments	9
1.1.5 Mechnotransductive Pathways in Cell Sensing	10
1.1.6 Conclusions	11
1.2 Examples of Methods for Surface Modifications in Cell Culture	11
1.2.1 Protein Coatings	11
1.2.2 Peptide Coatings	12
1.2.3 Micro-contact Printing	13
1.2.4 Self Assembled Monolayers	13
1.2.5 Topographical Patterning	14
1.2.6 Material Stiffness	15
1.2.7 Conclusions	16
1.3 Dissertation Scope and Outline	17
References	18
2 Nanopit Patterning Effects on Focal Adhesion Formation	23
2.1 Abstract	23
2.2 Introduction	24

2.3	Materials and Methods	28
2.3.1	Laser Ablation of Glass	28
2.3.2	Immunofluorescence	28
2.3.3	Focal Adhesion Size Quantification	28
2.3.4	Transfection of Talin-1	28
2.3.5	Motility & Directionality Measurements	29
2.4	Results and Discussion	29
2.4.1	Nanoscale Craters Reduce Focal Adhesion Size.	29
2.4.2	Directed Migration in Gradient Patterns	32
2.4.3	Talin-1 Integrin Activation	34
2.5	Future Direction and Conclusions	37
References		38
3	Using a Macrocyclic Polyphenol Coating to Block Absorption in PDMS-based Microfluidic Systems	39
3.1	Abstract	39
3.2	Introduction to Microphysiological Systems	41
3.3	PDMS Advantages and Challenges in Microphysiological Systems . .	41
3.4	Current Strategies for Reducing Small Molecule Absorption in PDMS	41
3.5	Materials and Methods	42
3.5.1	MPP 5 _{cone} Precursor Synthesis	42
3.5.2	High Pressure Liquid Chromatography	43
3.5.3	Nuclear Magnetic Resonance	43
3.5.4	Poly-dimethyl Silane (PDMS) Sample Fabrication	43
3.5.5	MPP 5 _{cone} Coating Procedure	44
3.5.6	Contact Angle Measurements	44
3.5.7	Fluorescent Dye Absorption and Effective Diffusivity Assay . .	44
3.5.8	Small Molecule Permeation Assay	45
3.5.9	Oxygen Permeation Assays	45
3.5.10	hiPSC-derived Cardiomyocyte Beat Rate Analysis Assay . . .	46
3.5.11	hiPSC-derived Cardiomyocyte Cell Viability Assay	46
3.5.12	Human Mesenchymal Stem Cell-derived White Adipose Tissue MPS Viability Assay	46
3.5.13	Scanning Electron Microscopy	46
3.5.14	X-ray Photoelectron Spectroscopy	47
3.6	Results and Discussion	47
3.6.1	Polyphenols Increase Hydrophilicity of PDMS	47
3.6.2	Reduction of Small Molecule Absorption	49
3.6.3	MPP 5 _{cone} Coating Characterization	56
3.6.4	Effective Diffusivity & Permeability Reduction	61
3.6.5	Coating Characterization and Performance in a Microfluidic Channel	70

3.6.6	Coating Biocompatibility	74
3.7	Conclusions & Future Directions	80
References		81
4	Future Work	83
4.1	Conclusions for Topographically Directed Migration	83
4.1.1	Topographical Patterning on Biologically Relevant Materials	83
4.2	Conclusions and Future Directions of Macrocyclic polyphenol Coatings	84
4.2.1	Elucidating Polyphenol Coating Kinetics	84
4.2.2	Using Macrocyclic Polyphenol Coatings for PDMS Functionalization	84
4.2.3	Improving Cell Adhesion with MPP 5_{cone} Coatings on PDMS	85
References		88

List of Figures

1.1	Basic Integrin Structure with Signaling Modes	3
1.2	Integrin Heterodimer Pairs and Associated ECM Proteins	4
1.3	Schematic Model of Focal Adhesion Architecture.	6
1.4	Dynamic nanoscale Structure of Focal Adhesions	7
2.1	Scanning Electron Micrograph of Isometric Nanopits	25
2.2	NIH 3T3 Mouse Fibroblasts on Nano-pit Pattern Lines.	26
2.3	NIH 3T3 Mouse Fibroblasts on Gradient Nano-pit Patterns.	27
2.4	Focal Adhesion Immunofluorescence Staining on Isometric Patterns	30
2.5	Focal Adhesion Size Distributions on Isometric Patterns	31
2.6	Gradient Patterns Reduce Focal Adhesion Size and Direct Cell Migration	33
2.7	Talin-1(405) Transfected NIH3T3 Fibroblasts on Isometric Patterns	35
2.8	Migration and Focal Adhesion Size Distribution of Talin+ NIH3T3 Fibroblasts on Nanopatterns	36
3.1	MPP 5_{cone} Precursor Synthesis.	43
3.2	MPP 5_{cone} Coating Method.	45
3.3	Polyphenol coatings increase hydrophilicity of PDMS	48
3.4	MPP 5_{cone} reduces Rhodamine B Absorption	49
3.5	MPP 5_{chair} and MPP 5_{cone} Absorption of Rhodamine B	50
3.6	MPP 5 Isomer Performance	51
3.7	Optical Density during MPP 5 Isomer Polymerization	52
3.8	MPP 5_{Cone} Isomer NMR	53
3.9	HPLC of MPP 5_{cone} Precursor	54
3.10	MPP 5_{cone} Reduces Absorption in Other Materials	55
3.11	MPP 5_{cone} stability on other polymers	56
3.12	MPP 5_{cone} Scanning Electron Microscopy	57
3.13	MPP 5_{cone} Scanning Electron Microscopy	58
3.14	MPP 5_{cone} X-Ray Photospectroscopy	59
3.15	MPP 5_{cone} Coating Drying Over Time	60

3.16	MPP 5_{cone} Coating Stability	61
3.17	Rhodamine B Diffusion Model Compared to Actual Data	63
3.18	Change in Effective Diffusivity and Area Under the Curve Intensity Measurements for Molecules with Range of Log Ps	64
3.19	Dye Molecules Used in Effective Diffusivity Models and Comparisons	65
3.19	Dye Molecules Used in Effective Diffusivity Models and Comparisons	66
3.19	Dye Molecules Used in Effective Diffusivity Models and Comparisons	67
3.20	Schematic of Franz Cell	68
3.21	Rhodamine B Permeability Measurements from Uncoated and MPP 5_{cone} Coated PDMS	69
3.22	Coating Thickness in Microfluidic Channel	70
3.23	Coating Thickness in Microfluidic Channel	71
3.24	Fluorescent Images of Rhodamine B and C ₁ -BODIPY-C ₁₂ Infused Microfluidic Channels	73
3.25	Normalized AUC of Rhodamine B and C ₁ -BODIPY-C ₁₂ Infused Microfluidic Channels	74
3.26	2D Alamar Blue Metabolism of glshiPSC-CMs after MPP 5_{cone}	75
3.27	Phase Contrast Images of hiPSC-CMs on MPP 5_{cone} coating	76
3.28	2D Beat Rate hiPSC-CM after MPP 5_{cone}	77
3.29	Vinculin and α -actinin Immunofluorescent Staining of CMs on MPP 5_{cone} coated PDMS	78
3.30	Oxygen Permeability	78
3.31	Toxicity of Direct Exposure to MPP 5_{cone}	79
3.32	White Adipose Tissue Microphysiological System Toxicity Assessment	80
4.1	Phase Contrast Images of iPSC-derived Cardiomyocytes on Coated and Uncoated PDMS	86
4.2	Immunofluorescent Staining of Vinculin and α -actinin in iPSC-derived Cardiomyocytes on MPP 5_{cone} and Uncoated PDMS 2D Surfaces	86

List of Tables

1.1	Examples of Integrin Tissue Distributions	5
-----	---	---

List of Abbreviations

- Arp2/3** actin-related proteins 2, 3
- AUC** area under the curve
- Cn** collagen
- D_{eff} effective diffusivity
- DI** de-ionized
- DIC** Differential Interference Contrast
- Dk** Permeability
- DMSO** Dimethylsulfoxide
- ECM** extracellular matrix
- EDTA** Ethylenediaminetetraacetic acid
- EHS** Engelbreth-Holm-Swarm
- ELISA** enzyme-linked immunosorbent assay
- ESC** embryonic stem cell
- EtOH** ethanol
- F-actin** filamentous actin
- FA** focal adhesions
- FAK** focal adhesion kinase
- Fg** fibrinogen
- Fn** fibronectin
- FWHM** full-width at half-maximum

G-actin globular actin

GFP Green Fluorescent Protein

HCl hydrochloric acid

hiPSC-CMs human induced pluripotent stem cell-derived cardiomyocytes

hMSC human mesenchymal stem cell

HPLC High Pressure Liquid Chromatography

IC₅₀ concentration of an inhibitor where the response is reduced by half

IKVAV Ile- Lys-Val-Ala-Val

iPALM Interferometric photoactivation and localization microscopic

iPSC induced pluripotent stem cells

LC/MS Liquid Chromatography with Mass Spectrometry

LG Lignin

Ln laminin

Log P Log of the partition coefficient

MPP macrocyclic polyphenol

MPP 5_{cone} Macrocyclic PolyPhenol 5 Cone Isomer

MPS Microphysiological Systems

MTOC microtubule organizing center

NAO nonyl acridine orange

NMR Nuclear Magnetic Resonance

P partition coefficient

PA Poly (acrylamide)

PDA polydopamine

PDMS Poly(dimethylsilane)

PEG polyethylene glycol

PG Pyrogallol

PHSRN Pro-His-Ser-Arg-Asn

PLL Poly-L-Lysine

PTKs protein tyrosine kinases

RGD arginine-glycine-aspartic acid

SAMs self assembled monolayers

SEM Scanning electron microscopy

TCPS tissue culture polystyrene

UV ultraviolet

VASP vasodilator-stimulated phosphoprotein

WASP Wisktt-Aldrich Syndrome Protein

WAT white adipose tissue

WT wild-type

XPS X-ray Photospectrometry

Acknowledgments

First, I would like to thank God, with him all things are possible.

I would like to thank my research advisor, Kevin E. Healy, for giving me the opportunity to be a member of his research group and fostering my intellectual growth and providing support to explore my research and personal interests. I would also like to thank other members of my committee, Phillip Messersmith and Sanjay Kumar, for their input and guidance in the development of my dissertation.

I would like to thank my parents, for always supporting me emotionally and financially. You have always believed in me encouraged me to cultivate my God given propensity for science. Thank you for being role models with integrity, initiative, and persistence. I love you both.

I'd like to thank my extended family. Particularly, my grandmother, Willie R. Miller, my aunt, Dr. Nancy Faith Reese-Durham, and my cousin, Gloria Waters. Your support through this 9.5 year journey is invaluable and thank you for being role models in pursuing education for its own sake.

To my lab mates throughout the past 5 and a half years, thank you for your guidance and support with research techniques and emotional well being. Dr. Naomi Kohen, thank you for on boarding me and spending time to meticulously teach me your scientific ways. Dr. Peter Loskill, thank you for being a mentor to me and taking interest not only in encouraging me to continue my pursuit of scientific knowledge, but also prowess. Dr. Anurag Mathur, thank you for your career and life advice. Peter and Anurag, thank you both for being dear friends and big brothers. Dr. Anusuya Ramasubramanian, thank you for our fruitful scientific discussions, helping me brainstorm, and for our therapeutic conversations about life. Dr. Shane Browne, thank you for helping me prepare presentations, reading my papers and abstracts, and being my healthy living buddy. Thank you, Professor Nathaniel Huebsch, who has been an exemplar role model of a scientist with integrity, compassion, and intelligence. Also, thank you to Brian Siemans and Natalie Marks, for being terrific lab managers, making sure the lab was functional and making amazing science possible. Thank you to all my lab mates and collaborators who have become good friends and supported me in so many ways.

I have been so fortunate to have a strong network of friends in the bay area that have made it feel like home. Thank you Luis Mendoza-Torres, Rosemarie de la Rosa, and Claudia Espinoza for our monthly meet ups to debrief, drink tea, and support each other in navigating life, love, and career. Thank you Samantha Akwei and Teshika Hatch for being amazing roommates with social consciences to remind me the world needs scientists who give back to the communities that support them. Thank you Dr. Heather Doyle for being a grounded emotional support and a true

friend with a big heart. Thank you Dr. Christopher Frances and (future Dr.) Steven Alvarez, for being great study buddies at the beginning of our time here at Berkeley in MSE and for becoming very close friends and confidants.

If I have forgotten anyone, please forgive me. I hope to help others in the future as the people here have helped me.

Chapter 1

Cell-Surface Interactions and Motivations for Surface Modifications

1.1 Overview: How Cells Interact with Interfaces

The mechanical integrity of tissues is due to the connections cells make with each other and with the surrounding protein matrix environment. These connections are appropriately called adhesions and can be highly specific. *In vivo* cells make adhesions with each other to create mechanical integrity for tissue, but also to the extracellular matrix (ECM). The chemical and topographical characteristics of a substrate surface have the ability to manipulate cell function, phenotype, behavior, and adhesion. Extrinsic mechanisms often begin with ligand interactions on the cell surface that mediate complex, dynamic signaling processes that can change internal gene and protein expression. Conversely, small or bio-molecules can be taken up by a cell and change intrinsic gene or protein expression to alter ligand-receptor kinetics externally. These processes of cell signaling influenced by mechanical forces and cues to produce biochemical signals and vice versa is referred to as mechanotransduction. Chapter 1 briefly overviews the structures in the cell that respond to substrate properties, the pathways that are involved in mechanotransduction, and the motivations and techniques to manipulate the dynamics of these systems in biomaterials engineering.

1.1.1 Integrins

The cell surface is covered with a variety of surface receptors that mediate the cell-cell and cell-substratum interactions. These interactions influence a diverse set of internal processes that regulate cellular growth, differentiation, senescence, junction formation, and polarity, among other properties. This work focuses on the interactions between the cell and the substratum and therefore integrins, which are trans-

membrane proteins responsible for mediating the cell-substratum interaction, will be discussed here.

Integrins are non-covalently associated heterodimers, consisting of an α and β subunit. Integrins have an external domain that interacts with ligands on extracellular matrix proteins and an internal domain that connects to the mechanical cytoskeletal structures of the cell through mediator proteins. **Figure 1.1** depicts two ways integrins can be activated. Outside-in signaling occurs when ligands external to the cell bind to and activate integrins and result in signaling through mechanotransductive pathways that can affect cell polarity, survival, proliferation, cytoskeletal structure and gene expression. Inside-out signaling happens when changes in gene or protein expression activate integrins from within the cell and cause changes in cell adhesion, migration, and motility.(1)

Specific pairs β and α units are known to interact. Current literature lists at least 8 different β subunits and at least 11 α subunits.(1, 2) Previously, it was thought that each β subunit had a particular α subunit pair, but now it is known that some α units can pair with more than one β unit. For example, α_v has been found to pair with β_1 and β_2 . Specific intergrin pairs are known to bind to certain ligands and may be expressed on specific cell types to create cell niche environments. For example, $\alpha_v\beta_5$ is known to be a crucial receptor for preserving embryonic stem cell (ESC) renewal. (3) **Figure 1.2** shows the current set of known integrin pairs and the ligands capable of binding each pair. Integrin-ligand binding is highly specific, but one integrin-ligand heterodimer is not sufficient to sustain the forces needed for cell attachment or migration. Therefore, integrin clustering, or the arrangement of multiple integrin hetero-dimers into hetero-oligomers, is necessary to produce the anchoring sites for cell adhesion and motility.

Integrin binding and clustering is essential for cells to sense their environment. The environment contains many signals such as topography, chemical composition and ligand presentation. Next, the discussion will move to the ligands in the cell niche environment that exist naturally on ECM proteins and their role in cell signaling.

1.1.2 Integrin Ligands in the Extracellular Matrix

The ECM serves many functional roles including providing mechanical integrity for tissues and organs and serving as ligands for cell signaling. The ECM is composed of approximately 300 types of proteins and proteoglycans, that are expressed differently depending on the tissue. The ECM is regulated dynamically throughout organism maturity and overall health.(4, 5) As scaffolds, ECM proteins help to regulate which cells are able to exist in certain tissues and can also affect their growth, activation, senescence, apoptosis, and maturity. Common ECM constituents include collagens, laminins, fibronectin, vitronectin, proteoglycans, and elastin, each providing different biochemical and mechanical signaling cues to give tissues unique dynamic functional abilities. For example, compared to normal tissue, aged tissue, wounded tissue, and tumor environments all have increased fibronectin content, resulting in increased stiff-

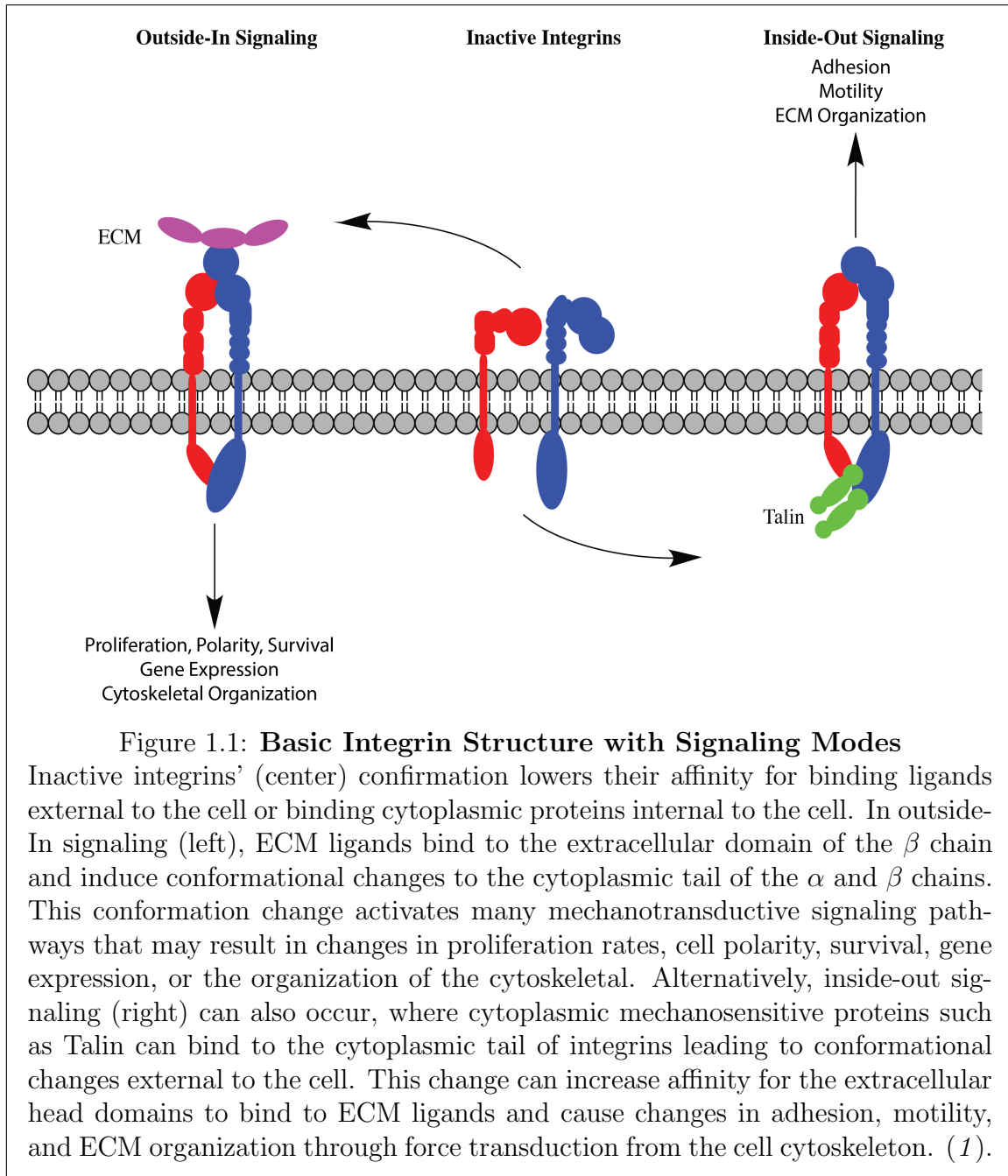
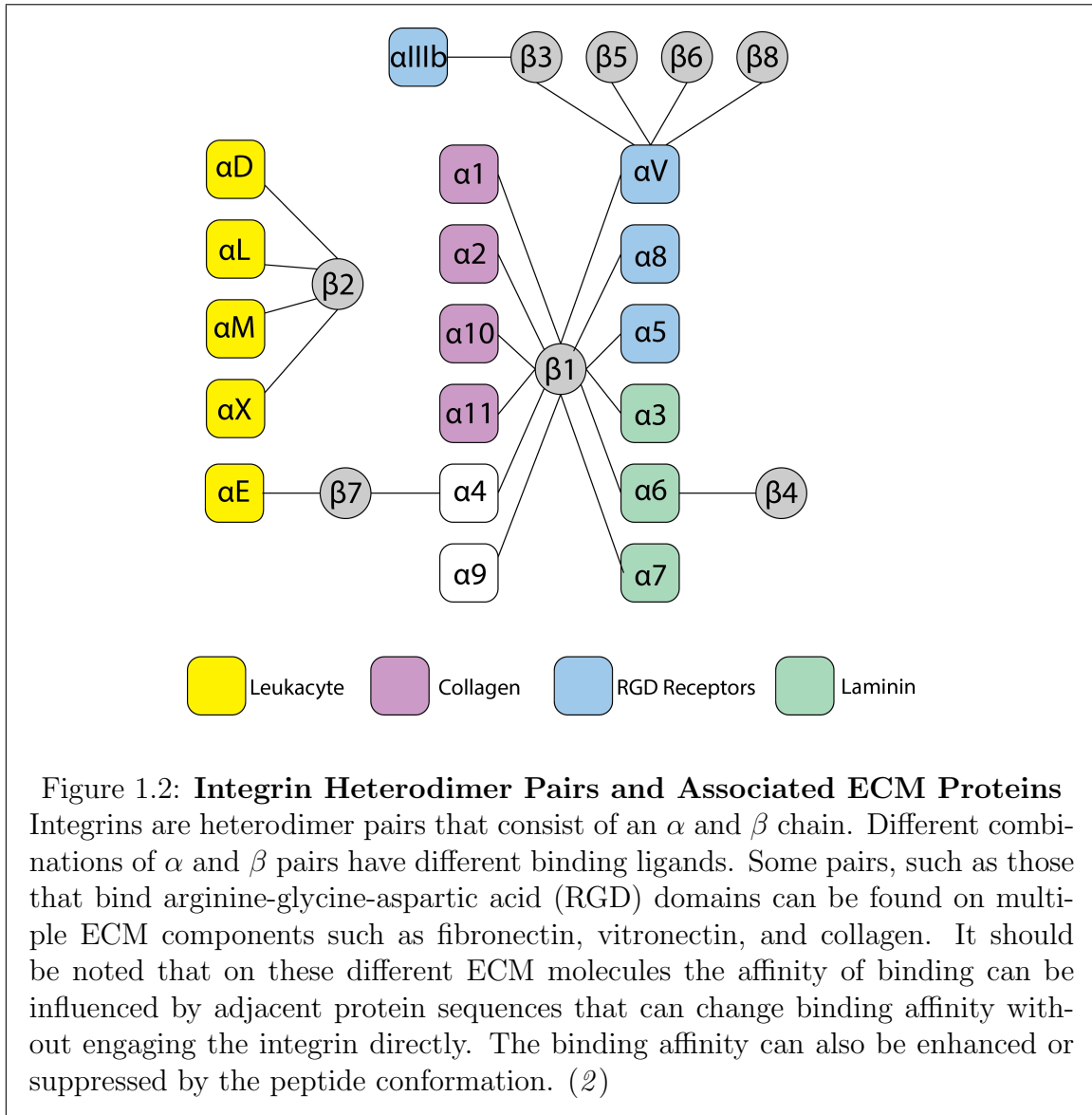


Figure 1.1: **Basic Integrin Structure with Signaling Modes**

Inactive integrins' (center) conformation lowers their affinity for binding ligands external to the cell or binding cytoplasmic proteins internal to the cell. In outside-In signaling (left), ECM ligands bind to the extracellular domain of the β chain and induce conformational changes to the cytoplasmic tail of the α and β chains. This conformation change activates many mechanotransductive signaling pathways that may result in changes in proliferation rates, cell polarity, survival, gene expression, or the organization of the cytoskeletal. Alternatively, inside-out signaling (right) can also occur, where cytoplasmic mechanosensitive proteins such as Talin can bind to the cytoplasmic tail of integrins leading to conformational changes external to the cell. This change can increase affinity for the extracellular head domains to bind to ECM ligands and cause changes in adhesion, motility, and ECM organization through force transduction from the cell cytoskeleton. (1).



Integrin	Ligand*	Cellular and Tissue Examples
$\alpha_v\beta_1$	Ln, Fn, Vn	fibroblasts, osteoclasts, tumor cells
$\alpha_v\beta_3$	Fg, Vn, Fn	fibroblasts, endothelial cells, osteoclasts
$\alpha_v\beta_5$	Fg, Vn, Fn	endothelial cells, osteoclasts, fibroblasts
$\alpha_v\beta_6$	Fg, Vn, Fn	epithelial cells, carcinoma cells
$\alpha_1\beta_1$	Cn VI, Cn I, Ln	chondrocytes, endothelial cells
$\alpha_2\beta_1$	Cn I, Cn IV, Ln	chondrocytes, endothelial cells

Table 1.1: **Examples of Integrin Tissue Distributions**

Some integrins can be expressed in multiple cell types and cells can also express multiple integrins. **Note** Not all integrins, ligands, or cell types are listed. * fibrinogen (Fg); fibronectin (Fn); laminin (Ln);collagen (Cn). (4)

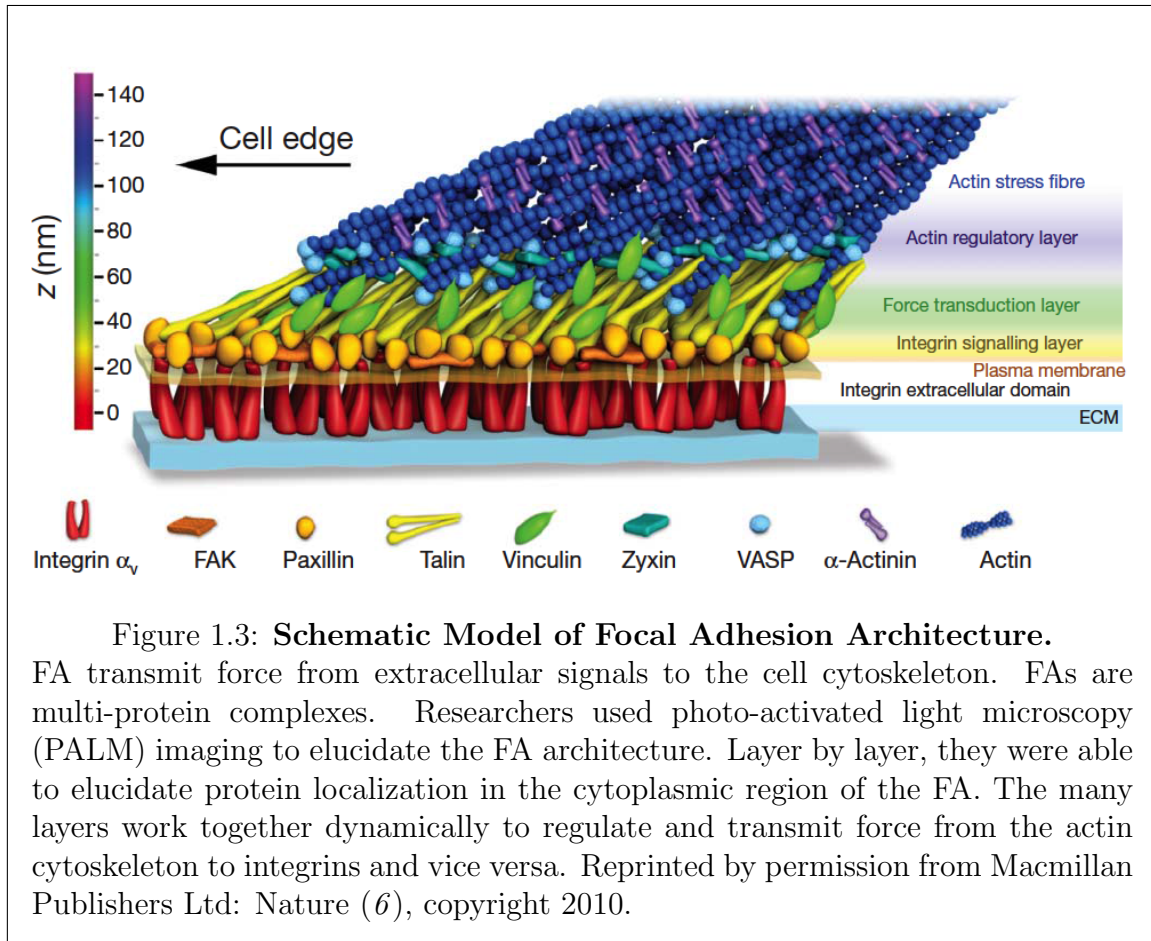
ness either directly, through the increased number of ligand binding sites that result in tissue crosslinking through cell binding, or indirectly, through ligand activated cell mechanotransductive pathways that increase the stiffness of the cell cytoskeleton.(5)

As shown in **Figure 1.2**, certain integrin pairs have the ability to bind to different ECM molecules. Cells may express one primary integrin or may have multiple integrins that enable different internal cell signaling to be activated depending on cell niche. **Table1.1** shows a few examples of integrins that appear in multiple tissues and cell types as well as cells that express multiple integrin modalities.

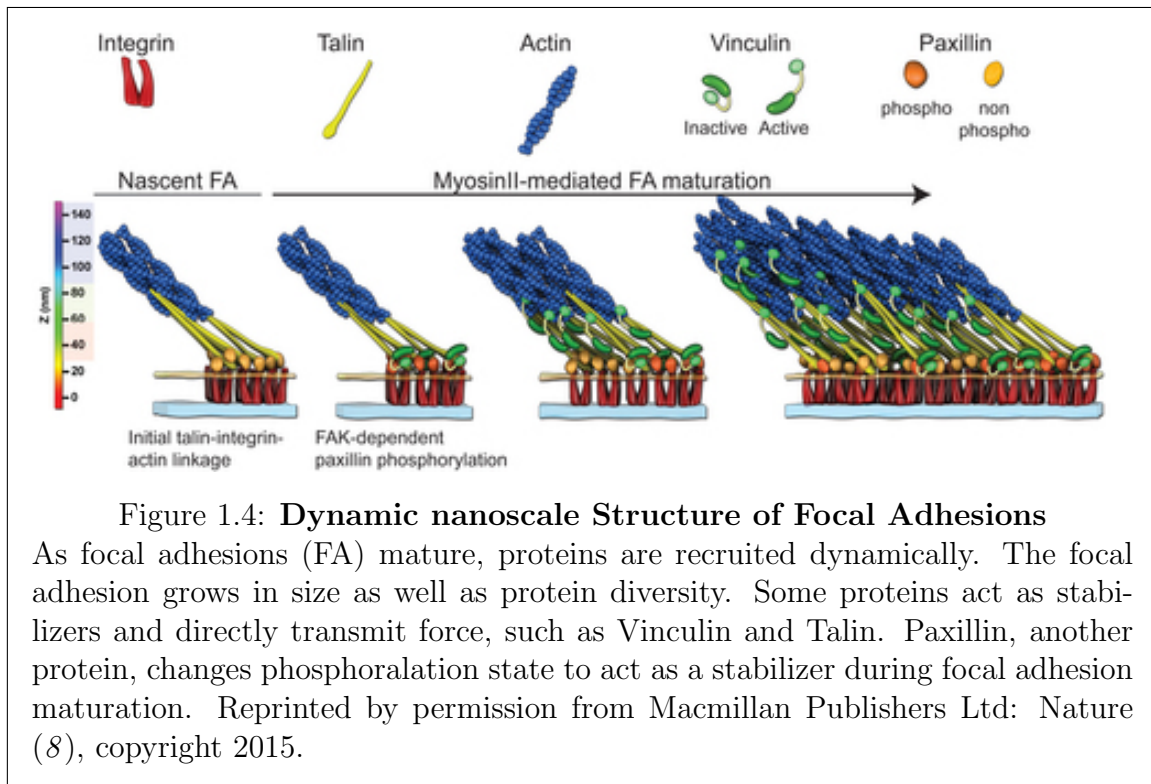
1.1.3 Focal Adhesions

Although the extracellular domain is important in cell adhesion, the cytoplasmic domain is critical for transmitting the external signals to other parts of the cell. The cytoplasmic domain is relatively short compared to the extracellular side with most having less than 70 amino acid residues.(2) The cytoplasmic side has no intrinsic kinase activity, but is bound to other proteins that serve as a bridge between integrins and the cell cytoskeleton (**See 1.1.4**). A number of biomolecules have been extensively studied as key proteins involved in forming a stable bridge that can transmit external signals to the cytoskeleton, as well as lead to changes in the extracellular activation of integrins increasing binding affinity for ligands. These multi-protein clusters are referred to as focal adhesions (FA).

Interferometric photoactivation and localization microscopic (iPALM) imaging revealed the spatial nanoscale cytoplasmic structure of these internal bridges called FA.(6) From the plasma membrane, the integrin cytoplasmic domain that binds to paxillian andfocal adhesion kinase (FAK) in the integrin signaling layer. Next, the force transduction layer consists of Talin and Vinculin, that together transmit forces on the extracellular ligand-integrin structure, with the help of zyxin and vasodilator-



stimulated phosphoprotein (VASP). **Figure 1.3** is a cartoon representation of the described structure. Proteins are not only spatially organized, but also temporally recruited to FA during outside-in signaling.(6–8) Waterman et al proposes that talin and unphosphorylated paxillin are bound to the externally-activated cytoplasmic integrin tail. Talin directly connects the cytoskeleton to the activated integrin, by binding the talin head domain to the cytoplasmic tail of the integrin and the talin tail domain to the cytoskeletal network, specifically actin. Subsequently, Vinculin is recruited, bound to talin, and then activated to help stabilize the bond between talin and the cytoskeletal network by binding its tail domain to the cytoskeleton as well. Finally, Waterman proposes that VASP then phosphorylates paxillin, allowing it to further stabilize integrin activation. VASP has also been linked to increasing vinculin activity by others.(9) Waterman was not able to provide sufficient data to prove the proposed temporal theory. **Figure 1.4** depicts the proposed maturation sequence from nascent FA to fibrillar adhesions. (8) Nascent FAs are short lived adhesions that turnover rapidly (~60s).(10) If stabilizing proteins such as vinculin are recruited, they become more stable and larger adhesions (~1 μ m) referred to as



focal complexes. α -actinin, a cytoskeletal cross linker, marks the maturity of focal adhesions since it has been found to be recruited at the end of nascent focal adhesion transformation into focal complexes.(10) If the maturation process continues, these focal complexes can mature into larger($2\mu\text{m}$ by $3\text{-}10\mu\text{m}$) adhesion sites termed fibrillar adhesions due to their long shape. Fibrillar adhesions last longer, support higher tensile forces, and align parallel to fibronectin fibers.(11)They are not seen in cells that are rapidly migrating due to their long lifetimes. Other than migration speed, the size distribution of FA depends on the stiffness and topography of the substrate, forces exerted on the cell, and cell type. The dynamics of focal adhesion assembly has been shown to be correlated with the fundamental processes of actin polymerization and myosin-II generated tension. These processes are discussed in the next section, Section 1.1.4.

1.1.4 The Cytoskeleton

The cytoskeleton is a network of actin (micro) filaments, intermediate filaments, microtubules. It is responsible for giving cells their shape and involved in processes including adhesion, proliferation, migration, nuclear signaling, intracellular transport, and others. To paraphrase Fletcher and Mullins, the cytoskeleton has three main functions(12):

1. Spatial Organization
2. Acts as a Physical and Biochemical Medium for Cell Sensing
3. Generates Forces for Motility and Cell Shape.

On shorter time scales, the cytoskeleton resembles the skeleton of an organism by its dynamic ability to remodel itself when subjected to external cues. The cues that affect the cytoskeleton can be physical or biochemical. There are several classes of proteins that regulate the cytoskeleton. Nucleation promoting factors initiate filament formation, while capping proteins terminate their growth. Polymerases also facilitate the growth of filaments through polymerization and cross-linking proteins, such as α -actinin, help to stabilize and orient filaments into more complex multi-filament structures. Through polymerization of the actin filaments and microfilaments, cells are able to change shape. Polymerization of these structures combined with protein based molecular motors that move along the filaments and tubules provide an intracellular transport system to move molecular components and organize them. Internal and external forces can alter the activity of regulatory proteins, providing a means for mechnosensing.

Actin filaments, microtubules, and intermediate filaments differ functionally in their architecture, mechanical stiffness, assembly dynamics, polarity, and their associated molecular motors. This section gives a brief overview of the main cytoskeletal systems and how they moderate cell adhesion and motility.

Actin filaments Actin is a collection of multi-functional proteins that can self-organize monomeric units, globular actin (G-actin), into fibrillar structures called filamentous actin (F-actin). Not only has it been found to play a role in motility and providing cell shape, but also helps create the complex transport systems needed for cell division and proliferation.⁽¹³⁾ G-actin is a asymmetric protein with a positive and negative end. The directed assembly of F-actin using this asymmetric monomer leads to a polarized network with positive ends of filaments oriented toward the plasma membrane and negative ends intersecting with microtubules, which will be described later. The polarization of the network allows associated motor proteins called myosin to preferentially travel along the F-actin network to allow cells to contract and sense the extracellular environment.

Actin can acquire different structural forms that perform various functions inside the cell. Bundles of aligned actin filaments provide structure for filopodia, which are involved in directed movement due to chemical gradients (chemotaxis) and cell-cell interactions. Highly branched filaments support the leading edge and provide forces needed to change cell shape which is needed for many processes such as phagocytosis. Isotropic or cortical networks of actin lack orientation but can be cross-linked with proteins such as fascin to resist tensile forces on the cell. Stress fibers, associated with myosin proteins, generate tensile forces on FA and the ECM. The type of

actin network formed is regulated by G-actin binding proteins such as profilin, which through interactions with actin bind proteins such as formin, can increase, in the case of formin, or decrease, in the case of Wisktt-Aldrich Syndrome Protein (WASP), polymerization rates.(13) Branching of actin fibers is mediated by actin-related proteins 2, 3 (Arp2/3) which bind to already growing actin fibers to create branches. These proteins are almost always membrane associated, ensuring that growing branches point to and support the membrane.

Actin polymerizes steadily in the presence of nucleotide bound monomers. The rate of this polymerization therefore is dependent on the concentration of these monomers, which is dictated by nuclear transcription and translation of the monomer protein. As the length of the protein monotonically increases, forces are likewise increased to support the steady growth of the leading edge required for migration. Capping proteins arrest the growth of individual fibers or branches. Disassembly mechanisms do occur and recycle G-actin to be used again.

Polymerization and de-polymerization signals have local affects on actin structures. For example, when an integrin is cytoplasmically activated through ECM binding, actin is bound and begins to polymerize locally and subsequently cross-link and organize, if maturation conditions are appropriate.

Microtubules Microtubules are the stiffest polymer in the cytoskeletal network. Unlike locally directed actin filaments, microtubules have a central microtubule organizing center (MTOC) near the nucleus.(14) Tubules branch out from the MTOC with persistence lengths as high as 5mm. With large stiffnesses and long persistence lengths, microtubules that almost linearly span from the MTOC to the cell membrane are common. Like F-actin, microtubules are composed of asymmetric protofilaments of $\alpha - \beta$ tubulin dimers with negative ends originating in the MTOC near the cell nucleus and positive ends interacting with F-actin near the plasma membrane. Again, polarization of tubules allows motor proteins in the dynein and kinesin families to travel preferentially in one direction along microtubules to perform transport processes needed for cell division and also transport cargo along their intracellular tracks.

Unlike the steadily polymerizing F-actin cytoskeleton, microtubules have two dynamic states of polymerization, steady growth and rapid depolymerization. The ability to rapidly deconstruct structures, gives microtubules the ability to globally respond to changes dictated at the MTOC. Microtubule stability has also been indicated in regulating F-actin polymerization and vice versa.(15)

Intermediate Filaments Intermediate filaments are the most pliable of the three cytoskeletal proteins. Their structure is more amenable to resisting tensile and shear forces compared to compressive forces. They are not polarized, like actin and microtubule networks and have not been implicated in any transport processes with motor proteins. Intermediate fibers can be cross-linked by a protein called plectin. Plectins

can also cross-link intermediate fibers to microtubule and actin structures. One example of intermediate filament proteins are lamins, which preserve the integrity of the eukaryotic nuclear membrane. The degradation of lamins by kinases helps to begin nuclear envelope breakdown during mitosis. Alberti notes that intermediate filaments play two roles in the cell:

1. linking the external stresses that many be tranferred directly from the cell membrane or indirectly through actin or microtubule networks to the nucleus
2. organizing membrane associated organelles (i.e.mitochondria, vesicles) in the cytoplasm, providing anchoring cites during migration and other processes. (14)

Intermediate filaments are thought of as a cytoskeletal integrating system directly connecting the actin and microtubules to important organelles such as the nucleus.

1.1.5 Mechnotransductive Pathways in Cell Sensing

Cells use integrins, focal adhesions, and the cytoskeletal network to sense the environment. Mechanotransduction is the process by which cells turn these physical cues into biochemical cues to affect cell processes, morphology and behavior. Environmental cues can be mechanical such as forces or be much more complex such as topographical. A complete understanding of the mechanisms that dictate cell response have yet to be elucidated, but over the past few decades, some light has been shed on the pathways that regulate mechanotransduction. (16, 17) However, the molecular complexity of these pathways is not well understood. For example, many researchers have been able to exploit the effect matrix stiffness has on stem cell differentiation, but the molecular mechanism that fully explains why different differentiation pathways can be accessed by changing stiffness is debatable. In mesenchymal stem cells, it has been found that the process is myosin II driven, but there still remain many questions about how these processes change nuclear gene expression, either directly or indirectly. (16, 18) Although integrin activation has been shown to be necessary, it is not sufficient to activate certain gene expression pathways. For example, Chen et al showed that the degree to which cells were able to spread was a better indicator for whether an endothelial cell would start DNA synthesis.(19)

Mechanotransductive pathways transmit large forces (10s of nanoNewtons) over long distances (10s of microns) covering the length of the cell in times (100s of milliseconds) that are much faster than soluble growth factors, which may take several minutes to invoke cellular responses.(16) Although, integrins have been proven to initiate the force transduction process, either in outside-in or inside-out signaling, other FA protein players such as talin and vinculin have also been implicated in signaling downstream.

This dissertation does not explore mechanotransductive signaling mechanisms and therefore, this chapter will not cover specific transduction pathways or proteins that

are involved in the cytoplasm. For an in depth review of mechanotransductive pathways please see (20) or (16).

1.1.6 Conclusions

Actin filaments, microtubules, and intermediate filaments work together to resist, generate, and transmit forces throughout the cell body. These forces can then lead to changes in cell structure, gene expression, motility, and other cell functions and behavior through mechanotransductive pathways. By engineering highly specific surfaces, researchers aim to control and understand the processes that dictate cell interactions with synthetic surfaces for cell culture systems. An overview of the motivations and methods is covered in the next section, Section 1.2.

1.2 Examples of Methods for Surface Modifications in Cell Culture

In the last 40 years, much progress has been made in some basic understandings of how cells interact with surfaces. Manipulating cell adhesion is critical for all laboratory experiments involving cells since adhesion signaling is needed to ensure healthy or representative phenotypes. This section, gives a brief overview of some of the more popular methods for understanding the role mechanotransduction plays in cell adhesion, motility, and differentiation. This section is in no way a complete survey of all the methods available, but gives the reader an idea of why understanding mechanobiology is so important to cell culture and the more common methods and variables for manipulating cells through engineered surfaces from the most widely used, simplest methods to more complicated protocols.

1.2.1 Protein Coatings

Protein coatings are often used to help facilitate cell attachment to promote healthy cell phenotypes in synthetic environments. Naturally occurring proteins are often used to recapitulate the cell adhesion environment. MatrigelTM, a trade marked gelatinous protein mixture, is a commonly used protein coating commercially available from BD Biosciences and Corning. It is harvested from Engelbreth-Holm-Swarm (EHS) mouse sarcoma cells, which secrete the ECM protein mixture. It is used for a wide array of applications to promote cell attachment on glass and tissue culture treated plastic among other surfaces that do not support cell attachment. The coating has often been criticized since it is exogenous, has significant lot to lot variability, and is also poorly defined. MatrigelTM contains fibronectin, collagen, laminin, and other adhesion proteins as well as growth factors that support normal cell phenotypes for an array of cells including primary cells, stem cells, and cell lines. Different lots can

contain different amounts of components leading to different cell behaviors and phenotypes, which is a undesired effect when trying to perform controlled experiments. Because of this some researchers prefer to use purified protein coatings of fibronectin and laminin or other proteins that can be also obtained from humans.

The method of coating for all these protein coatings is facile. The protein is reconstituted in either basal medium or phosphate buffered saline (PBS). The surface for cell attachment is then either immersed in the solution or covered with a thin layer of the solution at the desired protein concentration. The protein deposits onto the surface out of solution after some time and any unattached protein is washed away before cells are introduced. The simple method is accessible to any biology lab and is the reason for its wide spread use despite the concerns many have of its physiological validity.

1.2.2 Peptide Coatings

In 1984, the short peptide sequence, RGD, was found to block the adhesive ligand ability of the larger fibronectin protein by binding with integrins from solution. (21–23) Later, this peptide sequence, was chemically attached to other larger polymer structures to conjugate to surfaces either through covalent bonding in self-assembled monolayers or through adsorption by surface interactions. (15, 24) Not only the RGD sequence on fibronectin was found to be important, but also the binding affinity helper sequence Pro-His-Ser-Arg-Asn (PHSRN), was also found to further increase cell adhesion when combined on peptides with RGD. The RGD sequence is also found on other adhesive proteins including vitronectin, fibrinogen, osteopontin, and bone sialoprotein as well as some collagens and laminins. (25) Since the discovery of RGD on fibronectin, other sequences and peptide fragments have been found to mimic the ligand ability of other adhesive proteins such as Ile- Lys-Val-Ala-Val (IKVAV), in some laminins. (26, 27) Peptides provide advantages over full protein schemes in that they remove topographical and exogenous factors, can be easily conjugated to polymers to be used on surfaces and polymer matrices, and are well defined. Additionally, in some proteins such as collagen and laminin, the RGD sequence although included in their sequence is not always accessible due to conformation steric hinderance which can depend on the underlying surface hydrophobicity that is known to alter protein conformation through denaturing and exposing hydrophobic protein cores. (28) By using short peptide sequences, there are no steric effects that may cause the ligand sequence to become masked reducing confounding variables in experiments done on different surfaces. Although there are advantages of using short peptide sequences *in vitro*, results have not always been consistent when technologies are transferred *in vivo*. Bellis hypothesizes that the disparity *in vitro* and *in vivo* results, lies in the presentation of the sequence in isolation *in vitro* in terms of relative to other proteins that may attach to the biomaterial in *in vivo* as well as in terms of other parts in the sequence, since not only do flanking sequences such as PHSRN, as mentioned earlier, have an effect on integrin activation, but also integrin specificity. In the first case, the

sequence may be overshadowed by native proteins that can have a 1000 fold higher activity, blocking the interaction of the biomaterial with native cells. In the second case, the peptide sequence may not have enough specificity to interact with target cells. For example, although RGD is present on both fibronectin and vitronectin, the two bind different integrins. Additionally, the shape and flanking amino acids of RGD are known to have an effect on its affinity. The cyclic peptide version of RGD, which has bends before and after the RGD sequence, is known to have a different bioactivity than its linear counterpart. (29, 30)

1.2.3 Micro-contact Printing

Besides the type of the adhesion motif, the shape of cell colonies and also single cells has also been shown to affect differentiation outcomes, phenotype, and gene expression.(31) Micro-contact printing is a method that allows for the control of the adhesive area available to cell colonies as well as single cells and even single focal adhesions in high resolution methods. Simply, microcontact printing is the stamping of adhesion proteins or peptides onto non-adhesion backgrounds, restricting cells to adhesive islands where cells often take on the shape of the island. Soft lithography techniques are used to make patterns of different shapes such as circles, squares, spirals, etc of various sizes from hundreds of micrometers to tens of nanometers. By patterning adhesive islands, researchers can control cell aspect ratio, curvature, and attachment area among other variables. (32, 33) One study showed that by restricting the amount of area available for cell adhesion, human and bovine epithelial cells could be shifted from modes of proliferation to apoptosis.(19) This phenomenon has been duplicated with other cell types in different laboratories and is widely accepted. Studies using micro-contact printing with sub 100 nm high resolution lithography were used to find the threshold area necessary for cells to create stable focal adhesions with the ability to transmit force.(34) Coyer et al found that the ligand area threshold for integrin force transduction was dynamically dependent on talin and vinculin expression, confirming their critical roles in mechanotransduction.(35) Jiang found that controlling the asymmetric shape of a single cell defines its polarity as well as the direction in which it will move.(36) Geometric confinement studies using stem cells have shown that different lineages can be accessed by changing cell shape, although the molecular mechanism is not well understood. Cell shape has been shown to be a differentiation regulator in ESC and induced pluripotent stem cells (iPSC) important for cardiomyocytes, adipocytes, and endothelial cells among others.(32, 37, 38) Micro-contact printing is not the only technique used to geometrically confine cells, but is very common due to its ease of use and adaptability.

1.2.4 Self Assembled Monolayers

In 1946, Zisman published methods for creating well oriented mono-molecular layers on metallic substrates.(39) It wasn't until 1985, that methods were developed

using dilute solutions of long chain alkane-thiols on gold surfaces to create what is today's most widely used method to create self assembled monolayers (SAMs).⁽⁴⁰⁾ This method leverages the ability of gold surfaces to make covalent bonds with monothiolated molecules. Other conjugation schemes have since been discovered such as the reaction of silanes with silicon oxide based surfaces such as glass and PDMS, fatty acids with aluminum oxide or silver oxide, and more. Because of the high affinity of these reactions and the well oriented bond in aliphatic long chain molecules, dense carpets that expose the free functional end group can be created. Many researchers have leveraged the ability to create well defined interfaces to study how proteins and cells interact with different functional groups providing insight into interfacial biological studies.^(28, 41–43) Functional groups of interest vary wildly from simple molecular groups such as carboxylic acids and amines to more complicated, large biomolecules such as enzymes and antibodies. After Allara published the method for creating SAMS on gold, Lopez used the technique to create patterns of adhesive and non-adhesive motifs for cell patterning.⁽⁴⁴⁾ Today, this technique is widely used to create substrates in a standard protein detection protocol, enzyme-linked immunosorbent assay (ELISA).⁽¹⁵⁾ It is also widely used in methods of soft lithography fabrication to create non-stick surfaces for releasing PDMS or other materials from silicon wafers using fluoro-functional silanes.⁽⁴⁵⁾ polyethylene glycol (PEG) SAMs have been well known to reduce fouling and are often used to prevent protein adsorption and cell adhesion *in vitro* as well as *in vivo*.⁽⁴⁶⁾ PEG SAMS are often used in combination with micro-contact printing or stencil patterning techniques as way to create non-fouling backgrounds to increase the fidelity of adhesion patterns and reinforce geometric cell or colony confinement. ⁽⁴³⁾

As with micro-contact printing, the method for creating SAMS is simple and can be used in most biological settings without the need for complicated, expensive equipment. The quality of SAMS is; however, highly dependent on the quality of the underlying surface. Any contaminates or other surface irregularities such as roughness can cause defects in the tightly packed SAM layer. Also, for some conjugation schemes, such as silanes, well controlled humidity and temperature conditions are required for high fidelity patterning. Gold-thiol reactions from aqueous solutions are relatively easy as long as the gold surface is smooth and clean and probably the reason for their widespread adoption.

1.2.5 Topographical Patterning

The main driving motivation to create surfaces with topographical patterning lies in the function the native ECM plays as a physical architecture for cells. The ECM is constantly remodeled and has been shown to undergo drastic changes between healthy and disease states. In order to fully understand the ECM's role in the feedback loops of adhesion, proliferation, and differentiation, model systems are needed to systematically document the effects of changes in ECM topography in addition to biomolecular signaling pathways.

The native ECM is an anisotropic mixture of soluble and insoluble proteins, some with high orders of self assembly. For example, as noted earlier in this chapter, some types of collagen have the ability to organize themselves into fibrils composed of many individual collagen proteins. These fibers and other features of the ECM have nano-scale features that help to direct tissue organization on the microscale level through signaling pathways that are still not fully understood. (47) Cell shape, cytoskeletal organization, and force transduction are thought to be key players in the signaling pathways involved in proliferation, differentiation, and polarity among other cell states.

Laser ablation, lithography, and reactive ion etching, are just a few ways to alter the topography of a substrate. Laser ablation and lithography can create very well defined surfaces while reactive ion etching and plasma spraying; for instance, create surfaces that are defined by average roughnesses or geometries. Both types of surfaces have been used to investigate adhesion and motility of mammalian and bacterial cells with a variety of motivations. Guvendiren and Burdick showed that human mesenchymal stems cells could be more directed toward osteogenic lineages by encouraging cells to take on high aspect ratio shapes in differentially UV-crosslinked wrinkled hydrogel patterns compared to flat hydrogels or hexagonally patterned gels. (48) Hayman showed that post-induced differentiation neurite outgrowth could be significantly increased when seeded on highly porous polystyrene foams. (49) Many studies have reproducibly shown that topographical patterns with high aspect ratios such as grooves or fibers, encourage cardiomyocytes to elongate and function with higher contraction velocities and forces.(50–52) For more examples, Nikkhah provides a detailed review of strategies focused on engineering topographies for cell-substrate studies.(53)

1.2.6 Material Stiffness

Tissues in the body range in elasticity (Young's modulus) from 0.1kPa to 100kPa, many of orders of magnitude smaller than glass (50-90 GPa) or polystyrene (3-3.5 GPa), which are traditional cell culture surfaces. (47) Stiffness has been shown to regulate many mechanotransductive pathways involved in cell spreading, differentiation, and tumor formation. In 1998, Galbraith and Sheetz, wrote a review summarizing the current literature of the time. (54) There were several main theories presented in their opinion that are still widely accepted today. The most important is the mechanism through which most researchers believe substrate elasticity affects cell cytoskeletal organization. The understanding is that cells are only able to exert a force on a material that can in turn balance that force, from a simple physical explanation. In other words, the softer the substrate, the lower the force that can be generated in focal adhesions. If focal adhesions can only generate low tensile forces on the substrate, the internally induced tensile forces in the cytoskeleton will also be low due to an equilibrium force balance, resulting in low activation of pathways that respond to high tensile forces. Therefore, the tensile forces in the cell are proportional to ECM

stiffness. The regulation of these internal forces are dynamically regulated not only by focal adhesion contacts, but also by soluble growth factors; and conversely, changes in internally generated forces can create changes in gene and protein expression, resulting in a dynamic feedback loop. Internal stress fields have been shown to regulate cell viability, motility, signal transduction, nuclear shape and ECM organization or remodeling. (19, 20, 55, 56)

Gels are often used as substrates with tunable elasticity properties. By changing crosslinking density, it is very straightforward to change the gel stiffness. Poly (acrylamide) (PA) has been used in many studies to alter the static stiffness of gels.(56) Engler showed that myotubes optimally differentiate on substrates with "tissue-like" stiffness by using the PA gel protocol developed by Pelham and Wang(57) Gels with higher or lower stiffnesses, were not able to support myotube striation. A few years later, Engler also showed that human mesenchymal stem cell (hMSC) could be directed toward either neurogenic, myogenic, or osteogenic lineages by culture on PA gels with stiffness of 0.1-1 kPa, 8-17 kPa, or 25-40 kPa, respectively.(18) Khoutorsky combined PA gels to mimic a lower range of substrates and also added poly-dimethylsilane (PDMS) elastomers to access a higher stiffness range to a study on human fibroblast polarization. The data from this study showed that focal adhesion morphology was dependent on substrate stiffness and moderated through protein tyrosine kinases (PTKs). The changes in focal adhesion morphology led to changes cell traction force generation and cell polarization.(58) Although PA and PDMS elastomers have been extensively used to study cell response to substrate stiffness, they do not allow for the dynamic tuning of stiffness due to the irreversible nature of the covalent crosslinks. UV-crosslinking strategies present methods to at least mimic stiffening processes that occur in many biological processes such as aging, cardiovascular disease, wound healing, and tumor progression. (59) Guvendiren and Burdick presented a system for stiffening a substrate at different times after cell seeding. As a model, hMSCs were seeded on gels that were stiffened from 1-10 kPa at different time points in bipotential differentiation medium. The data showed that whichever stiffness the cells were cultured on longer determined whether the cells became adipogenic (soft surfaces) or osteogenic (stiffer surfaces).(60) These studies and others demonstrate the important role that substrate stiffness plays in cell phenotype and behavior and the need to understand mechanism that changes occur in order to produce effect materials for tissue culture, tissue regeneration studies and more.

1.2.7 Conclusions

In addition to soluble factors, physical characteristics of the ECM govern cell organization, phenotype, signal transduction, and function. Ligand presentation, chemical functionalization, substrate topography, and substrate stiffness are all properties that can be controlled in cell culture systems to mimic the native ECM or to manipulate cellular properties.

1.3 Dissertation Scope and Outline

The work in this dissertation is focused on using surface modifications in cell culture systems. The work is organized into 3 sections. Chapters 3 and 2 present the work on two different techniques to modify two very different surfaces. Chapter 4 proposes future directions for both projects as well as the potential for surface modifications in cell culture systems.

- **Chapter 2: Nanopit Patterning Effects on Focal Adhesion Formation** Investigation of the effects of laser ablated nano-pit patterning on focal adhesion formation in mouse fibroblasts. We hypothesize by changing the topography of the substrate, cells can be directed to migrate in specific directions. Immunofluorescence staining of focal adhesion components was used to reveal the effects of changes in nanopit patterning pitch (spacing). Observations in increased cell motility were correlated with shifts in focal adhesion size distributions. Finally,transfection experiments were performed to understand inside-out signaling could change focal adhesion formation.
- **Chapter 3: Using a Macrocyclic Polyphenol Coating to Block Absorption in PDMS.** Motivated by the need to reduce lipophilic drug absorption in PDMS based microphysiological systems, the development and characterization of a macrocyclic polyphenol coatings are described. We hypothesized that the ability of polyphenol coatings to improve PDMS wettability will decrease lipophilic drug loss by reducing the affinity of drugs for the PDMS surface. Standard surface characterization techniques, such as contact angle measurements, Scanning electron microscopy (SEM) and X-ray Photospectrometry (XPS) are performed to verify and characterize coating morphology. Absorption assays are developed to assess efficacy of the coating as a barrier to lipophilic drug absorption by measuring effective diffusivity and permeability. Biological characterization is also performed to assess toxicity of the coating using a variety of cell types, metabolic and functional assays. Coatings are also used to improve adhesion of human induced pluripotent stem cell derived cardiomyocytes to PDMS.
- **Chapter 4: Summary and Future Work** Summarizes the main findings from the research reported here and remaining questions for the field to answer.

References

- (1) Sanford J Shattil, Chunggho Kim, and Mark H Ginsberg. “The final steps of integrin activation : the end game”. In: 11 (2010), pp. 288–300.
- (2) “Integrin Structure and Function”. In: *Cell-Extracellular Matrix Interactions in Cancer*. Ed. by Manakan Betsy Srichai and Roy Zent. New York, NY: Springer-Verlag, 2010. Chap. 2, pp. 19–41. ISBN: 9781441908148. DOI: 10.1007/978-1-4419-0814-8.
- (3) Stefan Braam et al. “Recombinant Vitronectin Is a Functionally Defined Substrate That Supports Human Embryonic Stem Cell Self-Renewal via Alpha VBeta 5 Integrin”. In: *Stem Cells* August 2008 (2008). DOI: 10.1634/stemcells.2008-0291.
- (4) Gang Niu. “Why Integrin as a Primary Target for Imaging and Therapy”. In: *Theranostics* (2011), p. 30.
- (5) C. Frantz, K. M. Stewart, and V. M. Weaver. “The extracellular matrix at a glance”. In: *Journal of Cell Science* 123.24 (2010), pp. 4195–4200.
- (6) Pakorn Kanchanawong et al. “Nanoscale architecture of integrin-based cell adhesions.” In: *Nature* 468.7323 (Nov. 2010), pp. 580–4.
- (7) Daniel C Worth and Maddy Parsons. “Advances in imaging cell-matrix adhesions.” In: *J. Cell Sci.* 123.Pt 21 (Nov. 2010), pp. 3629–38.
- (8) Lindsay B. Case et al. “Molecular mechanism of vinculin activation and nanoscale spatial organization in focal adhesions”. In: *Nature Cell Biology* 17.7 (2015), pp. 880–892.
- (9) Ana M. Pasapera et al. “Myosin II activity regulates vinculin recruitment to focal adhesions through FAK-mediated paxillin phosphorylation”. In: *J. Cell Biol.* 188.6 (2010), pp. 877–890.
- (10) J Thomas Parsons, Alan Rick Horwitz, and Martin a Schwartz. “Cell adhesion: integrating cytoskeletal dynamics and cellular tension.” In: *Nature reviews. Molecular cell biology* 11.9 (Sept. 2010), pp. 633–43.
- (11) J. Angelo Green and Kenneth M. Yamada. “Three-dimensional microenvironments modulate fibroblast signaling responses”. In: *Adv. Drug Deliv. Rev.* 59.13 (2007), pp. 1293–1298.

- (12) Daniel A. Fletcher and R. Dyche Mullins. “Cell mechanics and the cytoskeleton”. In: *Nature* 463.7280 (2010), pp. 485–492.
- (13) Magdalena Bezanilla et al. “Cytoskeletal dynamics: A view from the membrane”. In: *J. Cell Biol.* 209.3 (2015), pp. 329–337.
- (14) C Alberti. “Cytoskeleton structure and dynamic behaviour: quick excursus from basic molecular mechanisms to some implications in cancer chemotherapy.” In: *Eur. Rev. Med. Pharmacol. Sci.* 13.1 (2009), pp. 13–21.
- (15) M Mrksich and G M Whitesides. “Using Self-Assembled Monolayers to Understand the Interactions of Man-made Surfaces with Proteins and Cells”. In: *Annu. Rev. Biophys. Biomol. Struct.* 25.1 (1996), pp. 55–78.
- (16) Benoit Ladoux, Alice Nicolas, and Ning Wang. “Review of cellular mechanotransduction”. In: *J. Phys. D Appl. Phys.* 50 (2017).
- (17) Stacey Lee and Sanjay Kumar. “Actomyosin stress fiber mechanosensing in 2D and 3D”. In: *F1000 Res.* 5 (2016), pp. 1–11.
- (18) Adam J Engler et al. “Matrix Elasticity Directs Stem Cell Lineage Specification”. In: *Cell* 126.4 (Aug. 2006), pp. 677–689.
- (19) C. S. Chen et al. “Geometric Control of Cell Life and Death”. In: *Science (80-.)*. 276.5317 (1997), pp. 1425–1428.
- (20) John Y J Shyy and Shu Chien. “Role of integrins in cellular responses to mechanical stress and adhesion”. In: *Curr. Opin. Cell Biol.* 9.5 (1997), pp. 707–713.
- (21) Michael D Pierschbacher and Erkki Ruoslahti. “Cell attachment activity of fibronectin can be duplicated by small synthetic fragments of the molecule”. In: *Nature* 309.5963 (1984), pp. 30–33.
- (22) K. M. Yamada and D. W. Kennedy. “Dualistic nature of adhesive protein function: Fibronectin and its biologically active peptide fragments can autoinhibit fibronectin function”. In: *J. Cell Biol.* 99.1 I (1984), pp. 29–36.
- (23) Stanley E. D’Souza, Mark H. Ginsberg, and Edward F. Plow. “Arginyl-glycyl-aspartic acid (RGD): a cell adhesion motif”. In: *Trends Biochem. Sci.* 16.C (1991), pp. 246–250.
- (24) Ulrich Hersel, Claudia Dahmen, and Horst Kessler. “RGD modified polymers: Biomaterials for stimulated cell adhesion and beyond”. In: *Biomaterials* 24.24 (2003), pp. 4385–4415.
- (25) Susan L Bellis. “Advantages of RGD peptides for directing cell association with biomaterials”. In: *Biomaterials* 32.18 (June 2011), pp. 4205–4210.
- (26) K Tashiro et al. “a Synthetic Peptide Containing the Ikvav Sequence From the α -Chain of Laminin Mediates Cell Attachment, Migration, and Neurite Outgrowth”. In: *J. Biol. Chem.* 264.27 (1989), pp. 16174–16182.

- (27) Xiaowei Li et al. “Short Laminin Peptide for Improved Neural Stem Cell Growth”. In: *Stem Cells Transl. Med.* 3.5 (May 2014), pp. 662–670.
- (28) K L Prime and G M Whitesides. “Self-assembled organic monolayers: model systems for studying adsorption of proteins at surfaces.” In: *Science* 252.5010 (1991), pp. 1164–1167.
- (29) Alireza Rezaia and Kevin E. Healy. “The effect of peptide surface density on mineralization of a matrix deposited by osteogenic cells”. In: *J. Biomed. Mater. Res.* 52.4 (2000), pp. 595–600.
- (30) M Heller et al. “Immobilisation of Linear and Cyclic Rgd-Peptides on Titanium Surfaces and Their Impact on Endothelial Cell Adhesion and Proliferation”. In: 21 (2011), pp. 364–372.
- (31) Zhen Ma et al. “Self-organizing human cardiac microchambers mediated by geometric confinement”. In: *Nat. Commun.* 6 (2015), pp. 1–10.
- (32) Farshid Guilak et al. “Control of Stem Cell Fate by Physical Interactions with the Extracellular Matrix”. In: *Cell Stem Cell* 5.1 (2009), pp. 17–26.
- (33) “Robust cardiomyocyte differentiation from human pluripotent stem cells via temporal modulation of canonical Wnt signaling.” In: *PNAS* 109.27 (July 2012), E1848–57.
- (34) Sean R. Coyer, Andrés J. García, and Emmanuel Delamarche. “Facile preparation of complex protein architectures with sub-100-nm resolution on surfaces”. In: *Angew. Chemie - Int. Ed.* 46.36 (2007), pp. 6837–6840.
- (35) Sean R Coyer et al. “Nanopatterning reveals an ECM area threshold for focal adhesion assembly and force transmission that is regulated by integrin activation and cytoskeleton tension.” In: *J. Cell Sci.* 125.Pt 21 (Nov. 2012), pp. 5110–23.
- (36) X. Jiang et al. “Directing cell migration with asymmetric micropatterns”. In: *Proc. Natl. Acad. Sci.* 102.4 (2005), pp. 975–978. URL: <http://www.pnas.org/cgi/doi/10.1073/pnas.0408954102>.
- (37) Max R Salick et al. “Micropattern width dependent sarcomere development in human ESC-derived cardiomyocytes”. In: *Biomaterials* 35.15 (May 2014), pp. 4454–4464.
- (38) Kristopher a Kilian et al. “Geometric cues for directing the differentiation of mesenchymal stem cells.” In: *Proc. Natl. Acad. Sci. U. S. A.* 107.11 (2010), pp. 4872–7.
- (39) W.C. Bigelow, D.L. Pickett, and W.a. Zisman. “Oleophobic monolayers. Films Adsorbed From Solution In Non-Polar Liquids”. In: *J. Colloid Sci.* 1.6 (1946), pp. 513–538.

- (40) David L Allara and Ralph G Nuzzo. “Spontaneously Organized Molecular Assemblies. 1. Formation, Dynamics, and Physical Properties of”. In: *Langmuir* 1.1 (1985), pp. 45–52.
- (41) Colin D Bain and George M Whitesides. “Correlations between wettability and structure in monolayers of alkanethiols adsorbed on gold”. In: *J. Am. Chem. Soc.* 110.11 (May 1988), pp. 3665–3666.
- (42) Robert G. Chapman et al. “Surveying for surfaces that resist the adsorption of proteins [3]”. In: *J. Am. Chem. Soc.* 122.34 (2000), pp. 8303–8304.
- (43) Emanuele Ostuni et al. “Self-Assembled Monolayers That Resist the Adsorption of Cells”. In: *Langmuir* 17.7 (2001), pp. 6336–6343.
- (44) Gabriel P. Lopez et al. “Convenient methods for patterning the adhesion of mammalian cells to surfaces using self-assembled monolayers of alkanethiolates on gold”. In: *J. Am. Chem. Soc.* 115.13 (1993), pp. 5877–5878.
- (45) Bharat Bhushan, Derek Hansford, and Kang Kug Lee. “Surface modification of silicon and polydimethylsiloxane surfaces with vapor-phase-deposited ultra-thin fluorosilane films for biomedical nanodevices”. In: *J. Vac. Sci. Technol. A Vacuum, Surfaces, Film.* 24.4 (2006), p. 1197.
- (46) Hongbin Zhang and Mu Chiao. “Anti-fouling coatings of poly(dimethylsiloxane) devices for biological and biomedical applications”. In: *J. Med. Biol. Eng.* 35.2 (2015), pp. 143–155.
- (47) Ryan J. Wade and Jason A. Burdick. “Engineering ECM signals into biomaterials”. In: *Mater. Today* 15.10 (2012), pp. 454–459.
- (48) Murat Guvendiren and Jason A. Burdick. “The control of stem cell morphology and differentiation by hydrogel surface wrinkles”. In: *Biomaterials* 25 (2010), pp. 6511–6518.
- (49) M. W. Hayman et al. “Growth of human stem cell-derived neurons on solid three-dimensional polymers”. In: *J. Biochem. Biophys. Methods* 62.3 (2005), pp. 231–240.
- (50) Peng Yuan Wang et al. “Modulation of alignment, elongation and contraction of cardiomyocytes through a combination of nanotopography and rigidity of substrates”. In: *Acta Biomater.* 7.9 (2011), pp. 3285–3293.
- (51) Nomin Erdene Oyunbaatar et al. “Biomechanical characterization of cardiomyocyte using PDMS pillar with microgrooves”. In: *Sensors (Switzerland)* 16.8 (2016), pp. 1–13.
- (52) Xia Liu et al. “3D cardiac cell culture on nanofiber bundle substrates for the investigation of cell morphology and contraction”. In: *Micromachines* 8.5 (2017).
- (53) Mehdi Nikkhah et al. “Engineering microscale topographies to control the cell-substrate interface”. In: *Biomaterials* 33.21 (2012), pp. 5230–5246.

- (54) Catherine G. Galbraith and Michael P. Sheetz. “Forces on adhesive contacts affect cell function”. In: *Curr. Opin. Cell Biol.* 10.5 (1998), pp. 566–571.
- (55) John R Sims, Seth Karp, and Donald E Ingber. “Altering the cellular mechanical force balance results in integrated changes in cell, cytoskeletal and nuclear shape.” In: *J. Cell Sci.* 103 (Pt 4 (1992), pp. 1215–1222.
- (56) R. J. Pelham and Y.-l. Wang. “Cell locomotion and focal adhesions are regulated by substrate flexibility”. In: *Proc. Natl. Acad. Sci.* 94.25 (Dec. 1997), pp. 13661–13665.
- (57) Adam J. Engler et al. “Myotubes differentiate optimally on substrates with tissue-like stiffness: Pathological implications for soft or stiff microenvironments”. In: *J. Cell Biol.* 166.6 (2004), pp. 877–887.
- (58) Masha Prager-Khoutorsky et al. “Fibroblast polarization is a matrix-rigidity-dependent process controlled by focal adhesion mechanosensing”. In: *Nat. Cell Biol.* 13.12 (2011), pp. 1457–65.
- (59) Sujata K. Bhatia. “Engineering biomaterials for regenerative medicine: Novel technologies for clinical applications”. In: *Eng. Biomater. Regen. Med. Nov. Technol. Clin. Appl.* (2012), pp. 1–352.
- (60) Murat Guvendiren and Jason A Burdick. “Stiffening hydrogels to probe short- and long-term cellular responses to dynamic mechanics”. In: *Nat. Commun.* 3 (Apr. 2012), p. 792.

Chapter 2

Nanopit Patterning Effects on Focal Adhesion Formation

2.1 Abstract

Although cell adhesion to nanostructured interfaces has been extensively studied, few studies have focused on tuning nano-topographical surfaces to direct cell migration for cell patterning. Using multi-photon ablation lithography, my collaborators fabricated arrays of nanoscale craters in quartz substrates with a variety of geometries and spacing (i.e. pitch). Changing the nanocrater diameter (600-1000 nm), depth (110-350 nm), or pitch (1-10 μm) alters the planar surface area available for cells to establish stable focal adhesions (FA) and induces migration away from regions of high nanocrater density. This persistent migration can be used to dictate cell patterning (e.g., lines, circles) according to the nanocrater parameters. By using immunofluorescence to visualize focal adhesion size, I was able to conclude that nanocrater features significantly dictated focal adhesion formation, which seems to lead to high turnover of focal adhesions and increased migration. To further investigate interactions of these patterned surfaces and cellular adhesion mechanisms, the effects of intracellular contractile protein Talin activation on patterning was probed. Cells that over express the N-terminus of Talin-1, which is one of the major proteins responsible for stable focal adhesion formation, lack the ability to quickly spread and migrate from low pitch to high pitch regions due to integrin over activation. Future studies to pattern similar nanoscale craters using nanoimprint technology in materials that are more relevant to biomaterial studies such as tissue culture polystyrene and other novel biomaterials should be done. These nanoscale surfaces can serve as tools for mechanobiology studies and further elucidate understanding the attributes of surfaces necessary to physically pattern cells.

2.2 Introduction

Surfaces that manipulate cell adhesion, motility, and differentiation are a large focus of many areas of biomaterials research including tissue regeneration, cell patterning, and bio-compatibility. Various methods have been extensively employed to alter the cell-substrate interaction through modification of surface chemistry, geometry, topography, and mechanical properties. One motivation for manipulating this interaction is to direct motility for cell patterning. Directed migration is involved in many biological processes such as development, wound healing, and tumor metastasis. Understanding all the factors that are involved in mechanotransductive signaling in these processes is essential to creating engineered devices and therapeutics for a variety of applications such as implants, injectable gels, etc. Each implantable device must be engineered with a set of with physical properties including elasticity, surface chemistry, topography, etc that encourage the successful long term operation of the device. A better understanding of how each of these characteristics influences cellular response adds to the engineering tool set that can be used to create more successful devices.

Many techniques have been explored to understand the different ways to direct migration. Chemotaxis involves using chemical gradients to drive cells to migrate along increasing or decreasing concentrations of a particular bioactive chemical substance. Durotaxis is the movement of cells caused by a gradient in the substrate stiffness usually towards stiffer substrates.(1, 2)

This study focuses on a phenomenon of spontaneous cell migration directed by nano-scale topographical features created using direct write multiphoton lithography in quartz substrates. The protocol uses a multi-photon laser beam pulse to ablate pits with diameters as small as a few hundred nanometers up to a micron into the substrate. Figure 2.1 is an SEM micrograph of isometrically (constantly) spaced pits. There are several variables that can be changed to systematically alter the topographical features of the surface. The depth and diameter of the pits can be altered by changing the energy and objective of the laser beam. The spacing of the pits can be changed by altering the code for the automated stage that rasters the sample relative to the beam. The last parameter, planar surface area, is defined by the diameter and pitch of the pits.

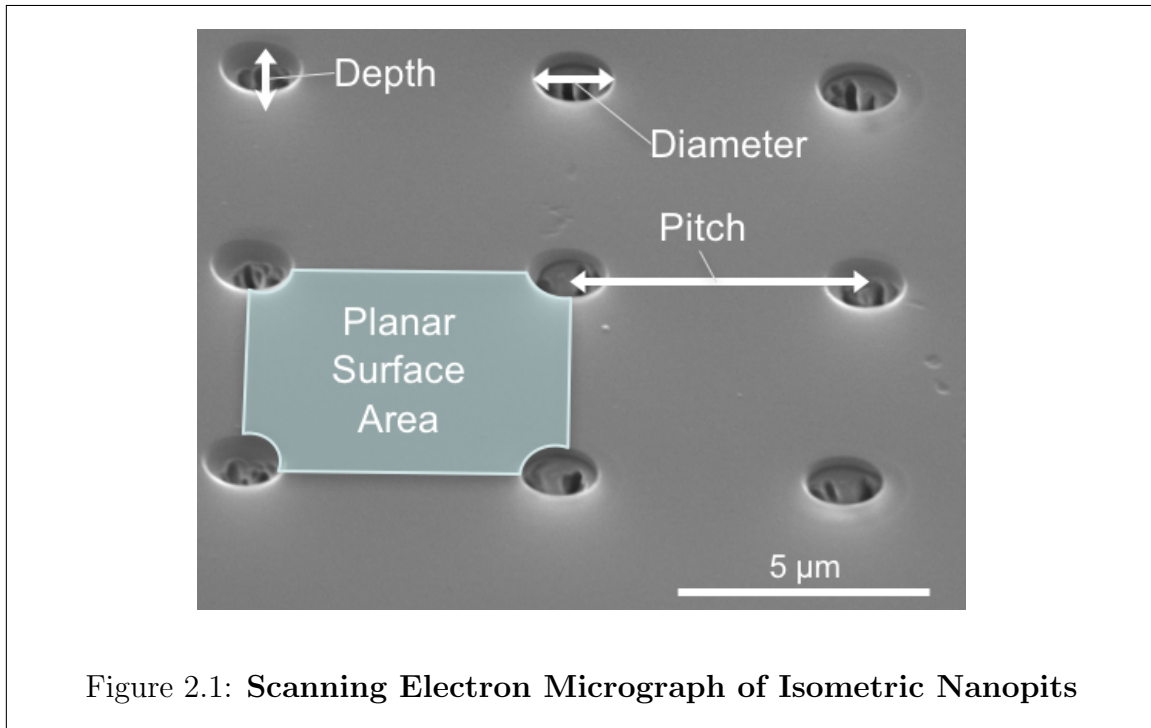
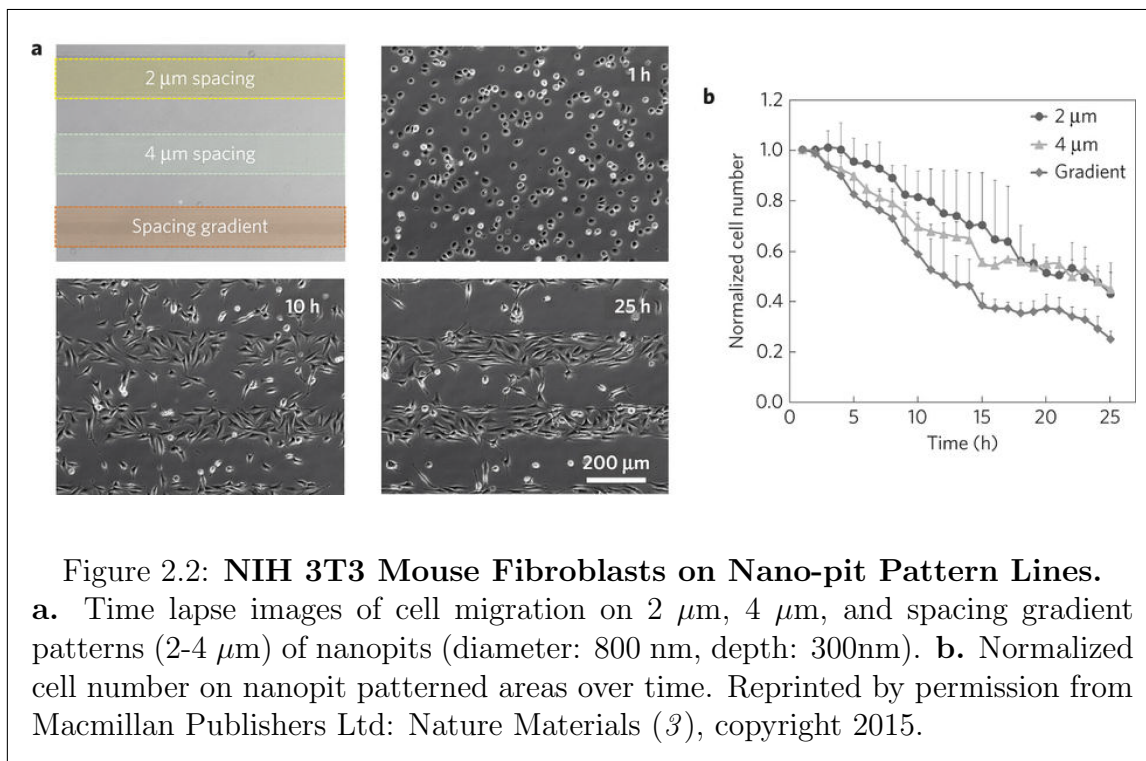
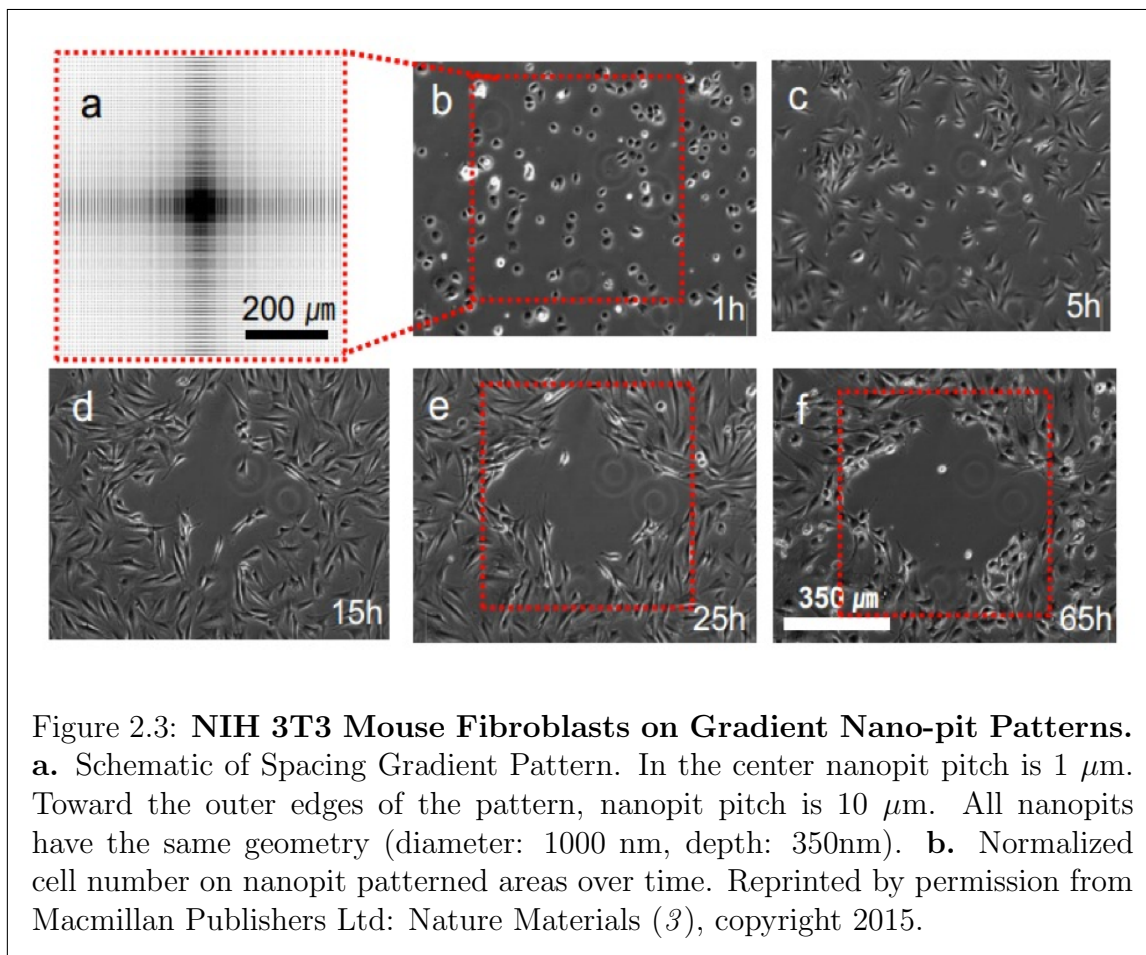


Figure 2.1: **Scanning Electron Micrograph of Isometric Nanopits**

Arrays of nano-sized craters with diameters of 1000 nm and depths of 350 nm were patterned in quartz using direct write multiphoton lithography. The initial study with Jeon began by exploring different diameters, pitches, and depths of the nanoscale craters and found the parameters in this study to be the most effective at promoting directed migration leading to self patterning of mouse fibroblasts (NIH 3T3). In Figure 2.2, Jeon displays the ability of patterns to direct cell migration. Cells were initially seed uniformly over the sample. The cells were able to attach everywhere, but cells attached to ablated regions migrated into planar regions. Visibly noticeable results occur within 10h after cell seeding. Over the course of 25 h, the cell density is reduced by $\sim 57\%$, $\sim 55\%$, and $\sim 75\%$ for $2\ \mu\text{m}$, $4\ \mu\text{m}$, and spacing gradient patterns, respectively.



Jeon then repeated this experiment with a larger gradient pattern. The schematic for the pattern is shown in Figure 2.3. The pattern possesses 4 fold rotational symmetry with the pitch varying in 2 dimensions. In the center, the lowest pitch patterns are 2 μm . In the corners of the pattern, the pitch is 10 μm . For example, down the vertical center line of the pattern the pitch in the horizontal plane is kept at 2 μm , while in the vertical direction the pitch increases as you move toward the edge of the pattern from the center to 10 μm along the vertical center line. The planar surface area gradient is highest in the direction from the center of the pattern at a 45 degree angle toward any of the corners. In these patterns, Jeon observed cells migrating away from areas of high density nanopits, but finding some sort of threshold defined by the planar surface area available (see Figure ??). In order to better understand the mechanotransductive mechanism responsible for the cell migration phenomenon, I explored the influence of the nano-pit features on FA size distribution and integrin activation.



First using isometric patterns, I explored the effects of the distance (i.e. pitch) between the pits in the pattern ($2 - 10 \mu\text{m}$). These experiments elucidated the complex interaction of cells and nano-pit topography. Next, we correlated motility properties of the cells with focal adhesion distributions on the gradient pattern to better understand the dynamics involved in the directed migration. Finally, I used over expression of the cytoplasmic focal adhesion protein, talin-1, to mimic and understand the role of integrin activation. The ability to pattern regular structures on the order of the FA size ($1 - 10 \mu\text{m}$) distinguishes these surfaces from other topographically patterned substrates by more closely mimicking the natural dimensions of the extracellular matrix topography in a systematic way.

2.3 Materials and Methods

2.3.1 Laser Ablation of Glass

Quartz glass coverslips were ablating using a Ti:sapphire regeneration amplifier system (Spectra-physics). The amplified laser beam was rastered over the sample using a user designed computer automated system under ambient conditions. The laser exposure had a 100 fs pulse length with full-width at half-maximum (FWHM) at a wavelength of 400 nm was obtained through frequency-doubling a fundamental 800 nm wavelength laser beam using a nonlinear crystal. Full methods developed by Jeon are described in (3).

2.3.2 Immunofluorescence

Samples were fixed 1 h and 12 h post seeding with 4% paraformaldehyde (Santa Cruz Biotech) for 15 min. Cell were permeabilized using 0.2% Triton X (Sigma) in dPBS. Blocking and fixation were performed with a solution of 2% bovine serum albumin (Sigma), 0.3 M glycine (Sigma), 0.2% Tween-20 (Sigma) in dPBS for at least 30 min. Samples were incubated with a primary mouse-anti-vinculin antibody (1:200) (Sigma) overnight at 4° C and then washed. Anti-mouse 633 secondary (1:100; molecular probes) and Actistain-555 (1:500; Cytoskeleton) were incubated for 1.5 h at room temperature and then washed. The nucleus was stained with DAPI (Molecular Probes) for 5 min and washed. Samples were inverted onto coverslips just before imaging. Images were acquired using the Zeiss 710 Axio-Observer with a 40 oil immersion objective. For immunofluorescence imaging of fibroblast cells on TCPS ablation patterns, a 40 water immersion objective was used.

2.3.3 Focal Adhesion Size Quantification

Vinculin fluorescent images were analyzed using ImageJ to measure focal-adhesion size. Vinculin is a focal-adhesion protein recruited slightly after initiation of focal-adhesion formation. First, background fluorescence was removed by subtracting background with a 4-pixel rolling ball radius. Only cells completely on patterns at the time of fixation were used for measurements. ImageJ built-in particle size analysis function was used to acquire the distribution of FA sizes in entire cells. At least 10 cells were analyzed for each pitch and also in different regions on gradient patterns. KruskalWallis tests were performed using Graphpad Prism.

2.3.4 Transfection of Talin-1

Overexpression of the first 405-amino-acid sequence of the globular N terminus of Talin-1 was accomplished using the Lonza Nucleofector 2B. GFP/Talin-1(1-405) plasmids obtained from Andreas Garcia's laboratory (Georgia Tech) included the entire

FERM domain and were shown to over-activate the $\alpha_5\beta_1$ and $\alpha_5\beta_3$ integrins in transfected cells. (4) For each transfection, approximately 10 million cells were suspended in 100 μl of Nucleofector 2 Solution R with 8 μg of plasmid and then transfected using program U-030. Immediately after transfection, 500 μl of DMEM (ATCC) supplemented with 10% fetal calf serum (ATCC) was added to the cell solution. The sample was then incubated at 37 C for 15 min. Cells were gently transferred into culture flasks and seeded at 90% confluency in normal growth medium. After 24 h, transfected cells were sorted using flow cytometry for Green Fluorescent Protein (GFP) fluorescence. Cells were seeded on patterned samples 48 h after transfection.

2.3.5 Motility & Directionality Measurements

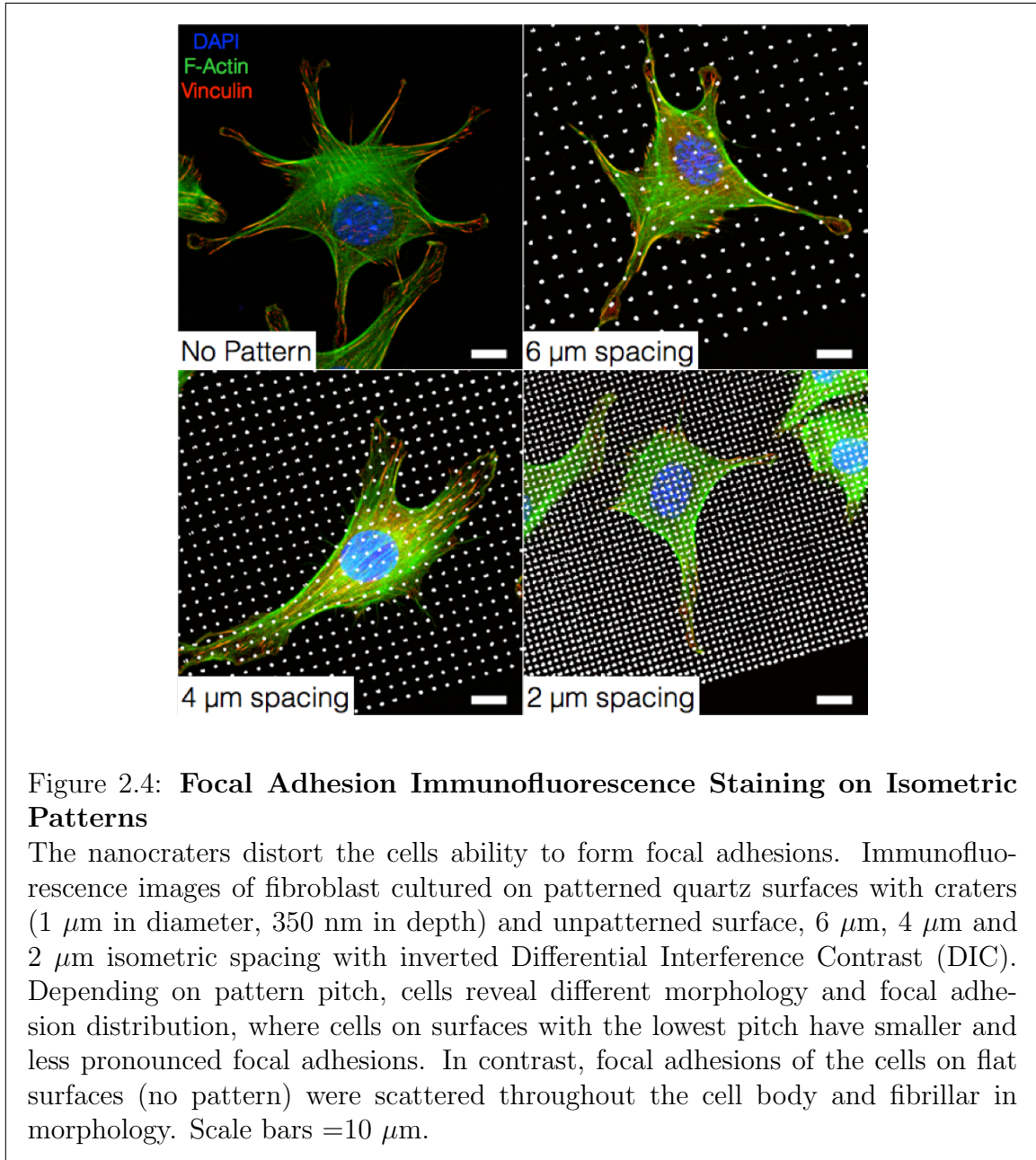
Motility and directionality measurement methods were developed by Koo and are fully described in (3).

2.4 Results and Discussion

2.4.1 Nanoscale Craters Reduce Focal Adhesion Size.

Previous studies showed that focal adhesion size (or area) is closely correlated ($r=0.93$) with cell migration speed, which dictates the ability cells to migrate into patterns.(5) Coyer also demonstrated that a threshold area is needed to form stable FAs, which are present in non-motile cells. (4). To investigate if FA size distribution could provide insight into the mechanism of cell patterning in the phenomenon seen by Jeon, cells were plated on isometric patterned surfaces with pitches of 2, 4, 6, and 8 μm . Focal adhesions were visualized using immunofluorescent staining of vinculin, an intercellular adhesion protein, to locate and measure FA area. Vinculin was chosen as a target because it is recruited dynamically unlike Talin, which is present in even nascent adhesions (see Figure 1.4). In Figure 2.4, cells are shown on different isometric patterns. On planar, unaltered quartz, cells exhibit the ability to form long stable FA with large areas throughout the cell body. As the pitch size decreases to 2 μm , the focal adhesion size decreases and is more localized to the leading and trailing edges on the planar areas between nanopits. It is visually hard to see the change in FA size distribution, since there are still large focal adhesions present even on the 2 μm pitch patterns. Using ImageJ, particle analysis tools were used to measure the area of each individual FA in an entire cell. Distribution of FA size are shown in Figure 2.5. The 8 and 6 μm pitch patterns, failed to alter the FA size distribution significantly. The 4 and 2 μm patterns reduced the FA size distribution mean by $41\% \pm 0.07\%$ and $28\% \pm 0.08\%$, respectively.

The data suggest that in order for cells to form stable, fibrillar adhesions a critical surface area is needed. Supported by the time lapse images taken by Jeon, the lower isometric pitch patterns inhibit large adhesions, which are present in more



nonmigratory cells. We propose that the mechanism is a statistically based one. Nascent adhesions turn over quickly within seconds. Rapid turnover allows the cells to create new adhesions on new areas of the substrate. If the new area the cell attaches to does not restrict the maturity of the adhesion, the adhesion is allowed to mature and becomes more stable, keeping the cell attached to the area longer. By inhibiting large focal adhesion formation by planar surface area restriction, the nanopits promote migration by reducing the average FA size within a cell.

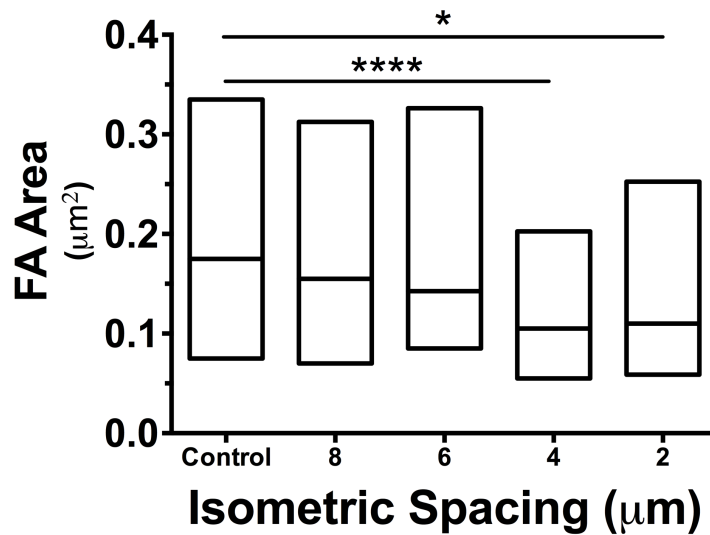


Figure 2.5: Focal Adhesion Size Distributions on Isometric Patterns
 Images acquired using immunofluorescence staining (see Figure 2.4) of Vinculin were analyzed to compare focal adhesion size distribution. Isometric patterns of 8 and 6 μm pitch were unable to significantly reduce the focal adhesion area distribution. 4 and 2 μm pitch patterns reduced focal adhesion mean area size by $41\% \pm 0.07\%$ and $28\% \pm 0.08\%$, respectively. 4 μm pitch patterns reduced focal adhesion size the most significantly with $**p \leq 0.0001$. For 2 μm pitch patterns, $*p \leq 0.05$.

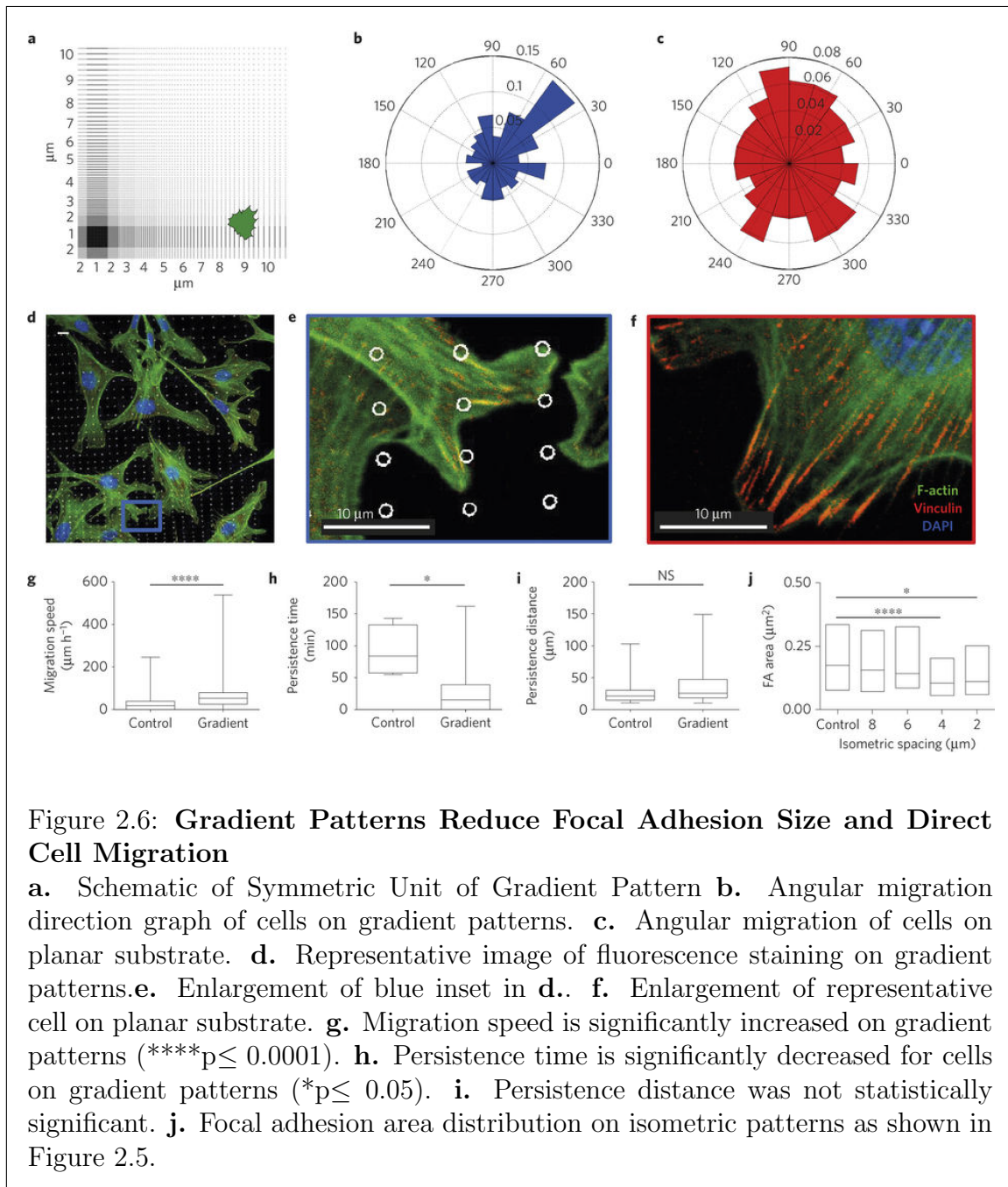
2.4.2 Directed Migration in Gradient Patterns

Our next aim was to understand and manipulate the mechanism that allows the nanopits to direct migration using pattern designs. In our hypothesis for the mechanism that promotes adhesion we lay great significance on the restriction of focal adhesion area and the stochastic nature of focal adhesion turnover. In the gradient patterns that Jeon designed, planar surface area increases fastest along the 45 degree angle from the center of the pattern to the corner, which is why we believe that cells are able to remain attached to regions closer to the center of the pattern along this direction compared to the direction along the horizontal or vertical directions from the center. This would explain the diamond like shape of the cell repellent area in the gradient pattern (see Figure 2.3).

Using the same methods to visualize focal adhesion size, immunofluorescent images were acquired of cells on gradient patterns and compared to images of cells on planar surfaces. Even without image analysis, focal adhesion size is noticeably smaller in the cell repellent regions toward the center of the pattern compared to focal adhesions on planar regions of the sample or FAs on areas of the pattern with larger planar surface area available. Figure 2.6 **e** and **f** show representative images taken from gradient patterns and planar substrates, respectively.

To better understand how FA size correlated with motility coefficients, four calculations or measurements were made and modeled by Koo from migration tracking data.⁽³⁾ Koo found the migration of cells also occurred preferentially along the 45 degree angle direction from the center of the pattern to the corners. This direction was the fastest route to larger planar surface area regions that did not inhibit large focal adhesion formation. On planar regions, cells had no directional preference for migration. Angular migration maps are shown in Figure 2.6 **b.** and **c.** Migration speed was increased from an average of 29 μm per hour to 65 μm per hour confirming the hypothesis that by limiting planar surface area available for focal adhesion maturity, cells are predisposed to migrate because they are only able to form nascent adhesion with high turnover rates. The persistence time is defined as the average time between changes in cell migration direction. For cells on planar substrates, the mean persistence time was calculated to be 91 ± 20 and for cells on gradient patterns, the mean time was 27 ± 10 , significantly lower ($p \leq 0.05$). Again, the data here suggest that the model is stochastic and still largely controlled by the random movements of the cell. The cells on the gradient pattern have a higher propensity to make new focal adhesions, but where these focal adhesions are allowed to mature is controlled by the planar area of the substrate; therefore, the cell is allowed to probe the substrate without limitation, but only forms stable adhesions when enough planar surface area is available. The persistence distance is defined as the length a cell moves in a relatively consistent direction (only lengths larger than 10 μm , changes in direction $\leq 30^\circ$). The persistence distance was not significantly different between the two groups, $27 \pm 3\mu\text{m}$ and $37 \pm 3\mu\text{m}$ for the control and gradient, respectively.

The motility data and the FA size distribution data (reproduced in **Figure 2.6j**)



confirm that focal adhesion size and migration speed are highly correlated, as suggested by others.⁽⁵⁾ The data also demonstrate the ability to create gradient patterns that leverage the stochastic nature of cell adhesion processes to produce cell guiding surface properties through topographical modifications.

2.4.3 Talin-1 Integrin Activation

Talin is a focal adhesion protein that has been shown to regulate extracellular integrin binding during cell adhesion, migration, and assembly.(6, 7) Talin binds to the cytoplasmic tail of the β integrin and F-actin. It is one of many proteins indicated in the mechanotransduction pathway as force transducers.

The first 405 N-terminal amino acids of Talin-1 are sufficient to activate both the $\alpha_5\beta_1$ and $\alpha_5\beta_3$ integrins.(8) Cells that over express Talin-1(405) are capable of forming mature focal adhesions with smaller adhesive pads area compared to wild type cells through the increased integrin affinity caused by increased inside-out signaling. The increased cytoplasmic activation of integrins enables sufficient integrin clustering needed for adhesion with lower available surface area.(4)

To test if integrin activation could promote the focal adhesion maturation and stabilization process disrupted by patterned nanopits, cells were transfected with DNA plasmids encoded with GFP/Talin-1(405). Focal adhesion maturity was quantified by the focal adhesion size, which uniquely predicts cell motility, as discussed by Kim and Wertz.(5)

Figure ?? shows wild-type (WT) cells and cells transfected with talin-1 (Talin+) on planar and 4 μ m pitch patterns. With no nanotopographical patterning, Talin overexpressing (Talin+) cells were able to form larger adhesions in the center of the cell body than wild type cells. On 4 μ m pitch patterns, which showed the greatest ability to reduce focal adhesion size in wild type cells, Talin+ cells are still able to make large focal adhesions. Talin-1 overexpressing cells were able to overcome the planar surface area limitation on nanopatterned surfaces and formed large, mature focal adhesions with lengths $\sim 10\mu$ m throughout the cell body.

Time lapse imaging in Figure ?? cells on the gradient pattern were unable to migrate away from low pitch pattern regions as seen in wild type cells. Figure ?? also shows the focal adhesion size distributions on planar, 2 and 4 μ m pitch patterns. Talin+ cells on all topographies formed much larger focal adhesion and the nanopits were unable to significantly alter the mean size of these distributions. The data suggest that integrin activation led to less turnover of focal adhesions and resulted in less migration. Cells retain their ability to adhere to the surface, but cannot turnover focal adhesions and form new ones, a necessary step of migration. These results support other studies in the conclusion that Talin activation of integrins enables cells to overcome area limitations to form larger focal adhesions. In the context of this study, this experiment shows that integrin activation is involved and somehow by the nanopatterned pits.

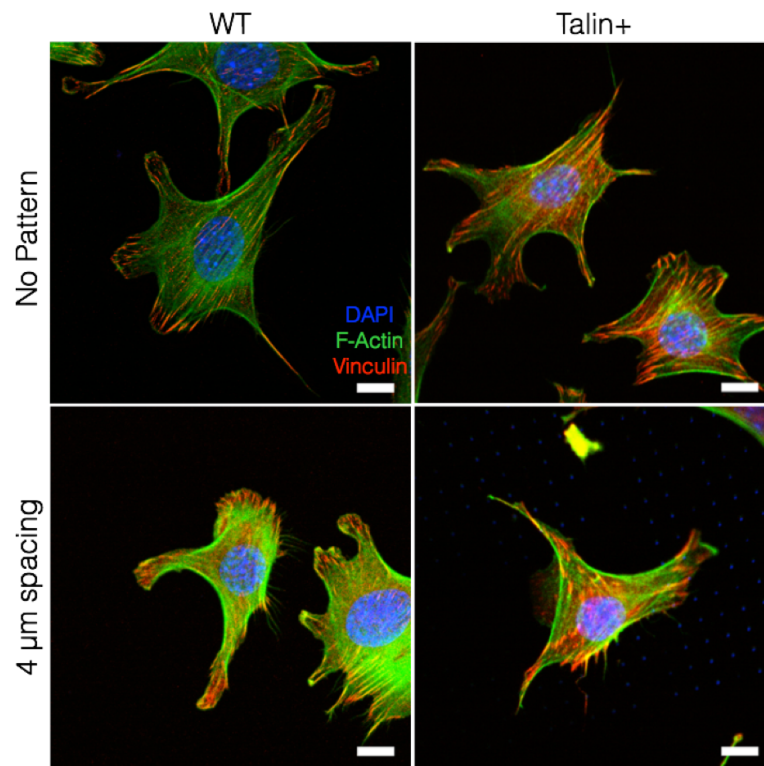


Figure 2.7: Talin-1(405) Transfected NIH3T3 Fibroblasts on Isometric Patterns

Talin+ cells have been transfected to overexpress the first 405 amino acids of the Talin protein. Compared to wild type (WT) cells, Talin+ cells have more focal adhesions throughout the cell body, which are revealed by vinculin immunofluorescent staining. On isometric 4 μm patterns, Talin+ retain their ability to form large adhesions throughout the cell body unlike wild type cells. Scale bars =10 μm .

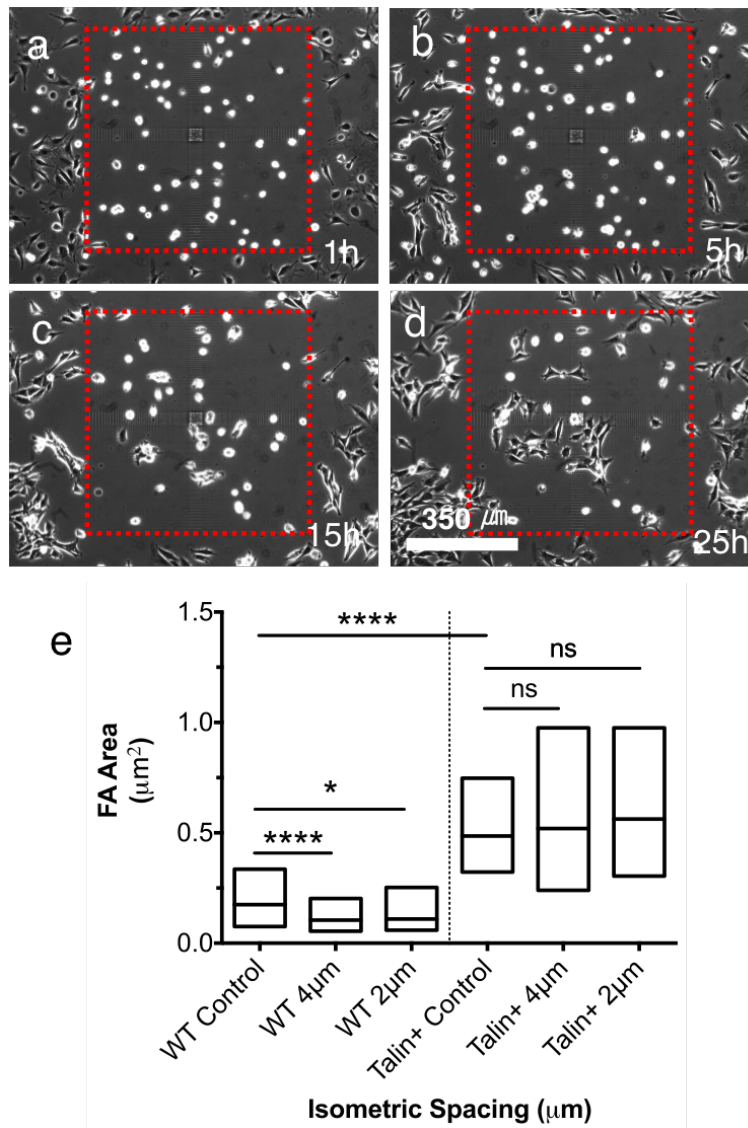


Figure 2.8: Migration and Focal Adhesion Size Distribution of Talin+ NIH3T3 Fibroblasts on Nanopatterns

a-d Time lapse images of Talin-1(405) over expressing fibroblasts (Talin+) on gradient patterns. Cells that attach in the first hour fail to migrate away from high density gradient regions. **e** Talin+ cells have much larger mean size of focal adhesions, quantified by area, than WT cells. Although, nanopatterning reduces focal adhesion size significantly for wild type cells, Talin+ focal adhesion size is not significantly affected. Scale bars =350 μm .

2.5 Future Direction and Conclusions

Our nano-patterned surfaces go beyond solely altering cell adhesion motifs, the prominent approach for cell patterning, and instead guide cell migration by disrupting mature FA formation. Certain combinations of diameter, depth, and pitch promote cell migration, which can be exploited to pattern cells into lines, circles, or other structures. This method could have great promise if used to pattern cells on relevant biomaterials. In this study, Koo and Jeon showed an extension of this method on tissue culture polystyrene. Other materials of interest might include implantable materials such as poly(urethanes), poly(dimethylsilane), or titanium. Patterning cells *in vivo* can be leveraged to reduce scarring or fibrous tissue encapsulation.

References

- (1) C M Lo et al. “Cell movement is guided by the rigidity of the substrate.” In: *Biophys. J.* 79.1 (2000), pp. 144–152.
- (2) R. J. Pelham and Y.-l. Wang. “Cell locomotion and focal adhesions are regulated by substrate flexibility”. In: *Proc. Natl. Acad. Sci.* 94.25 (Dec. 1997), pp. 13661–13665.
- (3) Hojeong Jeon et al. “Directing cell migration and organization via nanocrater-patterned cell-repellent interfaces”. In: *Nat. Mater.* 14.August (2015).
- (4) Sean R Coyer et al. “Nanopatterning reveals an ECM area threshold for focal adhesion assembly and force transmission that is regulated by integrin activation and cytoskeleton tension.” In: *J. Cell Sci.* 125.Pt 21 (Nov. 2012), pp. 5110–23.
- (5) Dong-Hwee Kim and Denis Wirtz. “Focal adhesion size uniquely predicts cell migration.” In: *FASEB J.* 27 (2013), pp. 1351–61.
- (6) Seiji Tadokoro et al. “Talin binding to integrin beta tails: a final common step in integrin activation.” In: *Science* 302 (2003), pp. 103–106.
- (7) Sanford J Shattil, Chungho Kim, and Mark H Ginsberg. “The final steps of integrin activation : the end game”. In: 11 (2010), pp. 288–300.
- (8) Mohamed Bouaouina, Yatish Lad, and David a Calderwood. “The N-terminal domains of talin cooperate with the phosphotyrosine binding-like domain to activate beta1 and beta3 integrins.” In: *J. Biol. Chem.* 283.10 (Mar. 2008), pp. 6118–25.

Chapter 3

Using a Macrocyclic Polyphenol Coating to Block Absorption in PDMS-based Microfluidic Systems

3.1 Abstract

There are many virtues of PDMS including ease of making a device, optical transparency, and high oxygen permeability. These qualities contribute to its widespread use in early MPS applications. One concern is that conventional PDMS as a substrate for microfluidic devices may result in significant absorption of over 90% of lipophilic compounds in unpredictable ways. The partition coefficient, partition coefficient (P) (specifically, Log of the partition coefficient (Log P)) of a drug can be used as a rough guide to predict absorption behavior. For drugs with $\text{Log P} \geq 2.4$, 90% absorption of the analyte into PDMS is expected. This chapter describes the development of a novel macrocyclic polyphenol coating that minimizes the absorption of small molecules.

In this work, we discovered a polyphenol coating precursor to prevent hydrophobic drug absorption into PDMS. Our coatings reduce the absorption of Rhodamine B ($\text{Log P}=2.4$) and $C_1\text{Bodipy}C_{12}$ into PDMS by 90% over a 3h period and remained stable for 24h in media conditions. This polyphenol, Macrocyclic PolyPhenol 5 Cone Isomer (MPP 5_{cone}), outperforms other solutions to drug absorption in terms of ease of use, associated costs, and universal applicability with absolutely no decrease in oxygen permeability or acute toxicity, which preserves the long-term cell culture amenability of PDMS. Compared to human induced pluripotent stem cell-derived cardiomyocytes (hiPSC-CMs) seeded on native PDMS, hiPSC-CMs beat the same or better on MPP 5_{cone} coated PDMS and exhibit similar metabolism in an alamar blue assay.

Surface modification of PDMS is notoriously challenging and often involves complex multi-step methods that produce inconsistent results even in experienced hands. Furthermore, translation of coating technologies from one material platform to another is often not possible due to highly specific chemical reactions on surfaces. To

address these challenges, we exploited the strong solidliquid interfacial activity of polyphenols to create coatings that act as physical barriers to prevent drug absorption in PDMS. Deposition of polyphenol coatings occurs by autooxidation of the phenolic precursor occurs in aqueous alkaline buffer making it easily translated into microfluidic systems. SEM, XPS, and contact angle were used to characterize the homogeneity, roughness and thickness of the polyphenol coating. Using a diffusion model with fluorescent dyes as drug surrogates, the effective diffusivity of the dyes was measured as well as an estimate of the amount absorbed by area under the curve analysis of confocal z-stack images after dye incubation. Using a Franz cell diffusion apparatus, we further quantified the barrier properties of the MPP 5_{cone} coating using Rhodamine B ($\log P = 2.74$) as a fluorescent drug surrogate to provide quick insight into coating performance and to compare effective diffusivity measurements. The coating was found to reduce absorption of a variety of drug surrogate molecules with $\log P$'s from 0.85 to 7.12, although not all molecules in this range were blocked. However, because this method is facile, simple, and inexpensive; thus, it has the potential to be a complete solution to the drug absorption problem in PDMS for some molecules.

3.2 Introduction to Microphysiological Systems

Drug development is an painstaking process with an estimated price tag of \$2.6 billion for a single compound.(1) Nearly 40% of drugs that make it to pre-clinical trials fail, and 89% of drugs that make it to clinical trials fail resulting in a great loss of resources and time. New models and methods are needed to increase the predictive power of in vitro testing to reduce the number of false positive and false negative candidates. MPS can be used to combine genetically relevant cell lines in micro-environments that recapitulate not only organ specific structure, but also organ system relationships to access not only on target, but also off-target toxicities and efficacies.

3.3 PDMS Advantages and Challenges in Microphysiological Systems

Most MPSs are easily manufactured using well known lithography techniques.(2) Briefly, photoresist is spin coated onto a silicon wafer, a mask is used to expose specific features to ultraviolet (UV) radiation to crosslink the photoresist. Next, the wafer is developed. Developing is the process when the un-crosslinked photoresist is removed with a solvent. PDMS is poured over the wafer to create a negative of the features. The features can be custom designed to hold cells in chambers with inlet and outlets for media perfusion using design software for the previously mentioned mask. PDMS has many characteristics that make it the most popular candidate for producing devices. PDMS is easily cross-linked by mixing a silicone base with a cross-linker and heating in an oven for a few hours. After crosslinking, the PDMS has been shown to be biologically compatible and amenable to many standard cell culture techniques due to its transparency, oxygen permeability, and low auto-fluorescence. Devices can be produced inexpensively with highly precise reproducible structures.

Although PDMS has several positive attributes, many have shown that due to its hydrophobicity, molecules that are also hydrophobic absorb into the PDMS.(3, 4) Specifically, Wang has found that molecules with a Log P value above 2.47 will partition into the PDMS to produce unpredictable concentrations in cell and media channels making it impossible to predict the actual dosing concentrations for drug investigations in MPS. This unpredictability is an obstacle for using MPS devices as screens for drug candidates in discovery stages.

3.4 Current Strategies for Reducing Small Molecule Absorption in PDMS

Many have attempted to develop methods to solve the problem of absorption and swelling of PDMS in the presence of hydrophobic molecules and solvents.

One group of methods involves using other less absorbent materials. Glass microfluidic devices completely eliminate absorption while remaining biocompatible, but require expensive fabrication techniques and instrumentation. Glass microfluidic devices also lack the gas permeability needed for microfluidic cell culture, and cannot incorporate flexible structures or surfaces for force-related experiments. One solution presented by Domansky replaces PDMS with casted poly(urethane) elastomers.(5) Although, this elastomer shows many of the positive characteristics of PDMS, the castable polyurethanes explored cannot be easily released from silicon-SU-8 master wafers and therefore require additional steps in molding, including a PDMS molding step, significantly increasing costs. Additionally, the gas permeability needed for long term culture has not yet been investigated as the primary structure of polyurethanes significantly influences oxygen permeability.(6)

Other solutions focus on developing barrier coatings for PDMS surfaces to prevent small molecule absorption. Silica sol-gel coatings were developed and showed great efficacy in preventing absorption of hydrophobic dyes, but the sol-gel coating effectively creates a glassy impermeable gas barrier making devices incompatible with long term cell culture.(7-9) Additionally, the precursors, usually silanes such as methyltriethoxysilane (MTES), present severe health and safety hazards and are costly. Parylene coatings were also used to prevent the absorption of hydrophobic fluorescent dyes, but again these coatings create a virtually impermeable barrier to gases needed for cell culture and require expensive equipment and complicated deposition processes.(10)

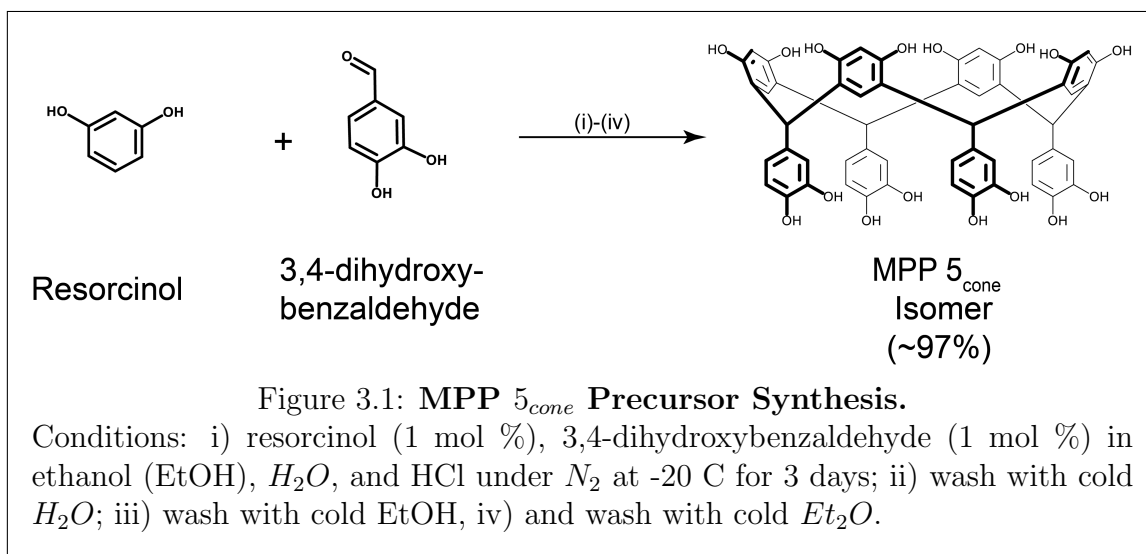
Although these approaches and others present solutions for decreasing absorbance of molecules into PDMS, they do not allow for long term cell culture conditions needed in microphysiological systems that are able to support cells for up to a month and also these solutions significantly increase costs.(11)

Other surface modification methods such as self-assembled monolayers and functionalized silanes have also been used, but again can only be employed on a small subset of substrates with great costs or complex processes that even in the best hands may not produce reliable barriers.(7) The ideal solution preserves the low cost of current PDMS-based microfluidic devices, can be employed through a facile, universally applicable protocol, is biocompatible and gas permeable.

3.5 Materials and Methods

3.5.1 MPP 5_{cone} Precursor Synthesis

Ethanol, de-ionized (DI) water, and 37% hydrochloric acid (HCl) (3:1:1) were stirred and cooled in an ice bath. Resorcinol and 3,4-dihydroxybenzaldehyde, 21.7 mmol each, were dissolved in the cooled solvent solution and sparged with nitrogen gas for 15 minutes. The flask was then sealed and the reaction mixture was stirred at -20 C for 3 days (see **Figure 3.1**). The reacted mixture was centrifuged (3500g, 10



min, -5 C) and the red supernatant was decanted. The precipitate was resuspended in 20 mL of cold DI water and centrifuged again. This purification process was repeated with ethanol and diethyl ether. The residue was then dried under vacuum.

3.5.2 High Pressure Liquid Chromatography

High Pressure Liquid Chromatography (HPLC) was performed on an Agilent HPLC system equipped with a C18 column and a UV detector. The solvents were HPLC-grade acetonitrile and DI water with 0.1% trifluoroacetic acid. MPP 5_{cone} was dissolved at 0.1 mgmL⁻¹ in water and acetonitrile (95:5). 20 μL were injected into the column, and MPP 5_{cone} eluted after 5 minutes of water and acetonitrile flow (95:5). The UV absorbance at 223 nm was detected.

3.5.3 Nuclear Magnetic Resonance

The Nuclear Magnetic Resonance (NMR)(¹H) spectrum of MPP 5_{cone} was recorded on a Bruker AVB-400 with Dimethylsulfoxide (DMSO) as the solvent and tetramethylsilane as an internal standard.

3.5.4 Poly-dimethyl Silane (PDMS) Sample Fabrication

Poly-dimethyl silane elastomer and curing agent (Sylgard 184) were mixed 10:1 by weight, then degassed for at least 30 minutes under vacuum. *Planar Samples Fabrication* | PDMS mixture was poured in an acrylic mold onto an unpatterned tridecafluoro-1,1,2,2-tetrahydrooctyl) trichlorosilanized (Gelest) silicon wafer. Upon demolding, PDMS pucks of 8mm diameter were created using a biopsy punch to make planar samples. Planar samples were cleaned by 10 minutes of sonication in

0.12 M HCl and 2-propanol, rinsed 3 times with Millipore filtered water and dried with nitrogen gas. *Microfluidic Channels Fabrication* | Wafers with patterned SU-8 channels were made using standard lithography techniques. Channels were cut to size and punched with inlet and outlets and cleaned with adhesive tape (Scotch) and bonded to glass slides using oxygen plasma (120 W, 60s). Channels were cleaned by pumping a solution of 0.12 M HCl and 2-propanol at $10 \mu\text{L}$ per min for 1 hour, then infused with Millipore filtered water for 1 hour at $10\mu\text{L}$ per min. *Membrane Fabrication* | Silanized blank silicon wafers were spin coated with PDMS mixture at 250 rpm for 11 s then ramped to 500 rpm for 31 s and cured for 2 hours at 90 C, then cleaned similar to planar samples.

3.5.5 MPP 5_{cone} Coating Procedure

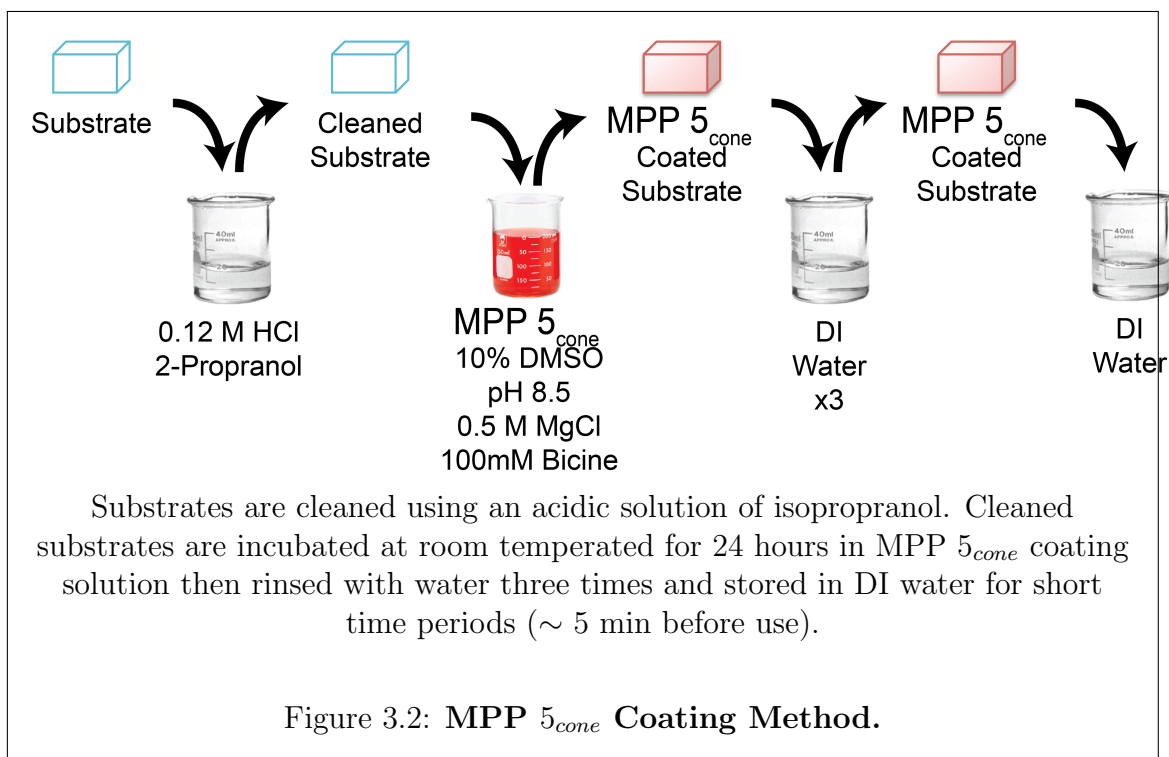
MPP 5_{cone} was first added to DMSO to make a 1% w/v solution and vortexed. The DMSO solution of MPP 5_{cone} was then diluted 1:9 in coating buffer solution (0.55 M MgCl, 0.11 M Bicine, pH 8.5) to make the final coating solution. The pH was immediately re-adjusted to 8.5 using NaOH. Membranes and planar samples were cleaned, then immersed in the coating solution and placed on an orbital shaker at 40 rpm at room temperature for 24 hours unless otherwise noted (see **Figure 3.2**). Samples were then rinsed with Millipore water and dried using nitrogen gas. Channels were infused with coating solution loaded into 1 mL syringes (Polypropylene, BD) and infused at $10 \mu\text{L min}^{-1}$ for 10 minutes and then $2 \mu\text{L hr}^{-1}$ for 24 hours, and then infused with Millipore water for 1 hour at a rate of $10\mu\text{L min}^{-1}$.

3.5.6 Contact Angle Measurements

Rame-Hart DropImage analysis software and hardware setup were used to obtain contact angle measurements with automated drop volume control module and video analysis.

3.5.7 Fluorescent Dye Absorption and Effective Diffusivity Assay

Planar samples of PDMS were then placed in separate baths of $100 \mu\text{M}$ dye solutions for 3 hours, removed, dried, and placed on glass coverslips. A 10x objective was used to acquire confocal z-stacks (Zeiss 710 Axio-Observer) The absorbance profile was then acquired using ImageJ software to plot Z-axis orthogonal profiles of image stacks. Graphpad Prism software was used to integrate the area under the Z-axis intensity profiles as one method of comparison. Computational models were fitted using Mathematica Non-linear model fit function to estimate values of effective diffusivity (D_{eff}), as another method of comparison. This methods was repeated on acquired samples of 3D printed acrylate as a gift from the lab of Teresa Woodruff and



nylon. Nylon samples were incubated in 100 μM Rhodamine B for 24 hours before imaging.

3.5.8 Small Molecule Permeation Assay

Membrane thickness was measured using a digital thickness gage (Mitutoyo 4.7 Throat). Unjacketed glass 15 mm Franz cells with 3 mL receptor volumes (PermeGear, Inc) were mounted with PDMS membranes. Receptor volumes were loaded with 10% DMSO by volume in PBS. 100 μM molecule solutions in PBS were loaded into donor compartment and capped with a rubber stop. All receptor compartments were stirred at the same speed. 200 μL aliquots from the receptor compartment were taken at noted time intervals. Liquid chromatography mass spectrometry (LC/MS) was used to quantify amount of drug at the drug's highest absorption wavelength.

3.5.9 Oxygen Permeation Assays

MOCON, inc performed oxygen flux measurements using ASTM F1927 standard with the modification of using the OxTran 210 sensor in order to reach higher oxygen flux readings. Samples were masked down to 5cm^2 .

3.5.10 hiPSC-derived Cardiomyocyte Beat Rate Analysis Assay

PDMS surfaces were prepared by pouring PDMS mixture into tissue culture polystyrene 12 wells and cured for 2 hours at 90 C. The plates were sterilized by 30 minutes of UV exposure. iPSC-derived cardiomyocytes produced using a robust directed differentiation method developed by Lian et al and optimized by Mathur et al were seeded at a density of 3×10^5 cells per cm^2 in RPMI +B27+ Y-27632 on PDMS surfaces coated with and without MPP 5_{cone} coating (N=6). (11, 12) After 24 hours, media was removed and cells were treated with the same media without Y-27632. Media was changed every 2 days over the 28 day study with video analysis occurring immediately before media changes. Video-based motion tracking software developed by Huebsch and Loskill was used to acquire beat rates for quantitative analysis.(13)

3.5.11 hiPSC-derived Cardiomyocyte Cell Viability Assay

Standard 96 well plates were coated or not coated with MPP 5_{cone} per the protocol mentioned previously. Matrigel was then coated on all wells for 1 hour at 37 C. hiPSC-CMs were then plated at a density of 3×10^5 cells per cm^2 in RPMI +B27+ Y-27632. After 24 hours, the media was changed to RPMI + B27. Cells were then cultured for 7 days with fresh media changes every 2 days. An Alamar Blue assay was performed on day 7 by changing the media to 200 μ L of DMEM+B27 with 20% Alamar Blue reagent (Thermofisher). Cells were incubated (37 C, 5% CO_2) for 3 hrs. The supernatant was then transferred to black well plates and read on Molecular Devices plate reader with fluorescence (540/585nm). Culture plates were then washed with PBS 1x, aspirated, and frozen at -20 C for 2 hrs. The plate was then thawed and standard CyQuant© protocol was followed using fluorescence (508/527nm) read on plate reader (Molecular Devices). The Alamar Blue data was then normalized by the relative Cyquant© fluorescence to get activity per cell.

3.5.12 Human Mesenchymal Stem Cell-derived White Adipose Tissue MPS Viability Assay

White adipose cells were loaded into WAT MPS developed by Loskill et al.(14) After 4 days, the cell chamber was infused with calcein AM and ethidium homodimer-1 in maintenance media to label live and dead cells, respectively. Fluorescent images were acquired using standard fluorescence microscopy.

3.5.13 Scanning Electron Microscopy

Planar samples were coated with a 80 nm gold conducting layer to reduce charging. SEM images were taken on FEI Quanta 3D FEG FIB/SEM.

3.5.14 X-ray Photoelectron Spectroscopy

XPS was performed using a Perkin Elmer PHI 5600 instrument. The X-ray source employed was a monochromatic Al $K\alpha$ (1486.6 eV) source operated at 100 W and 10^{-10} mbar.

3.6 Results and Discussion

3.6.1 Polyphenols Increase Hydrophilicity of PDMS

Polyphenols have been known to increase the hydrophilicity of PDMS for biological applications.^(15–18) Increasing wettability reduces the affinity for hydrophobic molecules to absorb into PDMS. To begin this study, a screen of polyphenol precursors was done to find the most effective polyphenol at increasing PDMS hydrophilicity through contact angle measurements.

Pyrogallol (PG), polydopamine (PDA), macrocyclic polyphenol (MPP) arenes, and Lignin (LG) among other precursors were explored. The MPP 5_{cone} coating decreased the sessile contact angle of PDMS from $\sim 102 \pm 2^\circ$ to $\sim 46 \pm 3^\circ$, lower than PG, LG, and PDA, $75 \pm 2^\circ$, $56 \pm 3^\circ$, and $50 \pm 2^\circ$, respectively. Monofunctional thiolated polyethylene glycol (SH-mPEG, 2kDa) was used to further functionalize the PG coating, decreasing the contact angle to $45 \pm 7^\circ$. This functionalization scheme comes at a great cost since thiolated PEGs are quite expensive compared to single component polyphenol coatings. Contact angle results are shown in Figure 3.4.

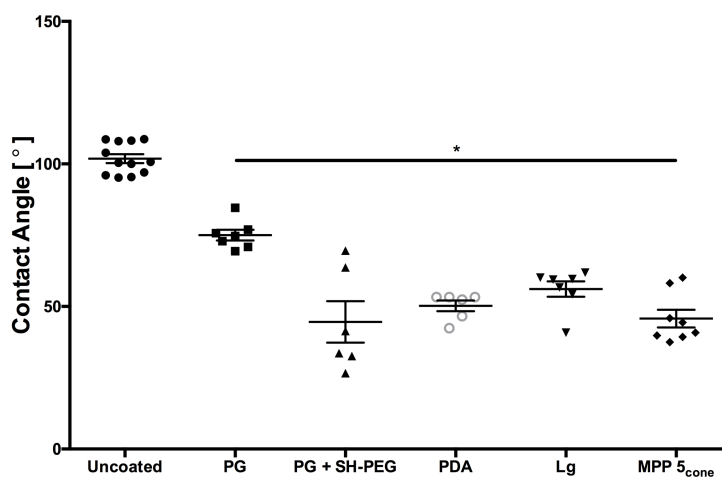
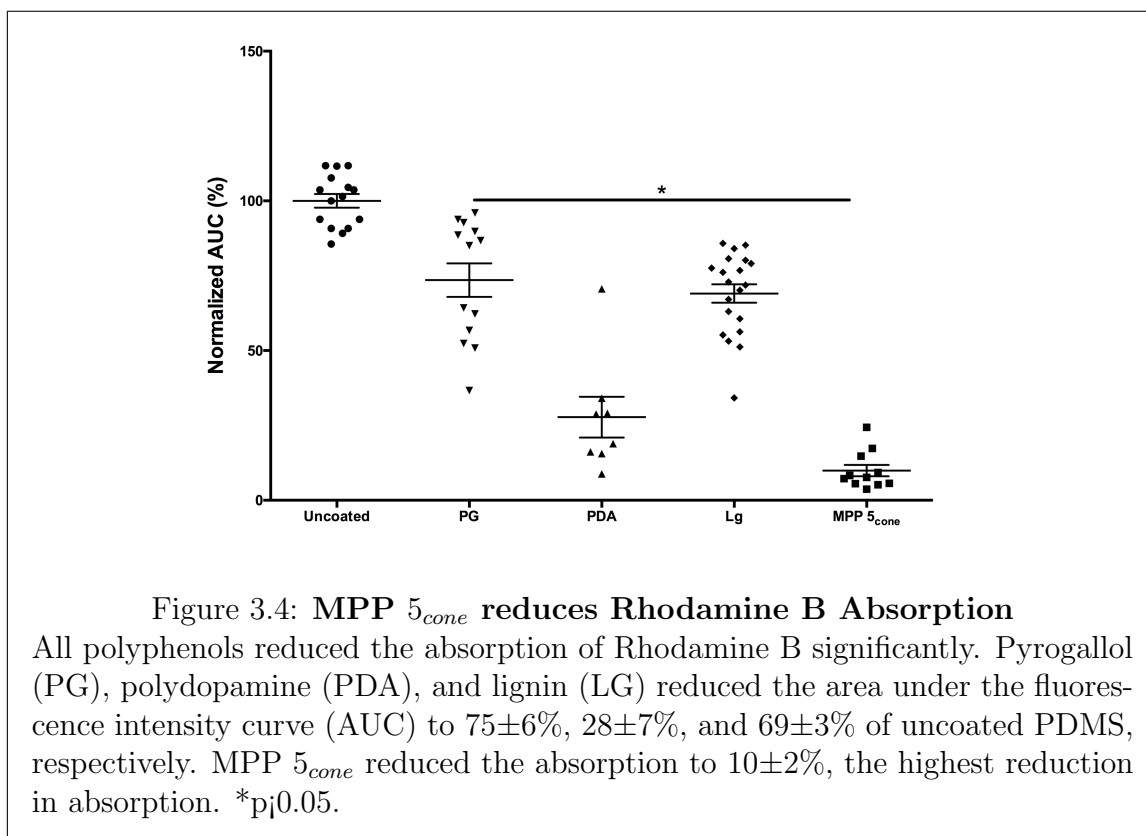


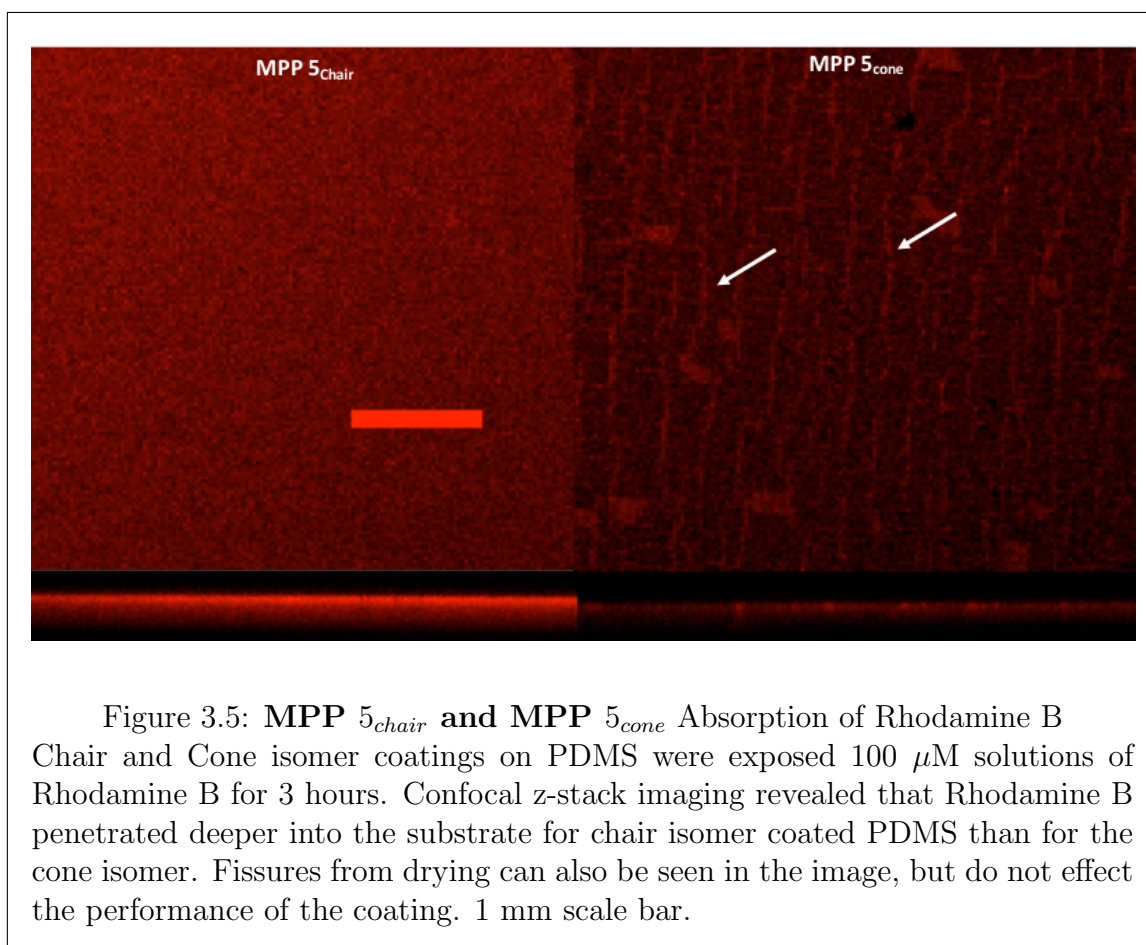
Figure 3.3: Polyphenol coatings increase hydrophilicity of PDMS
 Sessile contact angle measurements show a significant decrease in wetting angle for all polyphenol coatings. (PG - Pyrogallol, SH-PEG - monofunctional thiolated polyethylene glycol (2kDa), PDA - polydopamine, Lg - Lignin, MPP 5_{cone} - macrocyclic polyphenol 5 cone isomer). * $p < 0.05$.

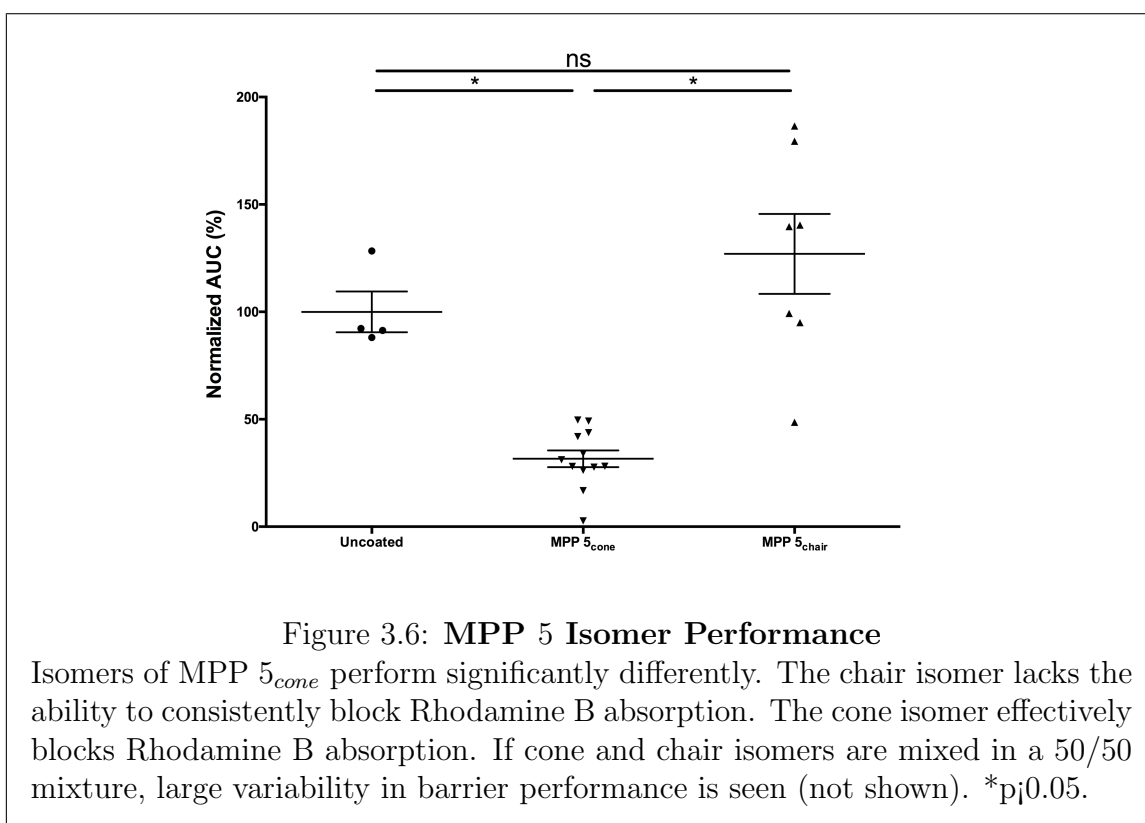
3.6.2 Reduction of Small Molecule Absorption

In order to access the barrier performance of PDMS treatments, Rhodamine B is often used as a drug surrogate to track absorption through fluorescent microscopy.^(3, 5, 10) After 3 hour incubations with 100 μ M Rhodamine B, confocal Z-stack images through the surface of PDMS blocks were used to produce intensity versus depth profiles and integrated to compare D_{eff} measurements. The AUC can be used as a proxy for the total amount absorbed since dye intensity is proportional to dye concentration for the range of concentrations used in this study. MPP 5_{cone} -coated PDMS showed significantly lower AUC compared to other polyphenol coatings, confirming MPP 5_{cone} as the most effective precursor of the testing group. Specifically the AUC analysis of the Rhodamine B intensity profiles showed that MPP 5_{cone} reduced the absorption of Rhodamine B by $90 \pm 2\%$, compared to $72 \pm 7\%$, $26 \pm 6\%$ and $31 \pm 3\%$ for PDA, PG, and LG, respectively.



In the development of the MPP 5_{cone} molecule, another isomer of MPP 5 was also produced under previously published reaction conditions. MPP 5_{chair} , was also tested for barrier capability, but showed a diminished ability to block Rhodamine B absorption compared to MPP 5_{cone} , despite its ability to also form a stable coating (see Figure 3.6). (19, 20). In Figure 3.5, both isomer coatings were exposed to 100 μ M Rhodamine B solution. The chair isomer failed to reduce the absorption of Rhodamine B as well as the chair isomer. The reason for this might be linked to our observation that the monomers in the cone isomer might form more complex conjugated systems measured by absorption (see Figure 3.7. Hence, the coating that is created from the cone isomer is more densely cross-linked than chair confirmation, resulting in a more effective barrier to small molecule absorption. The mechanism of most polyphenol polymerizations are not fully elucidated and for the purpose of this study was not necessary to understand for the application of barrier effectiveness. Instead, optimization of the reaction shown in Figure 3.1 was done to produce a higher amount of the cone isomer. As the cone isomer is less favorable energetically the temperature of the reaction was lowered to -20 C. At this temperature, the resulting product is 97% cone isomer, verified by NMR and HPLC.





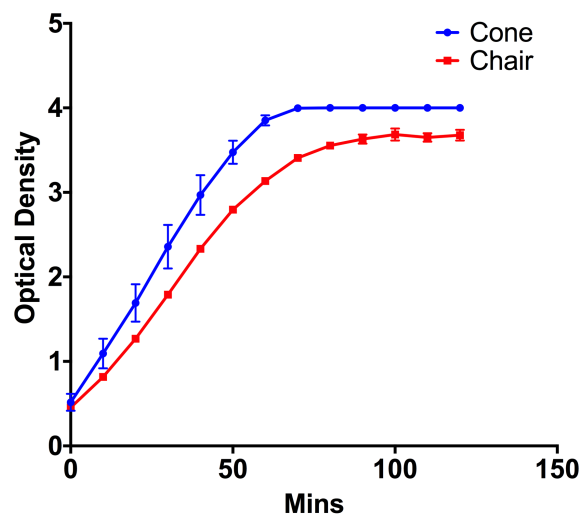
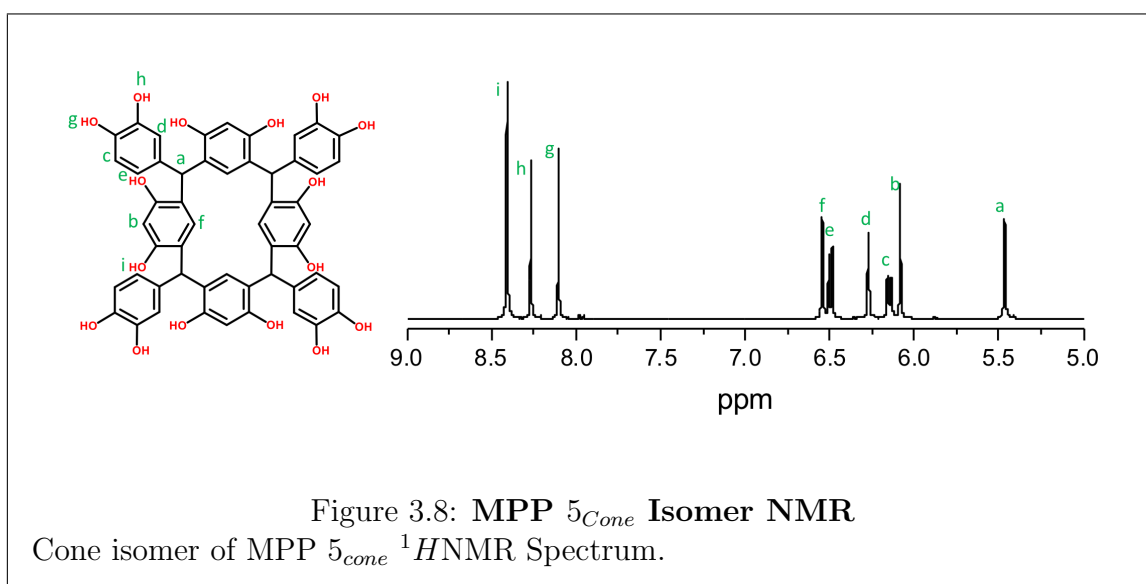


Figure 3.7: Optical Density during MPP 5 Isomer Polymerization

As polymerization of the MPP 5 monomer progresses, the optical density increases due to the increase in conjugated rings present in the polymer. The cone isomer reaches a significantly higher optical density, possibly due to higher system conjugation due to less steric hindrance in the monomer. Measurements were taken at 550 nm, $n=8$).



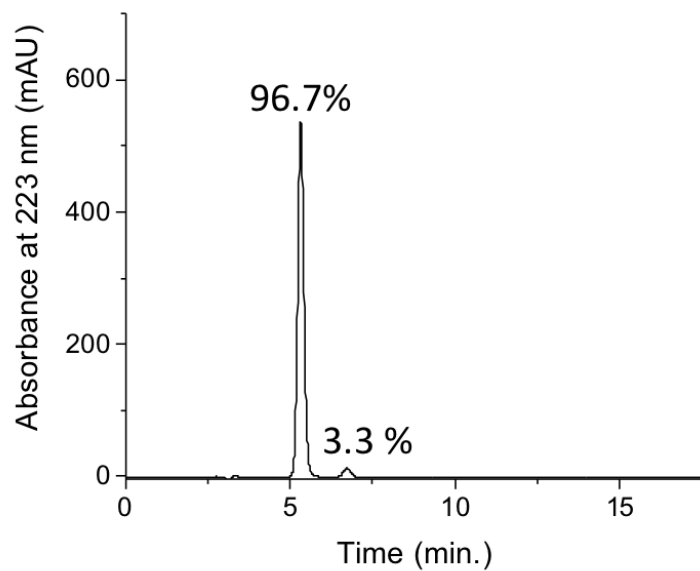
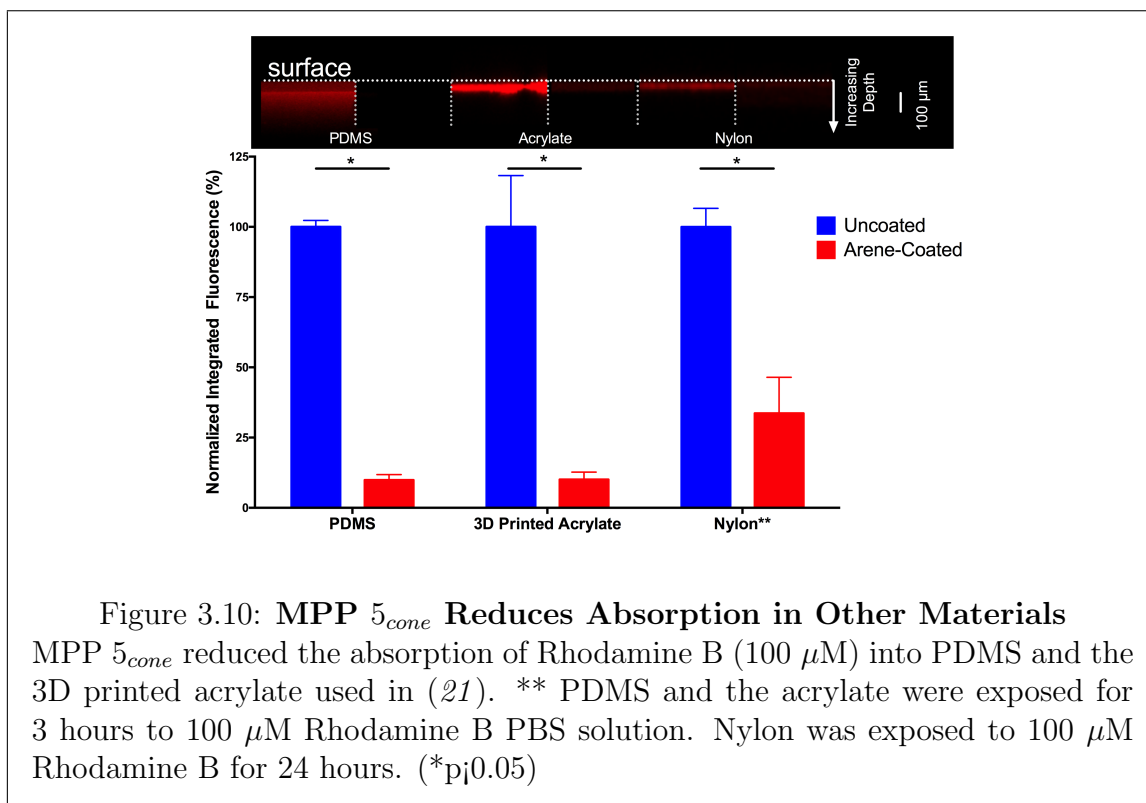


Figure 3.9: **HPLC of MPP 5_{cone} Precursor**
HPLC Spectrum of MPP 5_{cone} . Solvent gradient began with 95% water to 100% acetonitrile in 5 minutes.

Microphysiological system designs sometimes incorporate other materials such as membranes made from a variety of polymers. Additionally, devices are often connected to external pumps with Tygon tubing and polystyrene connectors. These materials also absorb small molecules, although to a lesser extent than PDMS. For example, the mini reproductive organ system from Xiao and Woodruff uses a 3D printed acrylate (21). Researchers in this lab noticed a loss of estradiol (Log P=3.5) during drug testing. The MPP 5_{cone} coating on the acrylate in that study showed similar ability to decrease absorption of Rhodamine B as shown in Figure 3.10. Nylon was also investigated. Although it does not readily absorb Rhodamine B as in PDMS and the acrylate, after 24 hours of exposure to 100 μM Rhodamine B solution, it also showed some absorption, which was also significantly decreased on samples coated with MPP 5_{cone} . The coating also showed to be stable on a variety of polymers shown in Figure 3.13. Other polymers were incubated in Rhodamine B to compare absorption but many of the harder polymers such as polystyrene, showed no detectable absorption even after 24 hours of exposure so it would not be necessary to coat these materials to block absorption. However, there may be other reasons to coat these materials covered in Chapter 4.



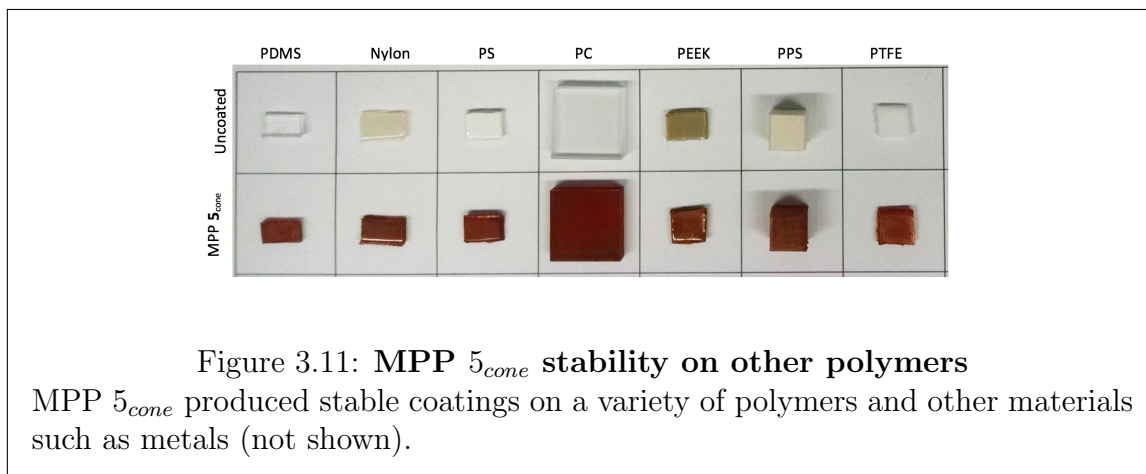


Figure 3.11: **MPP 5_{cone} stability on other polymers**

MPP 5_{cone} produced stable coatings on a variety of polymers and other materials such as metals (not shown).

3.6.3 MPP 5_{cone} Coating Characterization

The roughness and the thickness of the coating increase with incubation time, starting with a thin, smooth coating within a few hours. After 24 hours in a 1 mgmL^{-1} coating solution, the surface is rougher, covered with micron sized polyp structures visible with scanning electron microscopy, and is 400 nm thick (Figure 3.12). High resolution x-ray photoelectron spectroscopy (HR-XPS) (Figure 3.14) reveals a shift in the O1s peak due to the HO-aromatic bond on the MPP 5_{cone} structure. We hypothesize that the coating is not able to swell as much as the PDMS, and possibly more brittle, resulting in a cracked structure when dried (see Figure 3.15). Without cracking, it would be expected that the Si2p peak would be completely masked by a coating of this thickness. On other stiffer surfaces, such as titanium oxide (TiO₂), no formation of fissures occurs upon drying. However, we note that the barrier efficacy of the coating was not decreased due to fissure formation upon drying. In Figure 3.5, the fissure are visible through the Rhodamine B staining. There is slight penetration of the molecule in the cracks, but there still seems to be an underlying layer that blocks the Rhodamine B from penetrating to the extent it does in uncoated or MPP 5_{chair} coated PDMS.

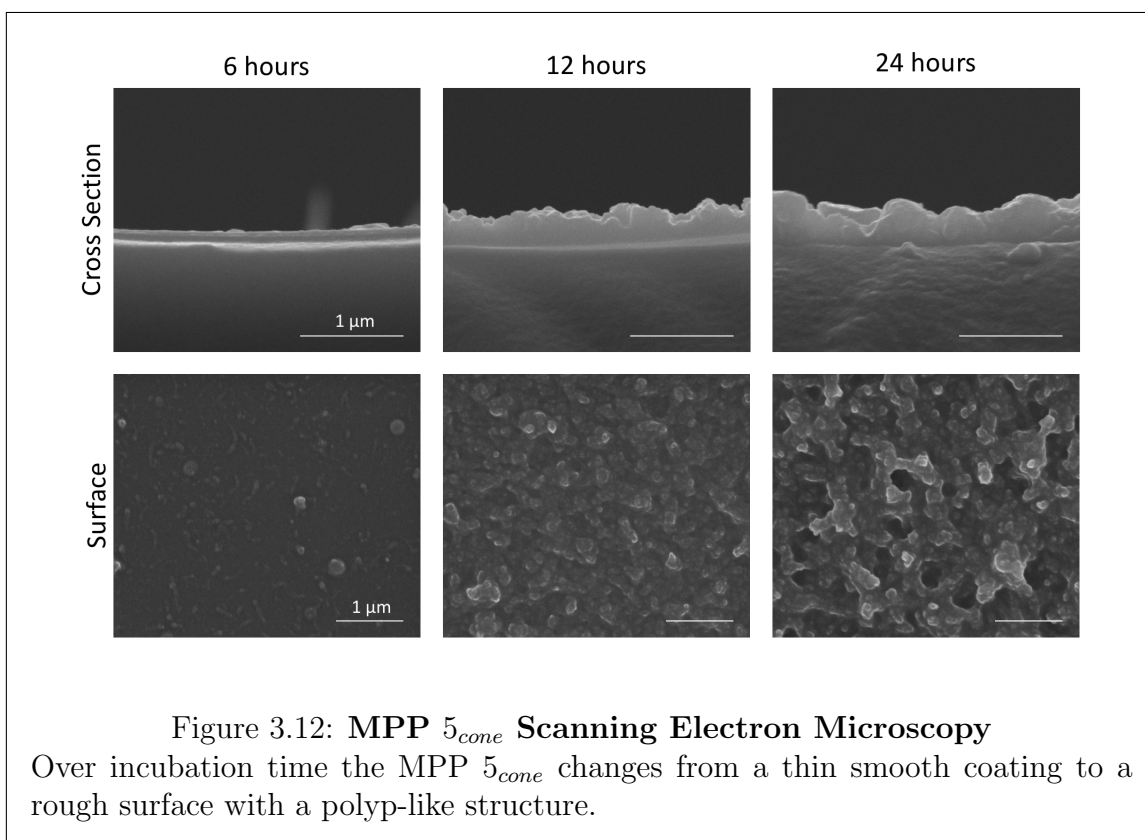


Figure 3.12: **MPP 5_{cone} Scanning Electron Microscopy**

Over incubation time the MPP 5_{cone} changes from a thin smooth coating to a rough surface with a polyp-like structure.

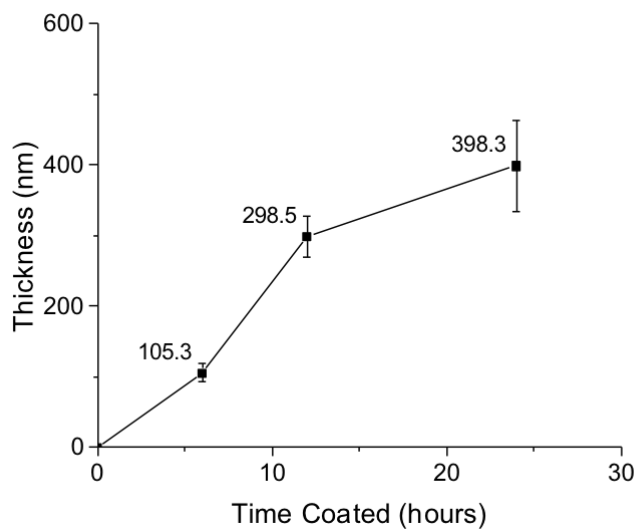
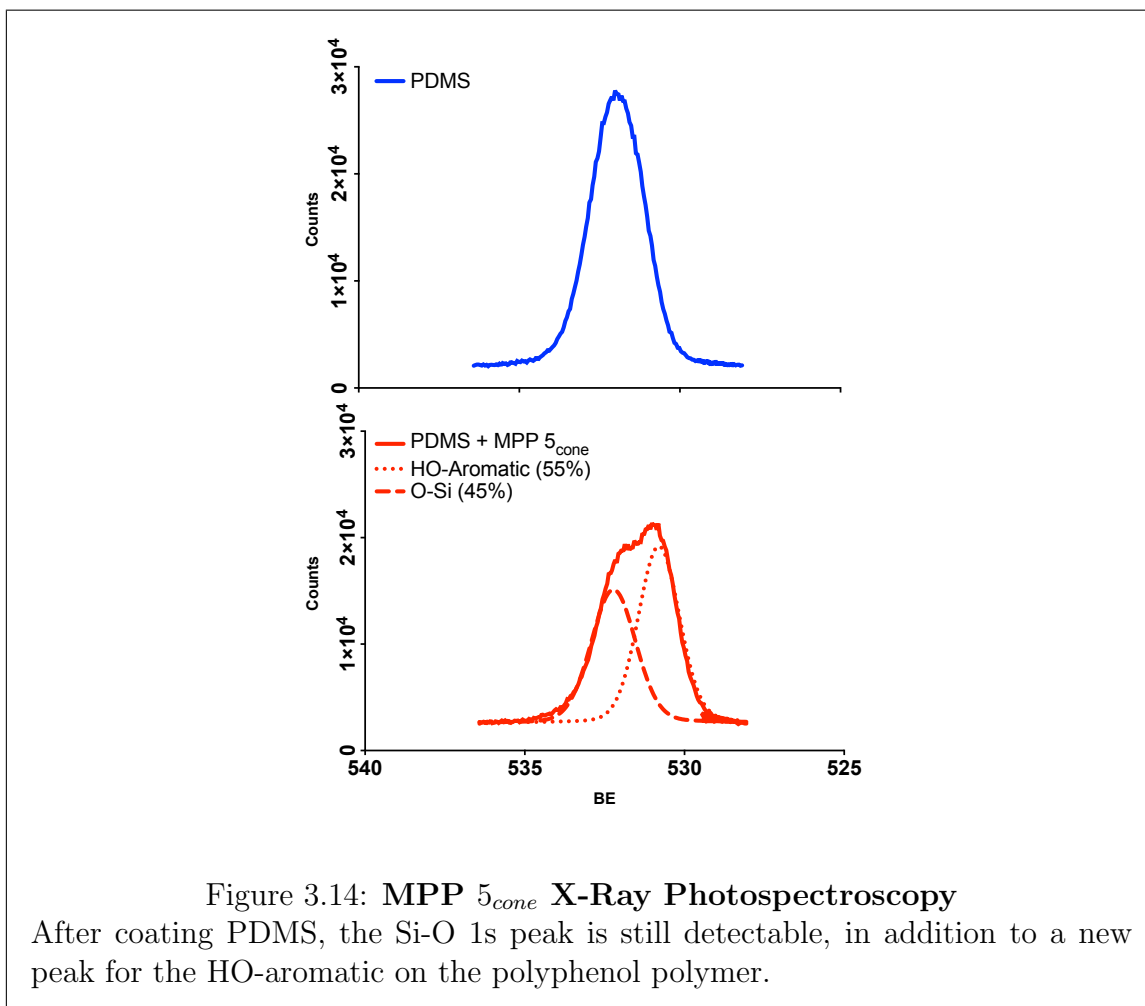
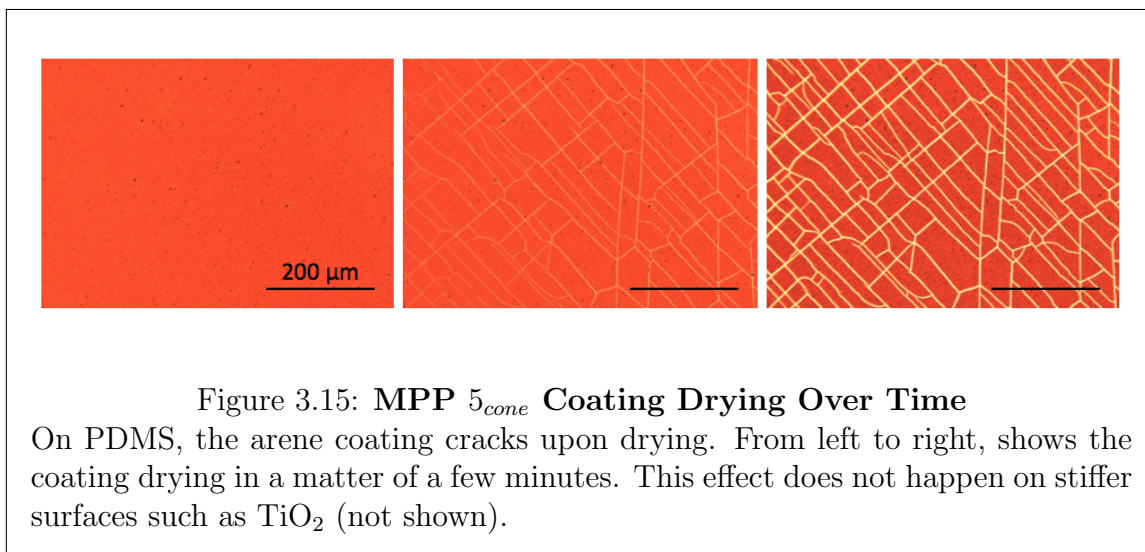


Figure 3.13: **MPP 5_{cone} Scanning Electron Microscopy**

Over incubation time the MPP 5_{cone} changes from a thin smooth coating to a rough surface with a polyp-like structure.





The stability of the coating was tested by incubation in a variety of solvents and acidities (Figure 3.16). The MPP 5_{cone} coating is stable in all conditions tested with the exception 2M NaOH, which almost completely removes the coating without significant agitation. We were able to exploit this property to clean the MPP 5_{cone} from unwanted surfaces for reuse. We also tested the coating stability at 75 C in water and 100 mM Ethylenediaminetetraacetic acid (EDTA), a chelating agent, for 24 hours to show that the coating is not held together by reversible metallic interactions (see Figure 3.16). This coating showed excellent stability in DMEM media, which is ideal for our bio-applications. Other conditions were also tested and the only condition able to remove the coating was 2M sodium hydroxide solution. This property was leveraged to remove the coating from surfaces where the coating was not desired.

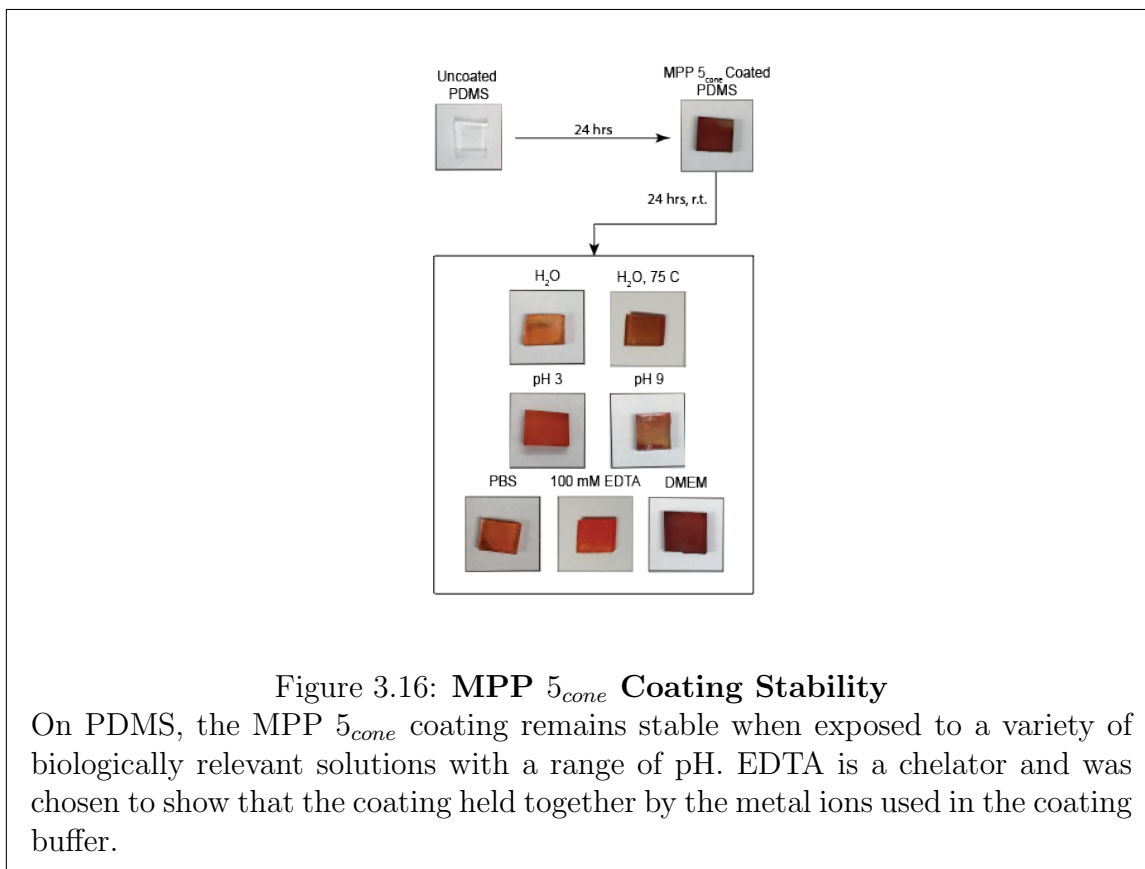


Figure 3.16: **MPP 5_{cone} Coating Stability**

On PDMS, the MPP 5_{cone} coating remains stable when exposed to a variety of biologically relevant solutions with a range of pH. EDTA is a chelator and was chosen to show that the coating held together by the metal ions used in the coating buffer.

3.6.4 Effective Diffusivity & Permeability Reduction

The loss of drug from media is controlled by the affinity of the drug for the PDMS wall, which is governed by equilibrium thermodynamics, and the rate at which the drug diffuses away from the media-channel wall interface, which is a matter of diffusion kinetics. Shirure and George propose using microfluidic design to reduce drug loss in MPS systems, but some deterministic parameters such as flow rate, solubility, and surface-area to volume ratio, are unalterable in order to recapitulate certain microphysiological environments.⁽²²⁾ For example, high fluid velocity decreases drug loss, but also prevents vital nutrients from reaching cells by decreasing the molecules ability diffuse through membranes or other barriers that are included to reduce shear stress on cells.

Our barrier coating affects the first step of the loss process by reducing the affinity of the drug for the surface. This affinity of molecules for hydrophilic vs hydrophobic environments is quantified by the partition coefficient, usually reported in its Log form, $\text{Log } P_{ow}$. $\text{Log } P_{ow}$, is the Log of the ratio of the equilibrium concentrations of the molecule in octanol, a hydrophobic solvent, and water, a hydrophilic solvent. The larger the value of $\text{Log } P_{ow}$, the more hydrophobic the molecule. $\text{Log } P_{ow}$ is

found to be a good estimate of the partition coefficient of PDMS and water, $\text{Log } P_{PDMS-W}$, which we will refer to as $\text{Log } P$ heretofore. (23) $\text{Log } P$ values of most biological molecules and drugs can be found online or estimated using software that analyzes molecular structure. Wang has found that molecules with a $\text{Log } P$ value above 2.47 will partition into the PDMS with estimated losses of $\sim 90\%$. [6] (3) The equilibrium concentration of the drug in the PDMS wall at the liquid-solid interface can be calculated from P by:

$$C_{i,P} = PC_{i,sl} \quad (3.1)$$

where $C_{i,P}$ is the concentration in the polymer at the liquid-solid interface, and $C_{i,sl}$ is the concentration in the solution at the liquid-solid interface. The barrier coating effectively reduces the partition (P) value and results in less dissolved drug in the polymer at the interface. After dissolution in the PDMS surface, the drug then can move, or diffuse, away from that interface into the bulk of the polymer by a concentration-driven thermodynamic force. This mass transport phenomenon is modeled by Ficks Second law of diffusion and follows the following partial differential equation in 3 dimensions (x, y, z):

$$\frac{\partial C_P}{\partial t} = D_P \left(\frac{\partial^2 C_P}{\partial x^2} + \frac{\partial^2 C_P}{\partial y^2} + \frac{\partial^2 C_P}{\partial z^2} \right) \quad (3.2)$$

where C_P is the concentration defined by space and time in the polymer and D_P is the diffusivity of the molecule in the polymer matrix. If we assume that we are looking at short times or large x -dimensions (compared to y and z), we can employ the semi-infinite media condition along with the equilibrium boundary condition (Equation 3.3) at the interface, and the solution to the diffusion equation becomes:

$$C_P(x, t) = C_{i,P} \text{Erfc} \left(\frac{x}{\sqrt{4D_P t}} \right) \quad (3.3)$$

If we assume that the intensity of the fluorophore varies linearly with its concentration, intensity can be used as a proxy for the concentration and then Equation 3.3 becomes:

$$\frac{I_P(x, t)}{I_{i,P}} = \text{Erfc} \left(\frac{x}{\sqrt{4D_P t}} \right) \quad (3.4)$$

Because we have a 2 layer system, instead of D_P , which assumes we have one constant diffusivity throughout the bulk material, we call this property the effective diffusivity, D_{eff} , of a molecule in our 2 layer system. Comparing the model to the actual intensity profile of Rhodamine B in PDMS, in Figure 3.17 we see the model closely predicts the intensity profile.

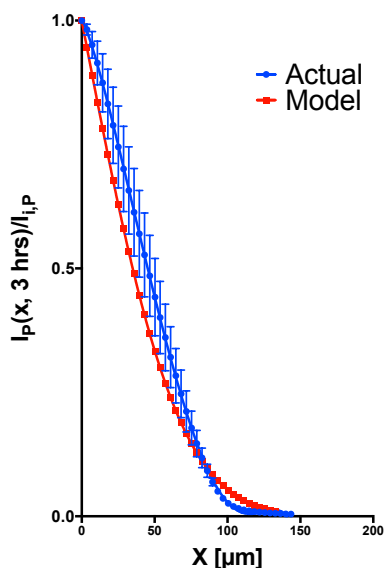
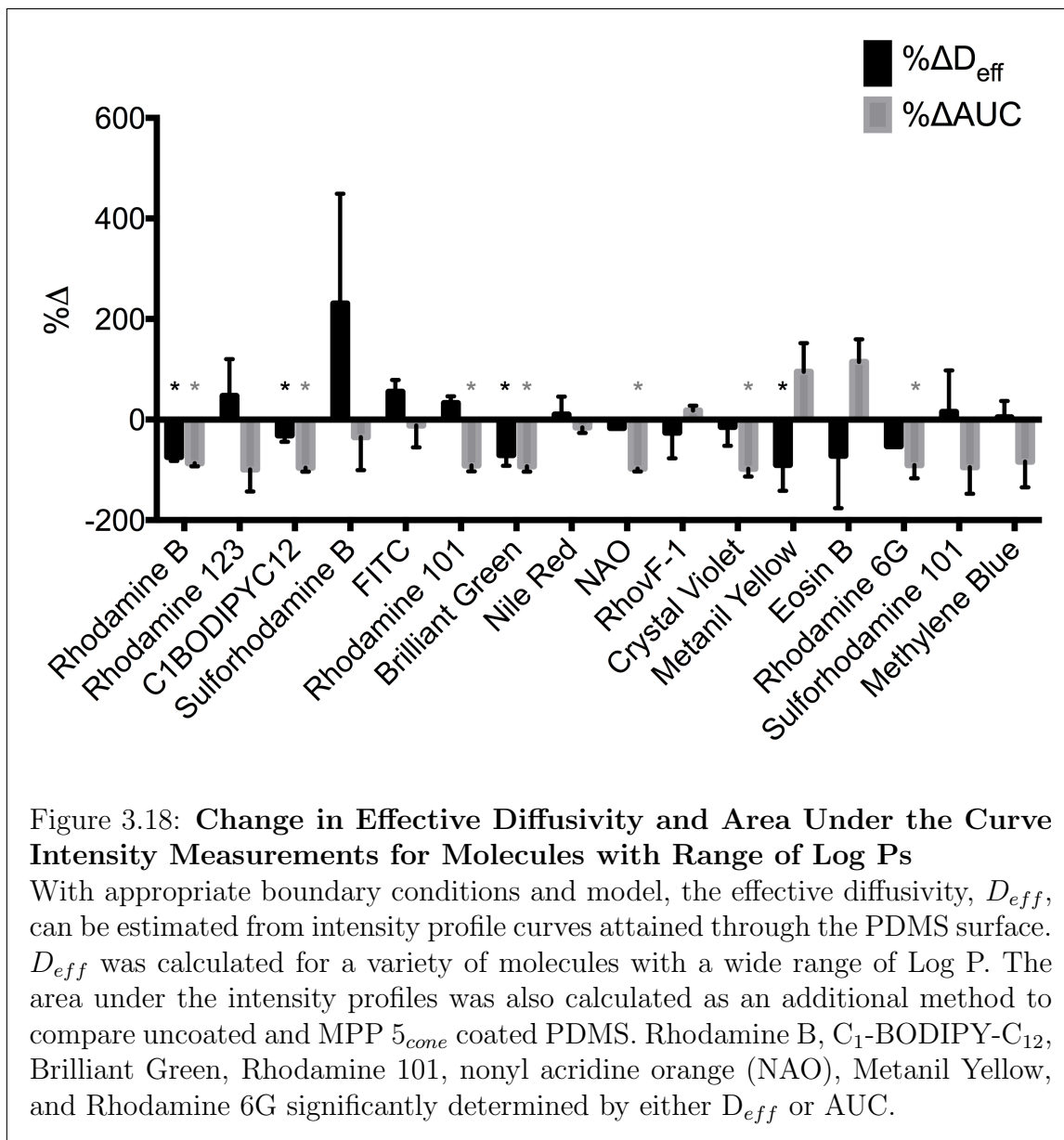


Figure 3.17: **Rhodamine B Diffusion Model Compared to Actual Data**
With appropriate boundary conditions and model, the effective diffusivity, D_{eff} , can be estimated from intensity profile curves attained through the PDMS surface. Here, the model very closely aligns with the actual data and can be used to estimate D_{eff} .

For dyes with a range of reported Log P values, D_{eff} was calculated for each dye by solving the intensity profiles in the form of Equation 3.4. The area under the curve (AUC) was always recorded and compared. The dye names and results are summarized in Figure 3.19. Rhodamine B, Brilliant Green, and Metanil Yellow were significantly reduced by D_{eff} comparison. While some dyes are increased, 8 out of the 11 dyes are reduced at least slightly.



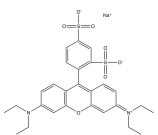
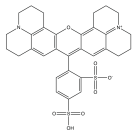
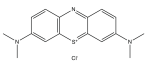
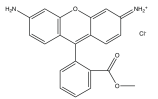
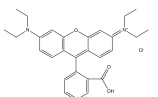
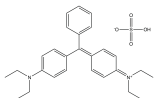
Name	Chemical Structure	cLog P (ChemDraw)	clog _P (ALOGPS)	% Δ D eff +/- SEM	Δ D eff Significance	% Δ AUC +/- SEM	Δ AUC Significance	# Enamine/Amine Groups	Molecular Weight (g/mol)	Nominal Charge
Sulforhodamine B		-8.7	1.06	231 +/- 218	0	-35 +/- 66	0	2	559	Zwitterionic
Sulforhodamine 101		-0.65	-0.43	15 +/- 83	0	-95 +/- 53	0	0	606	Zwitterionic
Methylene Blue		0.126	-1.08	5 +/- 32	0	-84 +/- 51	0	0	320	1
Rhodamine 123		1.5	0.45	47 +/- 73	0	-99 +/- 44	0	2	381	1
Rhodamine B		2.13	2.4	-74 +/- 7.8	-1	-87 +/- 6.3	-1	2	479	Zwitterionic
Brilliant Green		2.26	2.79	-70 +/- 22	-1	-93 +/- 11	-1	2	483	1

Figure 3.19: Dye Molecules Used in Effective Diffusivity Models and Comparisons

With appropriate boundary conditions and model, the effective diffusivity, D_{eff} , can be estimated from intensity profile curves attained through the PDMS surface. D_{eff} was calculated for a variety of molecules with a wide range of Log P. The area under the intensity profiles was also calculated as an additional method to compare uncoated and MPP 5_{cone} coated PDMS.

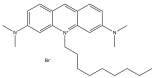
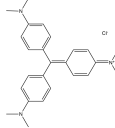
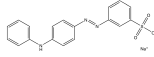
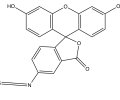
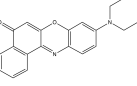
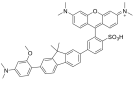
Name	Chemical Structure	cLog P (ChemDraw)	clog _P (ALOGPS)	% Δ D eff +/- SEM	Δ D eff Significance	% Δ AUC +/- SEM	Δ AUC Significance	# Enamine/Amine Groups	Molecular Weight (g/mol)	Nominal Charge
Nonyl Acridine Orange		3.1	4.37	-17 +/-	0	-98 +/- 6	-1	2	473	1
Crystal Violet		3.18	0.27	-14 +/- 38	0	-98 +/- 16	-1	3	408	1
Metanil Yellow		3.72	4.48	-90 +/- 52	-1	95 +/- 57	0	1	375	-1
FTIC		3.8	4.74	55 +/- 23	0	-12 +/- 44	0	0	389	0
Nile Red		4	4.39	10 +/- 36	0	-16 +/- 11	0	1	318	0
isoRhoF-1		4.6	4.6	-26 +/- 51	0	18 +/- 9.6	0	3	490	1

Figure 3.19 (Continued): Dye Molecules Used in Effective Diffusivity Models and Comparisons

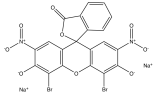
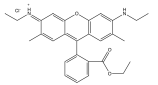
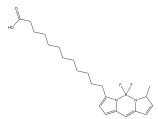
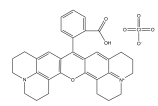
Name	Chemical Structure	cLog P (ChemDraw)	cLogP (ALOGPS)	% Δ D eff +/- SEM	Δ D eff Significance	% Δ AUC +/- SEM	Δ AUC Significance	# Enamine/Amine Groups	Molecular Weight (g/mol)	Nominal Charge
Eosin B		5.38	4.52	-72 +/- 104.2	0	114 +/- 45	0	0	580	-4
Rhodamine 6G		6.5	6.36	-53 +/-	0	-91 +/- 26	-1	2	479	1
CLBODIPYCL2		7.12	2.81	-32 +/- 12.5	-1	-96 +/- 8	-1	0	404	0
Rhodamine 101		7.8	2.37	33 +/- 13	0	-91 +/- 12	-1	0	491	1

Figure 3.19 (Continued): **Dye Molecules Used in Effective Diffusivity Models and Comparisons**

Another property used to quantify the ability of a molecule to absorb into and diffuse through a material is the permeability, which can be measured using Franz cell. Figure 3.20 shows a schematic of Franz cell. Franz cells are used to quantify the permeability of a molecule through a membrane. By tracking the concentration over time, you can calculate the amount of an analyte that has diffused through a membrane. From the time plot of the accumulation of analyte in the receptor chamber the flux kinetics can be elucidated and used to find the permeability constant of the experimental set up. Franz cells are often used to quantify permeability of drugs in skin, through other types of membranes, etc. Permeability is an important value for design considerations for drug delivery as well as microphysiological environment control.

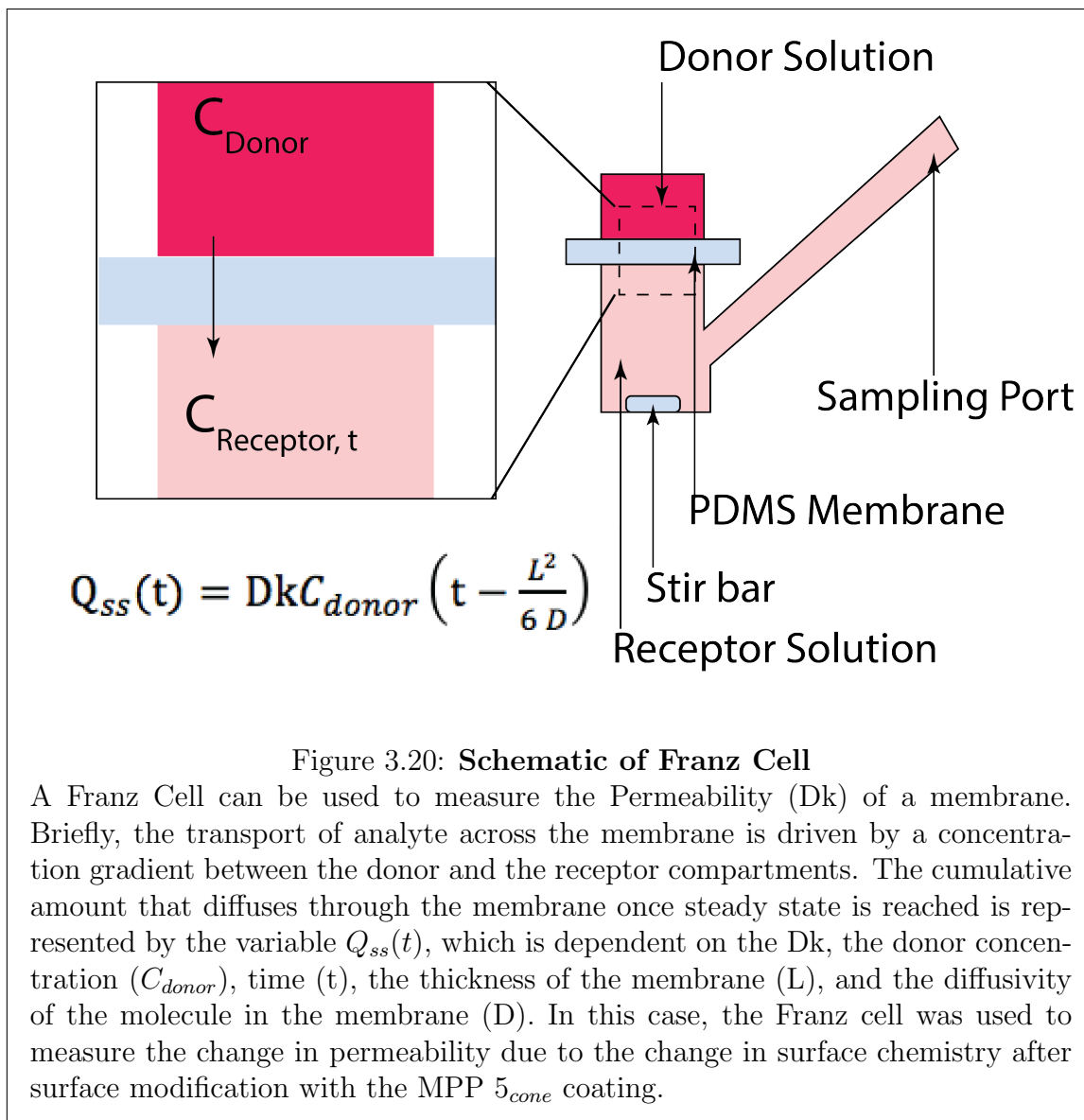


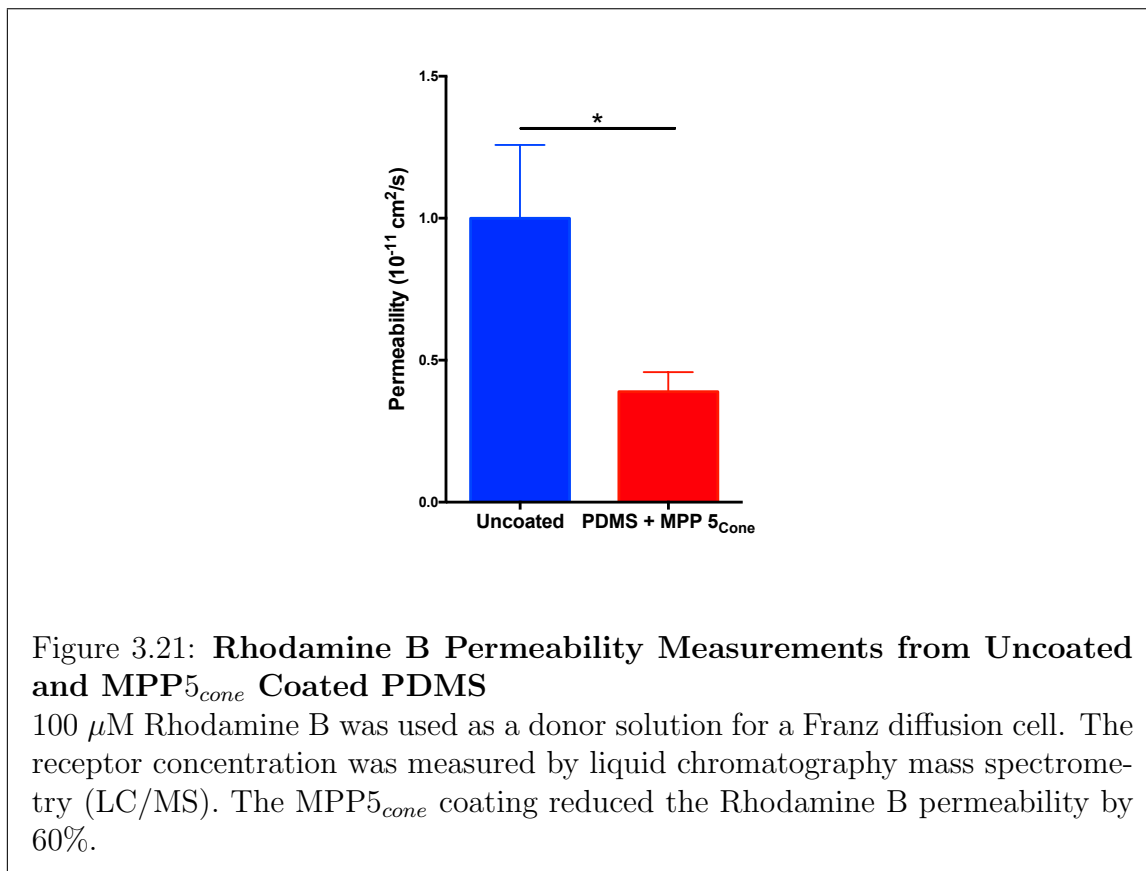
Figure 3.20: **Schematic of Franz Cell**

A Franz Cell can be used to measure the Permeability (Dk) of a membrane. Briefly, the transport of analyte across the membrane is driven by a concentration gradient between the donor and the receptor compartments. The cumulative amount that diffuses through the membrane once steady state is reached is represented by the variable $Q_{ss}(t)$, which is dependent on the Dk , the donor concentration (C_{donor}), time (t), the thickness of the membrane (L), and the diffusivity of the molecule in the membrane (D). In this case, the Franz cell was used to measure the change in permeability due to the change in surface chemistry after surface modification with the MPP 5_{cone} coating.

A donor solution with analyte is placed on one side of a membrane, with a receptor solution without analyte on the other side. The receiving side acts as a sink as long as the concentration remains relatively close to 0. If steady state is assumed and the boundary conditions on the membrane are applied, the solution to the diffusion equation becomes:

$$Q_{SS}(t) = DkC_{donor} \left(t - \frac{L^2}{6D} \right) \quad (3.5)$$

where Q_{SS} is the cumulative number of moles that has diffused through the membrane after time t during steady state diffusion, C_{donor} is the donor concentration, L is the thickness of the membrane, and Dk is the permeability of the molecule in the membrane. By plotting Q_{SS} , the permeability can be measured by the slope, since C_{donor} is known. Q_{SS} can be experimentally measured by quantifying the concentration of drug in the receptor compartment overtime using UV-vis spectrometry, HPLC, or Liquid Chromatography with Mass Spectrometry (LC/MS), without the need for fluorescent dyes. Using this experimental set up, we found the permeability of Rhodamine B was reduced by 60%, which is comparable to the 67% reduction in D_{eff} in the fluorescent confocal microscopy model. The results are shown in Figure 3.21.



3.6.5 Coating Characterization and Performance in a Microfluidic Channel

Coating the MPP 5_{cone} on microfluidic channel walls is simple and requires the same basic steps as coating any planar substrate. The cleaning, coating, and rinsing steps were all accomplished using a syringe pump that can be easily set to perform infusion over a range of flow rates. Instead of submerging PDMS into the coating solution, the solution is infused from syringes preloaded with the coating solution. Flow rates can be controlled to lower than $0.5 \mu\text{L min}^{-1}$ to as high as $10 \mu\text{L min}^{-1}$. The upper limit is restricted by the burst pressure of the PDMS device bonded to a glass slide through oxygen plasma activation. In order to gain access to the channels for SEM imaging after coating, the device bonding step was altered to use Poly-L-Lysine (PLL) reversible bonding with glass.⁽²⁴⁾ Using this method the PDMS could be removed from the glass slide and imaged on SEM to see the thickness of the MPP 5_{cone} coating. SEM micrographs revealed that lower infusion speeds produce thicker coatings as shown in Figure 3.22. Figure 3.23 is an SEM micrograph of a channel coated using a $1 \mu\text{L hr}^{-1}$ flow rate.

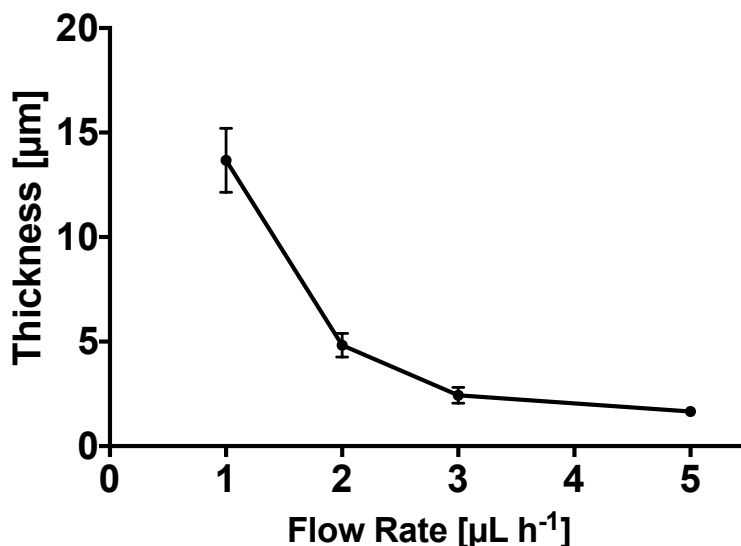


Figure 3.22: Coating Thickness in Microfluidic Channel

The coating protocol can be modified by using programmable infusion pumps. By decreasing the flow rate of the coating solution, the thickness of the MPP 5_{cone} coating increases.

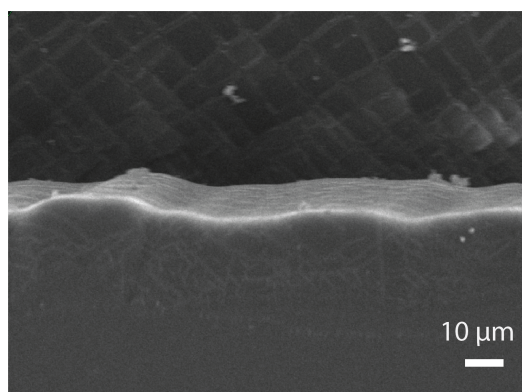


Figure 3.23: **Coating Thickness in Microfluidic Channel**

The coating protocol can be modified to use programmable infusion pumps. By decreasing the flow rate of the coating solution, the thickness of the MPP 5_{cone} coating increases.

For small molecule absorption measurements, samples were coated with flow rates of $1 \mu\text{L hr}^{-1}$ for 24 hours. Fluorescent microscopy images were taken at 4x and analyzed using ImageJ software to compare area under the curve (AUC) of intensity profiles. Channels 10mm long, $100 \mu\text{m}$ wide, and $150 \mu\text{m}$ high were fabricated in PDMS as testing platforms. After 3 hour infusion of $10\mu\text{M}$ Rhodamine B, MPP 5_{cone} coated channels had AUCs $92\pm 5\%$ smaller than uncoated channels. Likewise after infusion of $10\mu\text{M}$ of C1-BODIPY-C12 in media for 24 hours, MPP 5_{cone} coated channels had AUCs $78\pm 2\%$ smaller than in uncoated control samples, supporting the evidence for MPP 5_{cones} ability to reduce absorption. These data show that MPP 5_{cone} can be used in microfluidic systems to reduce lipophilic molecule absorption.

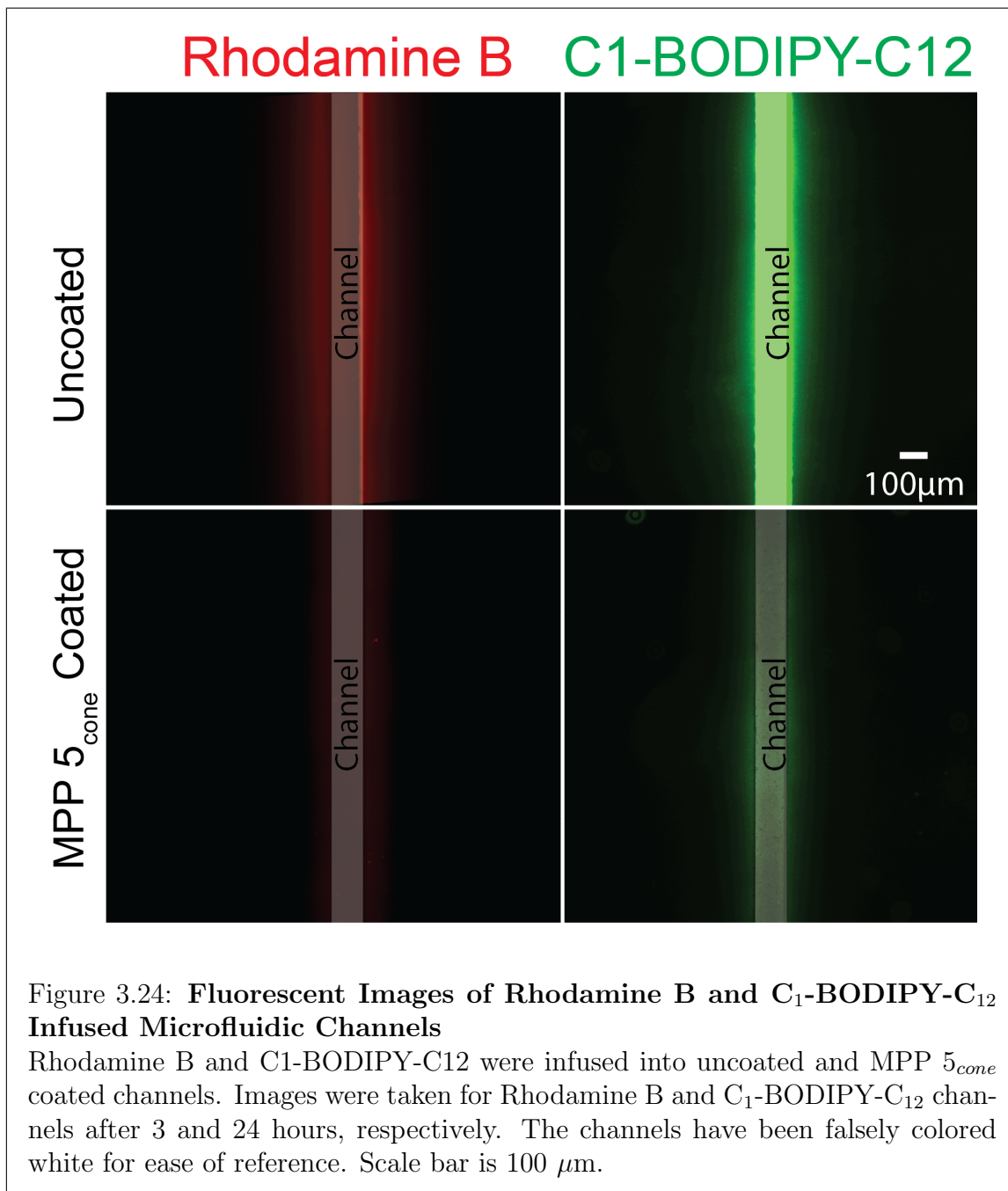


Figure 3.24: **Fluorescent Images of Rhodamine B and C₁-BODIPY-C₁₂ Infused Microfluidic Channels**

Rhodamine B and C₁-BODIPY-C₁₂ were infused into uncoated and MPP 5_{cone} coated channels. Images were taken for Rhodamine B and C₁-BODIPY-C₁₂ channels after 3 and 24 hours, respectively. The channels have been falsely colored white for ease of reference. Scale bar is 100 µm.

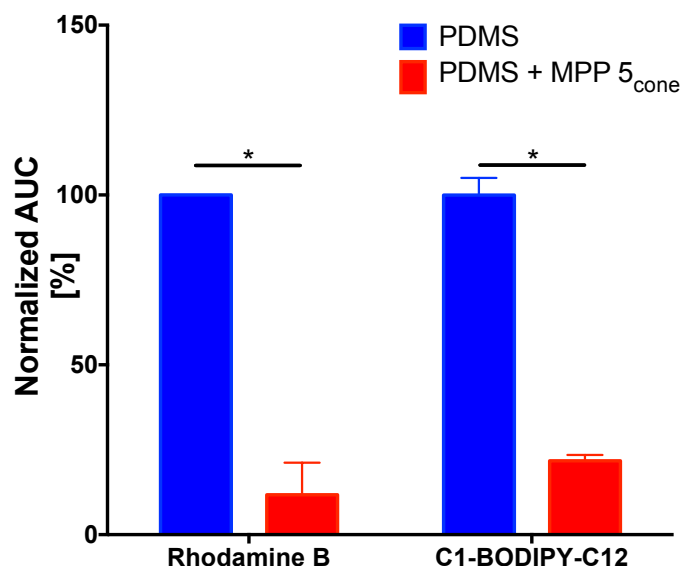


Figure 3.25: Normalized AUC of Rhodamine B and C₁-BODIPY-C₁₂ Infused Microfluidic Channels

Intensity profiles were averaged over the length of the channel and the area under the curve (AUC) was calculated and normalized to the uncoated channel average. Rhodamine B and C₁-BODIPY-C₁₂ AUC absorption was reduced $92\pm 5\%$ and $78\pm 2\%$, respectively, after treatment with the MPP 5_{cone} coating.

3.6.6 Coating Biocompatibility

The coating will be in contact with cells in a microfluidic system either directly, by adhering to the surface of the coating, or indirectly, through some residual loss of the coating into the media. Toxicity of the coating must be low in order to preserve the biocompatibility of current PDMS-based MPS. To verify the biocompatibility of the coating, several tests were designed to probe different ways the cells could be exposed to the coating in 2D and 3D. First, in 2D we verified that the MPP 5_{cone} coating did not significantly impair hiPSC-CMs metabolism after 7 days of direct exposure or function during 28 days of direct exposure (Figure 3.26 and 3.28), respectively. Figure 3.27 shows representative images of CMs during the 28 day beat rate study. In both of these assessments, there was no detectable difference in metabolism of Alamar Blue or beat rate. Immunofluorescent staining of vinculin and α -actinin did not reveal any toxicity on MPP 5_{cone} coated surfaces (see Figure 3.29).

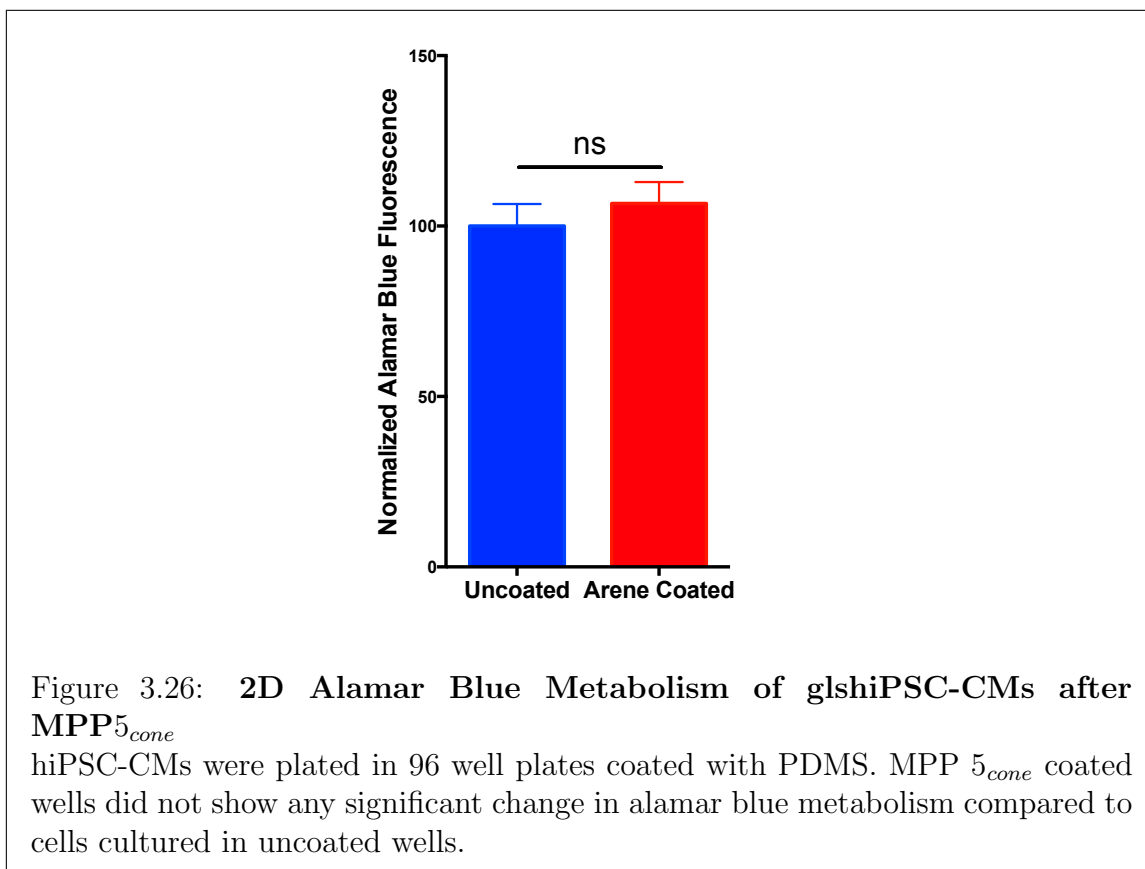


Figure 3.26: **2D Alamar Blue Metabolism of glshiPSC-CMs after $MPP5_{cone}$**

hiPSC-CMs were plated in 96 well plates coated with PDMS. $MPP5_{cone}$ coated wells did not show any significant change in alamar blue metabolism compared to cells cultured in uncoated wells.

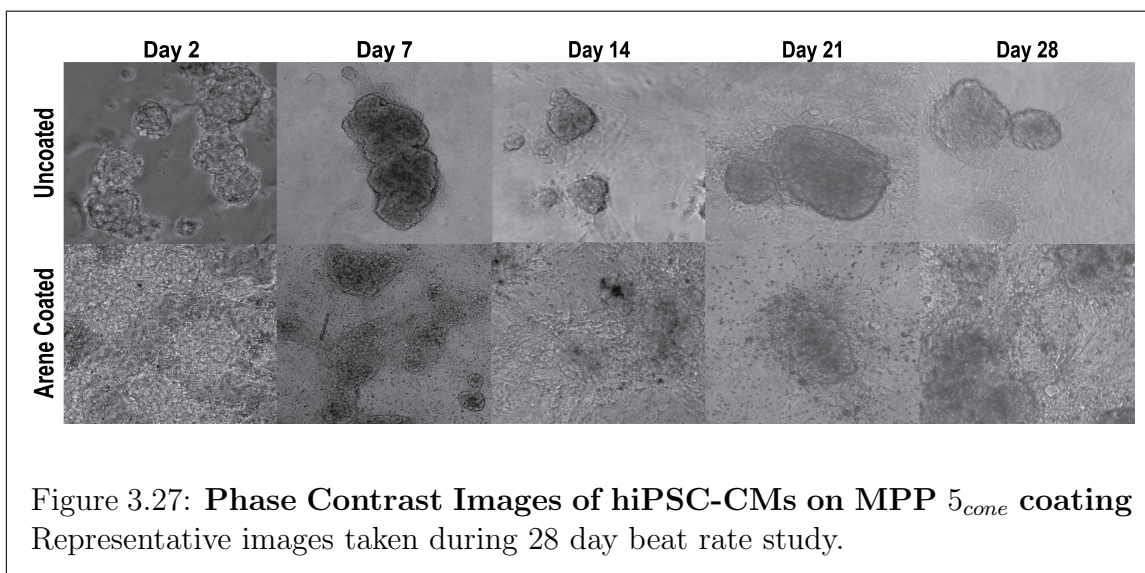
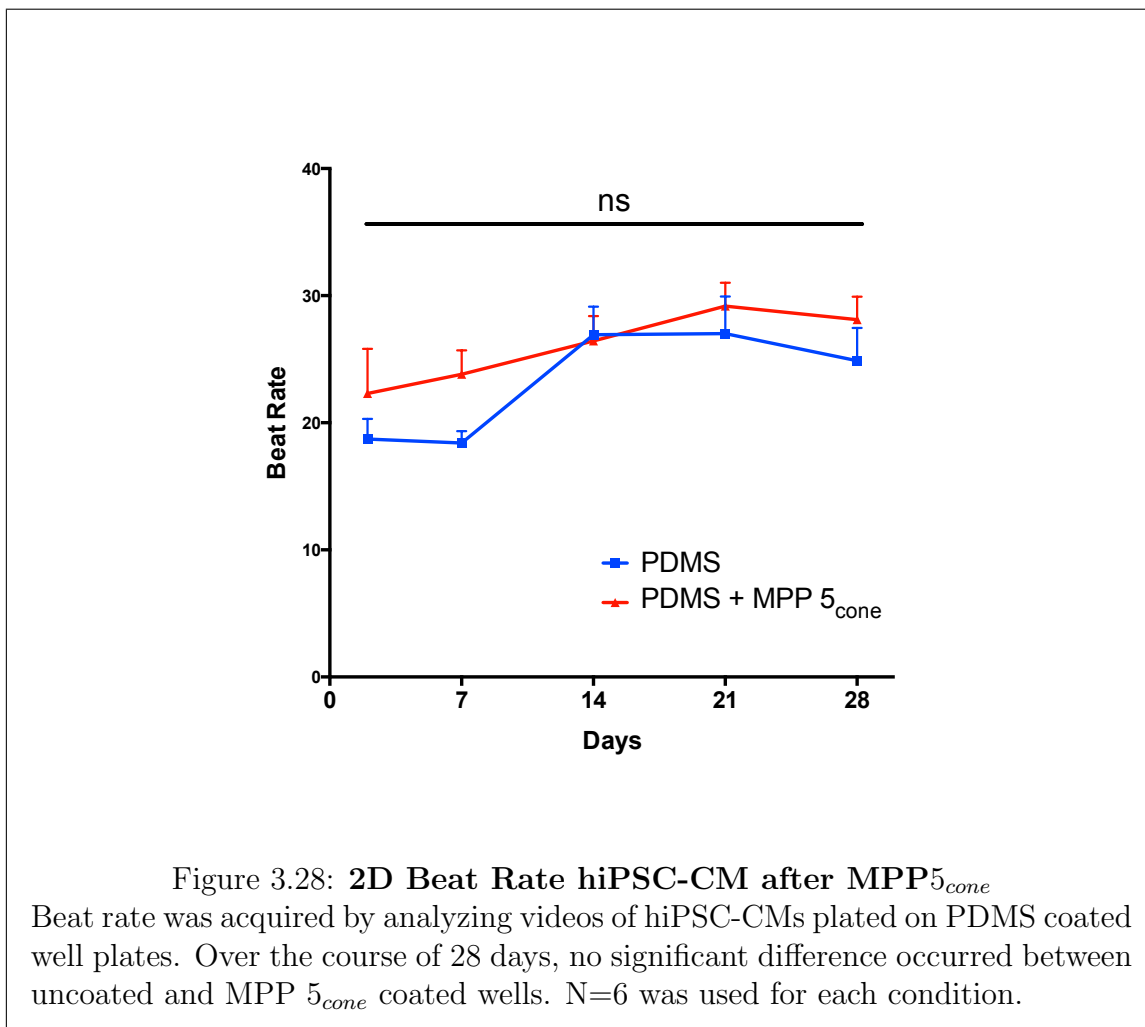
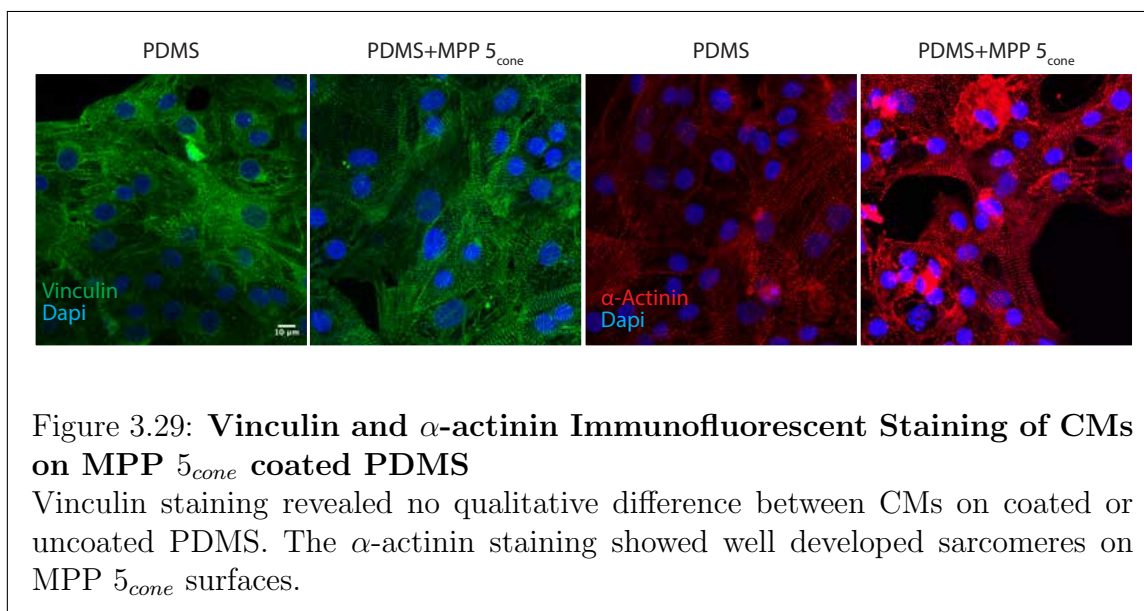
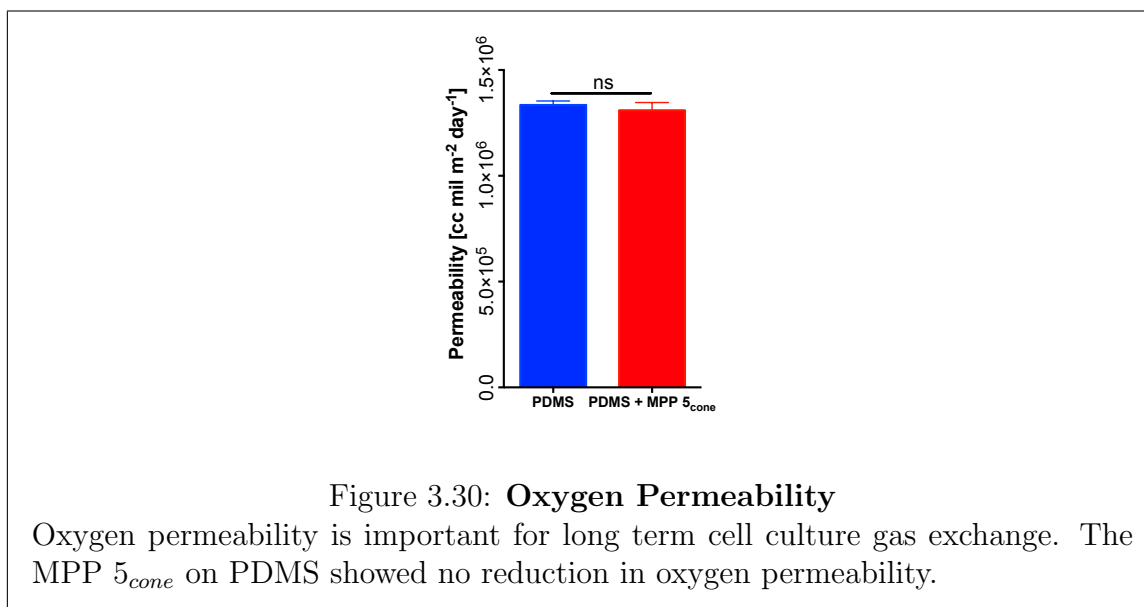


Figure 3.27: Phase Contrast Images of hiPSC-CMs on MPP 5_{cone} coating
Representative images taken during 28 day beat rate study.





Secondly, oxygen permeability is preserved, another major advantage of this coating over glassy coatings and necessary attribute for long term cell culture. Oxygen permeability measurements are shown in Figure 3.30. The high oxygen permeability of PDMS is preserved and showed no statistical difference between MPP 5_{cone} coated and native PDMS.



With a standard kill curve assay, we found the concentration of an inhibitor where the response is reduced by half (IC₅₀) for NIH3T3 fibroblast viability to be ~0.4 mg

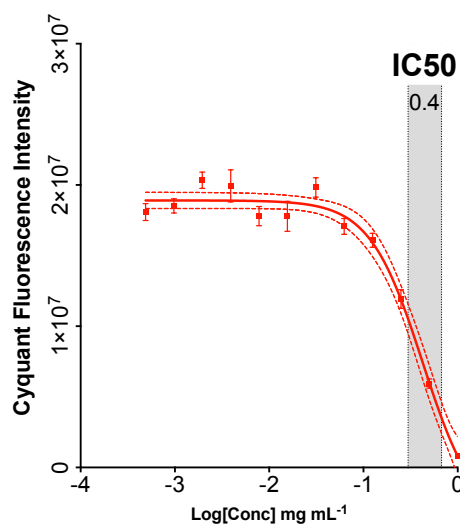


Figure 3.31: **Toxicity of Direct Exposure to MPP 5_{cone}**
NIH 3T3 mouse fibroblasts were exposed to MPP 5_{cone} polymer fragments in normal growth media at a range of concentration. The IC₅₀ for NIH 3T3 fibroblast viability was estimated at 0.4 mg mL⁻¹, far above exposure concentrations expected either in 2D or 3D culture systems.

mL⁻¹, far above concentration values expected due to residual coating loss (see Figure 3.31).

Finally, we loaded hMSC derived white adipose tissue (WAT) in an MPP 5_{cone} coated MPS reported by Loskill. (14) After 4 days of culture, there were no dead cells in the MPS. Figure 3.32 shows a side by side comparison of a MPP 5_{cone} coated WAT MPS and an uncoated MPS. It is important to show this result, since in an MPS the surface area to volume ratio is considerably higher and may result in the concentration being much higher.

From these experiments, the MPP 5_{cone} demonstrates tolerable biocompatibility with many different cell types in 2D and 3D systems.

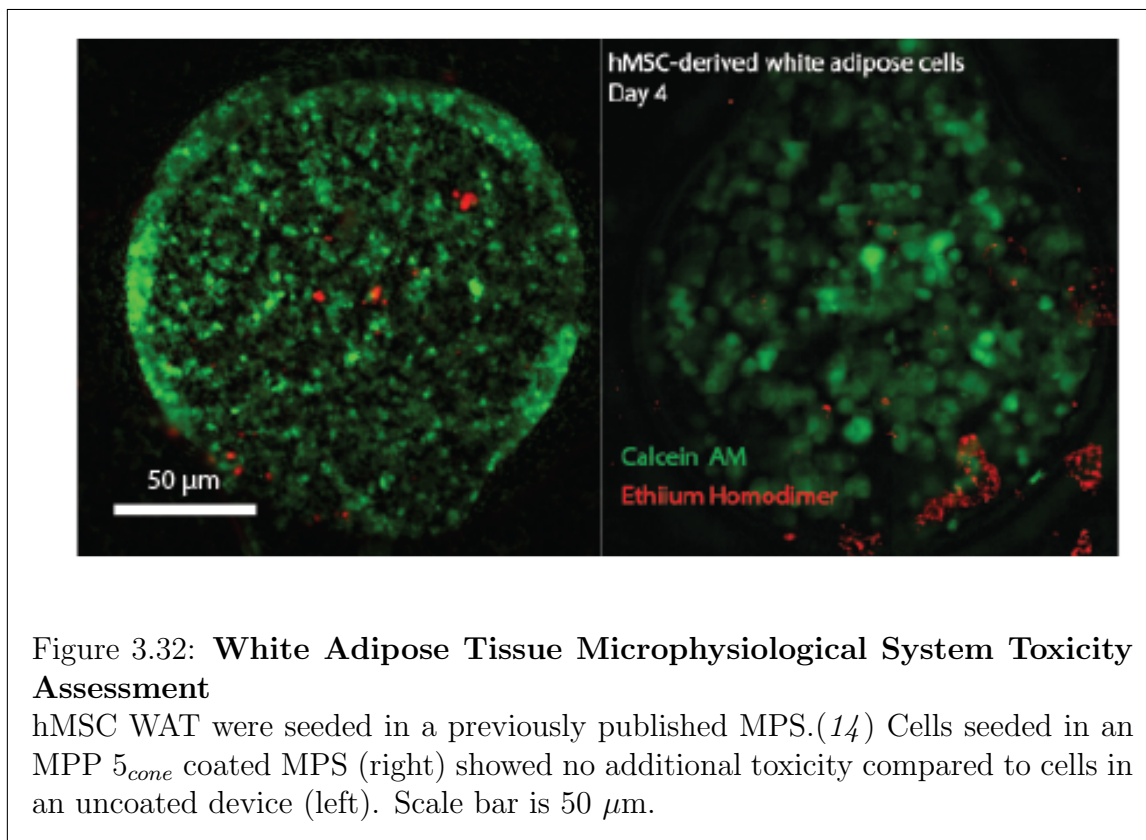


Figure 3.32: **White Adipose Tissue Microphysiological System Toxicity Assessment**

hMSC WAT were seeded in a previously published MPS.(14) Cells seeded in an MPP 5_{cone} coated MPS (right) showed no additional toxicity compared to cells in an uncoated device (left). Scale bar is 50 μm .

3.7 Conclusions & Future Directions

Our MPP 5_{cone} coating shows promise as a method to reduce drug absorption for PDMS-based microphysiological systems. It is able to block drug surrogates Rhodamine B, C₁-BODIPY-C₁₂, Brilliant Green, Rhodamine 101, NAO, Metanil Yellow, and Rhodamine 6G significantly determined by at least one of two fluorescent microscopy modeling methods. It should be noted that the MPP 5_{cone} is limited in its ability as a barrier coating compared to glassy-like coatings and results in selective blocking of analytes. This drawback is compensated by MPP 5_{cone} s low cost, high oxygen permeability, ease of use, and biocompatibility. Future studies should focus on understanding which types of molecules can be blocked by the coating and the mechanism which makes this blocking possible. Also, since the polymerization of many polyphenols is mostly misunderstood, some investigation on this process would also be insightful for optimization of the coating and its barrier abilities.

References

- (1) Joseph A. DiMasi. *Briefing Cost of Developing a New Drug Innovation in the Pharmaceutical Industry : New Estimates of R & D Costs*. Tech. rep. Boston, MA: Tufts Center for the Study of Drug Development, 2014.
- (2) Elveflow. *PDMS: A Review*. 2015. URL: <http://www.elveflow.com/microfluidic-tutorials/microfluidic-reviews-and-tutorials/the-poly-di-methyl-siloxane-pdms-and-microfluidics/>.
- (3) Jack D. Wang et al. “Quantitative analysis of molecular absorption into PDMS microfluidic channels”. In: *Ann. Biomed. Eng.* 40.9 (2012), pp. 1862–1873.
- (4) Skarphedinn Halldorsson et al. “Advantages and challenges of microfluidic cell culture in polydimethylsiloxane devices”. In: *Biosens. Bioelectron.* 63 (2015), pp. 218–231.
- (5) Karel Domansky et al. “Clear castable polyurethane elastomer for fabrication of microfluidic devices.” In: *Lab Chip* 13.19 (2013), pp. 3956–64.
- (6) Katsuji Matsunaga et al. “Gas Permeability of Thermoplastic Polyurethane Elastomers”. In: *Polym. J.* 37.6 (2005), pp. 413–417.
- (7) Ming Li and Dong Pyo Kim. “Silicate glass coated microchannels through a phase conversion process for glass-like electrokinetic performance.” In: *Lab Chip* 11.6 (Mar. 2011), pp. 1126–31.
- (8) Bo-Yeol Kim et al. “Solvent-Resistant PDMS Microfluidic Devices with Hybrid Inorganic/Organic Polymer Coatings”. In: *Adv. Funct. Mater.* 19.23 (Dec. 2009), pp. 3796–3803.
- (9) Adam R Abate et al. “Glass coating for PDMS microfluidic channels by sol-gel methods.” In: *Lab Chip* 8.4 (2008), pp. 516–518.
- (10) Hirotaka Sasaki et al. “Parylene-coating in PDMS microfluidic channels prevents the absorption of fluorescent dyes”. In: *Sensors Actuators, B Chem.* 150.1 (2010), pp. 478–482.
- (11) Anurag Mathur et al. “Human iPSC-based Cardiac Microphysiological System For Drug Screening Applications”. In: *Scientific Reports* 5 (Mar. 2015), p. 8883.

- (12) “Robust cardiomyocyte differentiation from human pluripotent stem cells via temporal modulation of canonical Wnt signaling.” In: *PNAS* 109.27 (July 2012), E1848–57.
- (13) Nathaniel Huebsch et al. “Automated Video-Based Analysis of Contractility and Calcium Flux in Human-Induced Pluripotent Stem-Derived Cardiomyocytes Cultured over Different Spatial Scales”. In: *Tissue Eng. Part C Methods* 21.5 (2014), pp. 467–479.
- (14) P. Loskill et al. “WAT-on-a-chip: A physiologically relevant microfluidic system incorporating white adipose tissue”. In: *Lab Chip* 17.9 (2017).
- (15) Haeshin Lee et al. “Mussel-Inspired Surface Chemistry for Multifunctional Coatings”. In: *Science* (80-.). 318.5849 (2007), pp. 426–430.
- (16) Min Yin et al. “Development of mussel adhesive polypeptide mimics coating for in-situ inducing re-endothelialization of intravascular stent devices.” In: *Biomaterials* 30.14 (May 2009), pp. 2764–73.
- (17) Tadas S. Sileika et al. “Colorless multifunctional coatings inspired by polyphenols found in tea, chocolate, and wine”. In: *Angew. Chemie - Int. Ed.* 52.41 (2013), pp. 10766–10770.
- (18) Seonki Hong et al. “Pyrogallol 2-Aminoethane: A Plant Flavonoid-Inspired Molecule for Material-Independent Surface Chemistry”. In: *Adv. Mater. Interfaces* 1.4 (2014).
- (19) Muriel Funck, Daniel P. Guest, and Gareth W V Cave. “Microwave-assisted synthesis of resorcin[4]arene and pyrogallol[4]arene macrocycles”. In: *Tetrahedron Lett.* 51.49 (2010), pp. 6399–6402.
- (20) Constance R. Pfeiffer et al. “Syntheses and characterization of aryl-substituted pyrogallol[4]arenes and resorcin[4]arenes”. In: *CrystEngComm* 18.2 (2016), pp. 222–229.
- (21) Shuo Xiao et al. “A microfluidic culture model of the human reproductive tract and 28-day menstrual cycle”. In: *Nat. Commun.* 8 (2017), p. 14584.
- (22) Venkatesh S Shirure and Steven C George. “Design considerations to minimize the impact of drug absorption in polymer-based organ-on-a-chip platforms”. In: *Lab Chip* 17.4 (2017), pp. 681–690.
- (23) Erica L. DiFilippo and Robert P. Eganhouse. “Assessment of PDMS-Water Partition Coefficients: Implications for Passive Environmental Sampling of Hydrophobic Organic Compounds”. In: *Environ. Sci. Technol.* 44.18 (Sept. 2010), pp. 6917–6925.
- (24) Joseph Harris et al. “Non-plasma Bonding of PDMS for Inexpensive Fabrication of Microfluidic Devices”. In: *J. Vis. Exp.* 9 (2007), pp. 4–6.

Chapter 4

Future Work

4.1 Conclusions for Topographically Directed Migration

Chapter 2 presents a method to direct cell migration on quartz. Laser-ablated direct write nanotopographical features reduce the area available for cell adhesion and focal adhesion maturation. Limiting focal adhesion size results in immature focal adhesions that turnover quickly and result in cells have short residence times on regions with nanopits spaced either 2 or 4 μm apart. When cells were seeded on regions with spacing of 6 or 8 μm , the effect of reducing focal adhesion size was diminished as well as cell repellent ability. On gradient patterns, cell migration also indicated a threshold for cell repellency indicating a minimum area needed for mature focal adhesion formation. Cells transfected with the functional head of intercellular protein Talin+1 were able to overcome the area limit and create stable, long lasting focal adhesions on all spacings of pits. This investigation indicates by purely altering the area available for cells to attach, cells can be repelled from a material surface.

4.1.1 Topographical Patterning on Biologically Relevant Materials

Chapter 2 presents a method to direct cell migration on quartz. Although the phenomenon is consistent on patterned quartz, the surface cannot be used for more than a tool to study mechanotransductive techniques for cell culture and is limited in application. A more interesting material for cell culture studies are tissue culture polystyrene (TCPS) and PDMS. These materials are used predominantly because they are very inexpensive, about hundreds of times cheaper than quartz. The direct-write method is not appropriate for these materials, however, because the material melts and instead of a clean pit, the ablation results in a pit surrounded by a hill of material around it, thereby increasing the roughness of the surface and confounding the effect of surface roughness and reduced surface area. Supplemental experiments

were done in laser ablated TCPS and showed that cells lost the ability to migrate in a directed manner.

Fortunately, there are other ways to create nanotopographical features on surfaces. Some methods include nano-imprint lithography which uses a quartz mold to increase the resolution of standard lithography techniques to nanoscale features. Unfortunately this technique is expensive.

New methods for patterning submicron feature sizes in polymer surfaces is needed. The feature sizes will need to be optimized individually since surface chemistry greatly affects protein adsorption and presentation, which leads to differences in cell adhesion and motility.

4.2 Conclusions and Future Directions of Macrocylic polyphenol Coatings

In Chapter 2, a macrocyclic polyphenol is presented to reduce drug absorption in PDMS. In this study, we use a novel macrocyclic polyphenol precursor to create a barrier coating on PDMS. The barrier coating increases the hydrophilicity and blocks fluorescent drug surrogates from being absorbed better than other polyphenols tested. The coating does not block all drug surrogates, but presents a facile, inexpensive method to reduce drug absorption over other strategies which makes it a viable solution for some lipophilic compounds.

4.2.1 Elucidating Polyphenol Coating Kinetics

Polyphenol coatings are not fully understood currently. More research into the fundamental kinetics of reaction, the products that are produced, and the driving force for this reaction needs to be done to help understand how to control these systems to produce desired coatings with particular properties. This was outside the scope of this dissertation that was focused more on proof of concept, but this understanding could improve performance of these coatings as barriers.

4.2.2 Using Macrocylic Polyphenol Coatings for PDMS Functionalization

Other polyphenols have been used to functionalize surfaces such as polydopamine and pyrogallol. These polyphenols are able to undergo a Michael addition reaction with primary thiols and amines on molecules such as thiolated PEG and other aliphatic compounds. It may be possible to further functionalize these macrocyclic polyphenols under optimized conditions.

Very limited investigation was done here. We were also able to incorporate a thiolated star PEG during coating. This can be investigated as a way to make the coating less brittle while retaining its barrier characteristic.

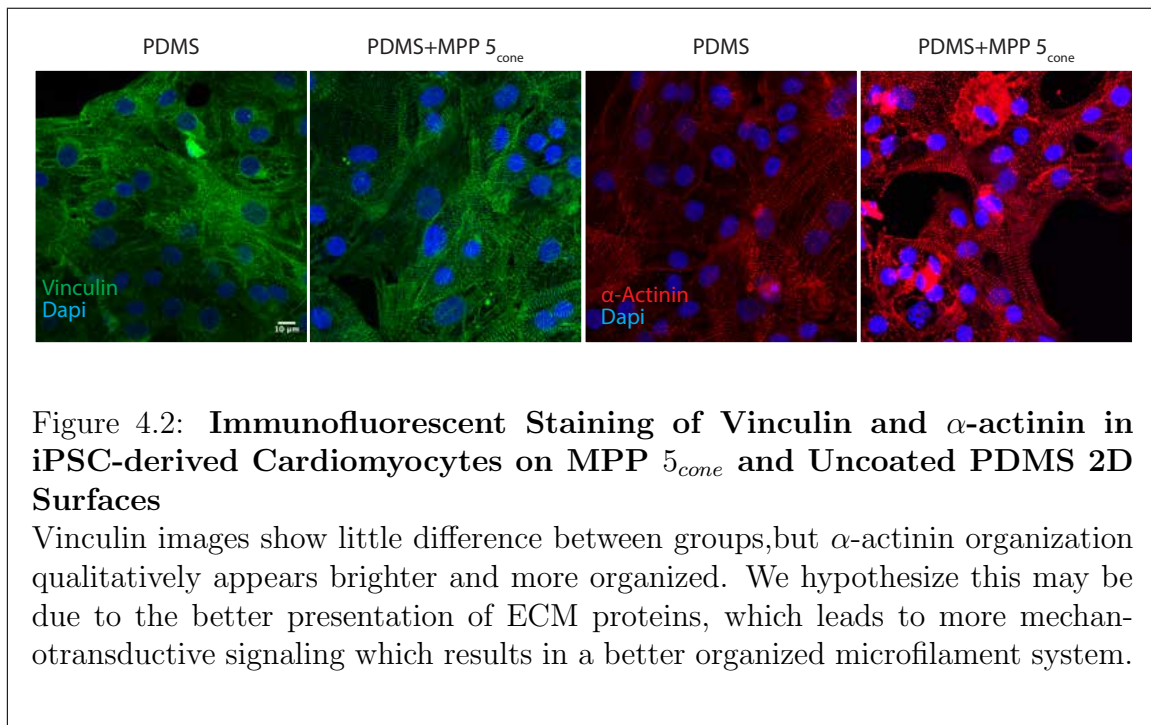
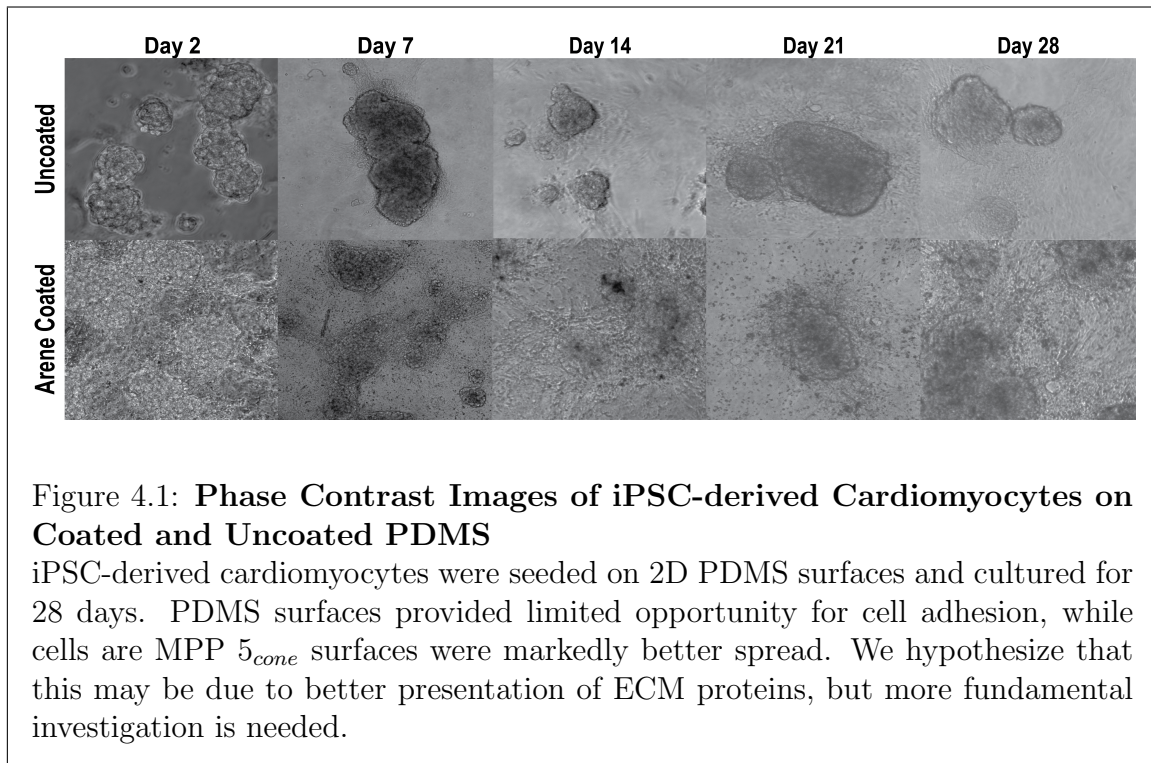
If functionalization of this polyphenol is possible, increasing its barrier performance may also be possible. A brush like PEG functionalization after polymerization of the polyphenol may further increase its barrier property to block a larger subset of lipophilic small molecules.

4.2.3 Improving Cell Adhesion with MPP 5_{cone} Coatings on PDMS

The discovery of iPSC as cell sources for studies has opened doors in clinical and research endeavors. In particular, hiPSC-CMs have recently shown potential in platforms for drug testing to augment current in vitro and in vivo toxicity drug development models and as sources for regenerative therapies for cardiac infarcts.(1, 2) Human iPSC sources for CMs overcome ethical concerns associated with differentiating these cells from ESC and increases the quantity of cells that can be attained without invasive and traumatic procedures. However, hiPSC-CMs demonstrate the maturity of fetal CMs showing a rounded morphology, mono-nucleated phenotype, ability to proliferate, similar electrophysiological signal, and similar gene expression of contractile and cytoskeletal markers.(3)

Many techniques have been used to accelerate or encourage the maturity of iPSC-derived cardiomyocytes through integrin activation, geometric confinement in 2 and 3D, surface topography, and electric stimulation among others. (Mathur2015 , 1, 3-6) Herrons study shows that Matrigel®coatings on PDMS increase conduction velocities by ~ 2 fold, promote hypertrophic growth, and increase expression of key sarcolemma and cardiac markers over other coating-substrate pairs. Herron hypothesizes that the improvement in conduction velocity and other mature cardiomyocyte markers is due to increased adhesion to the substrate, but in our experience even on Matrigel®coated PDMS, adhesion is much lower compared to other surfaces such as Matrigel®coated TCPS. To further investigate Herrons claim, experiments with PDMS with an intermediate protein adhesion layer that improves ECM presentation to further increase adhesion of cardiomyocytes (and other cell types) to PDMS needs to be done. These experiments will elucidate if it is indeed cell-substrate adhesion or possibly cell-cell adhesion that plays a role in improving iPSC-derived cardiomyocyte maturation as seen by Herron. MPP 5_{cone} in pilot studies has shown to improve CM adhesion significantly, as an intermediate adhesion layer between PDMS and Matrigel®. It is important to note that adhesion improvement with MPP 5_{cone} is seen even without optimization of the coating.

Figure 4.1 is a collection of images taken over the course of 28 days from seeding of iPSC-derived cardiomyocytes. Matrigel was used as an ECM coating for both conditions. Even without fluorescent staining, there is a marked difference in cell adhesion. Figure 4.2 shows vinculin, dapi and α -actinin staining. Vinculin is an intercellular adhesion protein and can be used to locate and quantify focal adhesion development as mentioned in Chapter 1. α -actinin has a banded structure in microfilament protein in



skeletal muscle cells such as cardiomyocytes. Between uncoated and coated groups, there is no qualitative disruption between either vinculin or α -actinin staining supporting the hypothesis that the coating is not negatively affecting the cardiomyocyte phenotype. Conversely, we noticed that the α -actinin staining is much brighter and more organized than on uncoated PDMS. More investigation into gene expression should be done to confirm that the cells are actually producing more α -actinin. Also, using cells that have fluorescently labeled α -actinin would provide more insight into this observation and confirm that it is not an artifact of immunofluorescent staining and simply a loss of antibody on uncoated substrates.

If this coating and possibly other polyphenols can be used to improve hiPSC-derived cardiomyocyte cytoskeletal organization and possibly maturity, it would help supply a more reliable cell source for toxicity testing in many platforms and possibly for tissue regeneration applications.

References

- (1) Xiulan Yang, Lil Pabon, and Charles E Murry. “Engineering Adolescence: Maturation of Human Pluripotent Stem Cell-Derived Cardiomyocytes”. In: *Circ. Res.* 114.3 (Jan. 2014), pp. 511–523.
- (2) Anurag Mathur et al. “Human iPSC-based Cardiac Microphysiological System For Drug Screening Applications”. In: *Scientific Reports* 5 (Mar. 2015), p. 8883.
- (3) Scott D Lundy et al. “Structural and Functional Maturation of Cardiomyocytes Derived from Human Pluripotent Stem Cells”. In: *Stem Cells Dev.* 22.14 (July 2013), pp. 1991–2002.
- (4) Todd J. Herron et al. “Extracellular matrix-mediated maturation of human pluripotent stem cell-derived cardiac monolayer structure and electrophysiological function”. In: *Circ. Arrhythmia Electrophysiol.* 9.4 (2016), pp. 1–12.
- (5) Zhen Ma et al. “Self-organizing human cardiac microchambers mediated by geometric confinement”. In: *Nat. Commun.* 6 (2015), pp. 1–10.
- (6) Sara S. Nunes et al. “Biowire: a platform for maturation of human pluripotent stem cell-derived cardiomyocytes”. In: *Nat Methods* 49.2 (2013), pp. 781–787.